Characterizing Heart Failure-Associated Myopathy: Skeletal Muscle Structure and Function in Late-Stage Patients

By

Jared Hartung

A dissertation submitted in partial fulfillment of the requirements for the degree of

Doctor of Philosophy

Kinesiology (Exercise Physiology)

at the

University of Wisconsin-Madison

2026

Date of Final Examination: 04/17/2026

This dissertation is approved by the following members of the Final Oral Committee:

Gary M Diffee, Professor, Kinesiology

Adam Kuchnia, Associate Professor, Nutritional Sciences

Jill Barnes, Associate Professor, Kinesiology

William G Schrage, Associate Professor, Kinesiology

Joshua Hermsen, Associate Professor, Cardiothoracic Surgery

Acknowledgements

During my six years of graduate school here at the University of Wisconsin-Madison I have developed and refined my skill set as an academic. I have learned so much about science, research, physiology, professionalism, and even myself. However, these insights would not have been possible without the incredible work of select individuals, and therefore, these acknowledgements recognize their significant contributions.

First, I would like to express my sincere gratitude to my mentor, Dr. Gary Diffee. His continued support, guidance, and instruction helped shape my doctoral education. Dr. Diffee's willingness to step out of his comfort zone of rodent research into human subjects, his dedication to facilitating assistantship support, and his innate ability to know when to let us learn through our mistakes and when to step in and save the day all demonstrate his incredible mentorship abilities. Throughout these six years, he has been essential in cultivating my academic, professional, and personal skill sets, which will guide me in all future endeavors. I truly cannot fully express my gratitude to him.

Second, I am deeply grateful to my committee members: Dr. Adam Kuchnia, Dr. Jill Barnes, Dr. Bill Schrage, and Dr. Josh Hermsen. Their roles, both as educators and experts, helped guide me and transform this project into the best possible version of itself. I am sincerely thankful for the time they dedicated, their thoughtful feedback, and their support throughout the process. Moreover, I'd especially like to thank Dr. Kuchnia for continuing to serve as PI for this project, despite balancing other studies. His willingness to continue this project, purely for my benefit, is nothing short of amazing.

I'd also like to thank the instructing supervisors I've had during my time as a teaching assistant in physiology- Dr. Drew Lokuta, Dr. Janet Branchaw, and Eric Walsh. Their mentorship

helped to shape my appreciation for teaching, my teaching philosophy, and even how I view scientific research. They taught me about the interconnectedness of physiology, which played a significant role in the way we designed and analyzed this project. Observing and learning from their lecture abilities instilled a confidence in my capability to present both academic and research material. Finally, they helped to foster my mentorship abilities, not only with undergraduates, but graduate peers as well.

I would also like to thank my lab partner, Justin Lopez. I am appreciative for him always being there to bounce ideas off one another, to commiserate together in misery, and to celebrate all our accomplishments. I'd like to thank him for his willingness to always be the first to hear a *rough* presentation or read a draft, for taking the lead on research protocols when we were stuck, and for just being a great friend. I cannot imagine a better lab partner.

Finally, I am incredibly grateful to my wife, Kasey. Her unwavering, unending support was critical. She constantly believed in me, encouraged me when I was down, and carried an enormous share of the financial burden. I truly cannot thank her enough. This achievement is as much hers as it is mine.

Abstract

Heart failure (HF) is a chronic, progressive clinical syndrome affecting more than 7 million Americans, with prevalence projected to reach approximately 3% of the U.S. population by 2030. While the condition is characterized primarily by impaired cardiac output, it is now well recognized that peripheral skeletal muscle dysfunction, rather than central hemodynamic compromise alone, accounts for a significant portion of patients' exercise intolerance, fatigue, and diminished quality of life. Despite this recognition, the mechanistic underpinnings of heart failure-associated myopathy remain incompletely characterized. Most existing research has focused on stable, moderate-stage patients using single biopsy sites and symptom-based classification systems (NYHA functional classification), which are known to poorly reflect objective disease severity. Moreover, no prior study has simultaneously investigated multiple domains of skeletal muscle pathology, namely functional, structural, and metabolic, within the same cohort of late-stage heart failure patients. This dissertation addresses these gaps through a comprehensive, multi-domain characterization of skeletal muscle biology in patients with ACC/AHA Stage D heart failure.

Ten patients with late-stage heart failure undergoing either orthotopic heart transplantation or ventricular assist device (VAD) implantation at the University of Wisconsin Hospital were enrolled. Eight non-heart failure organ donors from the University of Kentucky served as controls. Skeletal muscle biopsies were collected from two functionally distinct sites, the sternal pectoralis major and the proximal rectus abdominis, during their respective surgeries. This design allows for direct within-subject comparisons of systemic versus localized myopathy. Biopsy samples were subdivided and processed for three separate analyses: 1) skinned muscle fiber (SMF) contractile experiments measuring peak isometric force, maximal unloaded shortening velocity, and peak power output; 2) comprehensive morphohistological assessment via immunofluorescence for fiber type, cross-sectional area, fiber morphology, myonuclear content, and fibrosis; and 3)

quantification of mitochondrial content via citrate synthase activity assay and neutral lipid accumulation via Oil Red O staining. Linear mixed-effects modeling with repeated measures was the primary statistical approach across all aims.

We found that late-stage HF caused a profound intrinsic contractile dysfunction, with reduced force (~70%) and specific force (~61%) compared to controls. In parallel, peak power output and normalized power showed trend-level reductions (~68% and ~55%, respectively). No significant difference was found in intrinsic contractile parameters across muscle groups. Morphohistological analysis also revealed extensive fiber atrophy in the HF group, with Type 1 fibers reduced by 36% and Type 2 by 41%, compared to controls. Moreover, a marked fiber type shift from oxidative to glycolytic fiber types was detected in the patients with heart failure. Morphological assessment showed that heart failure fibers deviated from the typical polygonal shape and resulted in a less round, more convex fiber. Further analysis of the skeletal muscle extracellular landscape through Oil Red O and Picrosirius Red staining detected no differences between the groups. However, mitochondrial content, measured by citrate synthase activity, demonstrated decreased mitochondrial content (~35%) in the HF group compared to controls. To establish clinical relevance, we utilized correlational analysis to identify meaningful relationships between functional, structural, and metabolic muscle data with clinical parameters routinely acquired during standard care of heart failure. We found significant relationships between CT radiodensity and skeletal muscle lipid content, suggesting that these clinical metrics may serve as a non-invasive tool to inform us about the skeletal muscle metabolic phenotype.

Overall, the present studies indicate that heart failure-associated myopathy is a systemic process rather than a localized, site-specific response. Moreover, these findings present a mechanistic rationale for the observed exercise intolerance, fatigue, and reduced quality of life in patients with heart failure. The peripheral maladaptations induced in skeletal muscle extend

through multiple domains of muscle biology, including functional alterations, structural remodeling, and metabolic disarray. To the best of our knowledge, these studies are the first to utilize a comprehensive multi-domain investigation into the skeletal muscle of late-stage heart failure patients. Our hope is that studies help to provide a foundation for future works that aspire to more deeply investigation the mechanisms driving heart failure-induced myopathy.

Table of Contents

List of Abbreviations

Ab: Abdominis (rectus abdominis)

ACC: American College of Cardiology

AHA: American Heart Association

AIC: Akaike information criterion

ANOVA: Analysis of variance

BNP: Brain (or B-Type) natriuretic peptide

BSA: Bovine serum albumin

CON: control group

CS: Citrate synthase

CSA: Cross-sectional area

CT: Computed tomography

DAPI: 4’,6-diamidino-2-phenylindole

DEXA: Dual-energy X-ray absorptiometry

Df: degrees of freedom

EMM: Estimated marginal means

EtOH: Ethanol

FFP: Fried Frailty Phenotype

FI: Fibrosis index

FOV: Field of view

FT: Fiber type

HF: Heart failure

HFpEF: Heart failure with preserved ejection fraction

HFrEF: Heart failure with reduced ejection fraction

HU: Hounsfield units

LAI: Lipid area index

LME: Linear mixed effects

MyHC: Myosin heavy chain

NP: Normalized peak power output

NYHA: New York Heart Association

OCT: Optimal cutting temperature compound

OHT: Orthotopic heart transplant

OPTN: Organ Procurement and Transplantation Network

ORO: Oil Red O stain

P_0: Peak isometric force

PAD: Peripheral artery disease

PBS: Phosphate buffered saline

PBST: Phosphate buffered saline with Tween

PBST-B: Phosphate buffered saline with Tween and BSA

Pec: Pectoralis (pectoralis major)

PPO: Peak power output

PSR: Picrosirius red stain

REML: Restricted maximum likelihood

SD: Standard deviation

SDS-PAGE: Sodium dodecyl sulfate-polyacrylamide gel electrophoresis

SE: Standard error

SF: Specific force (P_0/CSA)

SMF: Skinned muscle fiber

TEC: Thermoelectric cooler controller

UNOS: United Network for Organ Sharing

(L)VAD: (Left) Ventricular assist device

V_{max}: Maximal unloaded shortening velocity (extrapolated from force-velocity curve)

VO_2max: Maximal oxygen uptake

Chapter I. Review of Literature

General Introduction

Heart failure (HF) is a debilitating, chronic, and progressive clinical syndrome is which the heart is unable to sufficiently match perfusion with tissue demands, producing a cascade of systemic maladaptations that impair quality of life.[1] Regardless of the etiology, systolic or diastolic dysfunction, HF is a multi-systemic syndrome that causes an array of symptoms, including lethargy, shortness of breath, edema, pulmonary congestion, and reduced exercise capacity; all of which increases the risk for frailty, morbidity, and mortality. Heart failure currently affects more than 7 million Americans, and its prevalence continues to rise in parallel with the aging population, with a roughly 3% of the American population affected by 2030.[2–4] The average HF patient is hospitalized more than twice annually, with a greater than 40% 90-day readmission rate, generating an enormous economic burden on both the individual and healthy system.[5]

Heart failure is treated through careful management of a variety of pharmacological agents and lifestyle facts. However, despite optimized therapies, HF can progress. In these advanced stages, when medical therapy alone proves inadequate to sustain quality of life or prolong survival, more definitive interventions such as implantation of a ventricular assist device (VAD) or orthotopic heart transplant (OHT) may become necessary.[1] In 2022 there was roughly 4,200 heart transplants in the United States.[6] Unfortunately, this number pales in comparison to the number of individuals on the waiting list.[7] Although record numbers of heart transplants have been regularly occurring year to year, there is still a significantly elevated demand for organs compared to their current supply.[6] The financial burden is equally staggering, with pre-transplant admission through one-year post-operative costs estimated at nearly $1.7 million.[8] Due to the limited supply and significant financial demands, it is vital to determine which patients will have the greatest probability of favorable outcomes following OHT. To aid this process, there is an organ matching system in place.

In the United States the Organ Procurement and Transplantation Network (OPTN) oversees organ transplant processes, including organ matching. The OPTN is a unique public-private partnership developed in response to the National Organ Transplant Act of 1984. Specifically, the OPTN establishes and maintains policies regarding organ transplant while addressing concerns in the transplant community.[9] Currently, the United Network for Organ Sharing (UNOS) is serving at the OPTN under contract with the U.S. Department of Health and Human Services. This organization serves as a forum for transplant professionals to come together and work to improve the national system for organ procurement and transplantation. Additionally, UNOS maintains the centralized computer network that links all organ procurement organizations, transplant hospitals, and histocompatibility labs, allowing for appropriate organ allocation.[10]

A variety of factors are considered during organ matching, such as immunological compatibility through blood and tissue type matching, organ size agreement, and duration on the transplant list. Another important factor for organ matching is the urgency a patient needs a transplant. Often this is related to the immediacy of mortality without transplantation and is determined by the patient's organ function and frailty.[9] Understanding the factors considered in organ matching is crucial for ensuring equitable allocation of organs to patients in need. However, beyond medical criteria, it is essential to consider the overall health status of transplant candidates, particularly regarding frailty and comorbidities, which can significantly impact outcomes following transplantation.[11,12]

Specific Aims

Skeletal muscle dysfunction is a key factor in the symptoms and progression of heart failure, making it a critical target for researchers and clinicians. These impairments in skeletal muscle mass and function increase the risk of frailty, disability, morbidity, and mortality. While the consequences of reduced skeletal muscle function are well understood, the mechanisms leading to heart failure-associated myopathy remain unclear. Currently, most research on heart failure is cross-sectional and conducted in stable, moderate-stage disease, making it difficult to fully capture cellular adaptations with disease progression. Moreover, studies involving human subjects typically involve grouping patients by similar symptomology using the New York Heart Association (NYHA) functional classification system, which is known to poorly correlate with disease progression and physical capacity, potentially obscuring significant mechanisms at play.

In order to address the current gaps in our understanding of the mechanisms of heart failure-associated myopathy, we utilized skeletal muscle biopsies from the pectoralis major and rectus abdominus in late-stage (ACC/AHA stage D) heart failure patients that were undergoing heart transplantation or VAD implantation. From these biopsies, we probed into multiple domains of skeletal muscle, namely functional, structural, and metabolic, in order to elucidate the mechanisms driving heart failure-associated myopathy. Specifically, we investigated changes in skinned muscle fiber (SMF) contractile properties, muscle quality changes, and mitochondrial maladaptations. Changes in any one of these skeletal muscle dimensions can result in reduced whole muscle function and diminished exercise capacity. Thus, by determining changes in these skeletal muscle characteristics in heart failure patients compared to non-heart failure controls, we can identify mechanisms for skeletal muscle myopathy and consequent increased incidence of frailty, disability, morbidity, and mortality in this patient population. Identification of the primary

mechanisms of myopathy is paramount for beginning to improve standards of care and development of novel pharmacological and lifestyle interventions.

To the best of our knowledge, this project is the first to investigate SMF contractile properties in late-stage heart failure patients. As such, this investigation compared heart failure patients at similar states of disease progression instead of based on symptoms (i.e. NYHA classes). While knowledge of the mechanisms leading to skeletal muscle myopathy is currently lacking, this project aimed to provide novel insights into the etiologies of reduced functional performance in this population. These understandings may provide a framework for future scientific research into the treatment and prevention of diminished functional performance in heart failure that has not previously been possible.

To address these issues, we had the following specific aims for this study:

1. Determine SMF contractile function in late-stage heart failure patients compared to non-heart failure controls.

    Utilizing multiple, functionally distinct biopsy sites, determine whether there is a difference in absolute contractile characteristics- such as peak isometric force, unloaded shortening velocity, and peak power output- as well as cross-sectionally normalized contractile properties- specific force and normalized peak power output.

    We hypothesized that heart failure patients will have significantly reduced SMF contractile function compared to non-heart failure controls. Specifically, we expected to see a reduction in specific force, unloaded shortening velocity, and normalized peak power output.

2. Characterize skeletal muscle quality in heart failure patients and quantify muscle quality differences to non-heart failure controls.

We hypothesized that skeletal muscle quality would be poorer in heart failure patients compared to non-heart failure controls. Namely, there would be significantly more fiber atrophy, increased fibrous infiltration, and reduced markers of regeneration, specifically centrally located nuclei.

3. Evaluate differences in mitochondrial content between heart failure patients and controls.

We hypothesized that there would be a decrease in mitochondrial content as measured by citrate synthase activity. We also hypothesized that there would be a greater lipid burden in heart failure compared to controls.

Research Strategy

Significance

Heart failure is a chronic, progressive condition for which there is no cure. While more definitive measures, such as a variety of advanced cardiac interventions, do exist, heart failure is primarily managed through meticulous treatment plans. This treatment is often through diligent supervision of a variety of pharmacological interventions and modifications of lifestyle factors. Currently, about 6.7 million individuals in the United States have heart failure, but that number is expected to rise, with an estimated 3% of the US population affected by 2030.[4] Additionally, the average patient with heart failure is hospitalized more than twice a year with a >40% 90-day readmission rate.[5] This high rate of hospitalization and readmission generates a significant economic burden, not only on the individual, but the healthcare system as a whole. As such, it is imperative to improve our understanding of the mechanisms driving worsening patient symptoms and heart failure progression in order to appropriately identify novel targets for both pharmacologic and lifestyle interventions.

Skeletal muscle, as the primary determinant of physical capacity, is an appropriate candidate for further investigation in this population. While diminished cardiac output and impaired hemodynamic reserve are implicated in exercise intolerance, it is now appreciated that central dysfunction alone cannot fully account for the degree of functional limitation. Extensive prior works have demonstrated that skeletal muscle dysfunction is a consequence of heart failure and better explains the observed exercise intolerance in heart failure patients.[13–18] Moreover, deficits of skeletal muscle mass and function in the setting of heart failure are independent predictors of patient symptoms, morbidity, and mortality.[19–22] Frailty, a clinical syndrome of reduced functional reserve and resistance to stressors, is of particular interest in the context of advanced cardiac interventions, as it is both a relative contraindication and an established independent predictor of adverse post-operative outcomes.[23–28] Therefore, understanding the peripheral skeletal muscle contributions to frailty in the context of HF is not merely of mechanistic interest, but contains significant clinical relevance, allowing for pre-operative risk stratification. As such, it is imperative to unravel the mechanistic underpinnings driving these maladaptive responses in skeletal muscle.

The neuromuscular system is an integrated, multitiered system beginning in the motor cortex and ending within the sarcomere with crossbridge cycling. Disruption of any node along this pathway can confer negative consequences as seen through impaired physical capacity. Consequently, many domains along the neuromuscular system must be investigated. Investigation into the functional properties within the myofiber, structural and compositional landscape of the whole muscle, and metabolic infrastructure to sustain repeated contractions is essential for our understanding. This dissertation does exactly that by characterizing the intrinsic contractile properties, morphohistological composition, and metabolic content within two functionally distinct skeletal muscle sites in patients with late-stage heart failure.

Addressing Gaps in Our Understanding

There are four gaps existing in the current literature that have limited our understanding of the effects underlying heart failure-induced myopathy. This project was designed to specifically address the following: 1) the focus on the stable, moderate-stage, ambulatory heart failure population; 2) use of single biopsy sites that prevent inference about systemic versus localized myopathy; 3) conflicting and incomplete data on single muscle fiber intrinsic contractile properties; and 4) absence of a comprehensive, multi-domain morphohistological assessment of heart failure patients utilizing the same cohort. Below, is a discussion on how we address each gap through careful methodological design in order to resolve these matters.

1. Late-stage heart failure as an understudied population

The vast majority of studies examining skeletal muscle biology in human models of heart failure have recruited patients with stable disease, usually classified as NYHA class II or III. Additionally, common exclusion criteria prevents enrollment of patients that were hospitalized in the last 90 days. The most critically ill patients, those with late-stage (AHA/ACC Stage D) heart failure, are routinely excluded from studies. Notably, the NYHA classification is a symptom-based tool that poorly correlates with objective measures of disease severity, cardiac function, and physical capacity, suggesting that grouping subjects by NHYA class may obscure significant findings. By recruiting exclusively patients that are undergoing heart transplantation or VAD implantation (AHA/ACC Stage D), we are studying the skeletal muscle phenotype during the most extensive progression of the disease, where deficits are expected to be both substantial and clinically meaningful. Recruitment from this specific subpopulation allows for us to ensure that all patients are at a comparable, objective stage of disease, allowing for increased subject homogeneity than by symptom-based classification alone.

2. Multiple biopsy design to test systemic versus localized myopathy

Virtually all prior studies involving muscle biopsies employ the use of a single site and often of the same muscle (vastus lateralis). This becomes problematic when trying to extrapolate findings to the skeletal musculature as a whole. Additionally, some conditions, such as weightlessness, injury, and decondition, have disparate effects on different muscle groups. In order to appropriately capture a broader picture of the effects of heart failure on skeletal muscle, this project utilized two functionally distinct muscle groups- the pectoralis major and rectus abdominis. This approach allows us to identify whether heart failure-induced myopathy is a systemic process or rather a localized, site-specific pathology. This within-subject design is a unique approach, made possible by the surgical context of biopsy acquisition, and allows for paired comparison of skeletal muscle properties across these distinct muscles.

3. Single muscle fiber analysis to identify intrinsic contractile dysfunction

Functional assessments; such as grip strength, 6-minute walk test, and sit-to-stand; are informative about clinical function, but are heavily confounded by motivational, neural, and hemodynamic factors that make interpretation of dysfunction difficult. Skinned muscle fiber preparations, on the other hand, offer a methodological solution to isolate dysfunction to the functional unit of muscle- the sarcomere. By chemical permeabilization, the sarcomeric proteins are left intact and eliminates everything upstream of the functional unit, including the central nervous system, α-motor neurons, neuromuscular junction, sarcolemma, and sarcoplasmic reticulum. This approach allows for direct investigation into the contractile apparatus of skeletal muscle, where contractile parameters of force, velocity, and power can be directly measured. Previous research examining SMF contractile function in heart failure has yielded ambiguous results, with reports of reduced specific reports in all, some, or no fiber types. These discrepancies

across prior works is likely reflected in both methodological approach and patient selection. As mentioned above, recruitment of late-stage heart failure patients may produce a more homogenous experimental group and a larger effect size, allowing for better resolution into the effects of heart failure-induced myopathy. To the best of our knowledge, this is the first study to apply SMF contractile analysis in patients undergoing advanced cardiac intervention.

4. Comprehensive morphohistological characterization

Prior histological works of skeletal muscle in the setting of heart failure have primarily focused on fiber atrophy and fiber type distribution. However, this characterization is incomplete. Beyond fiber size and type, the morphological quality of individual fibers, myonuclear content, and deposition of fibrofatty infiltration provide additional information regarding the remodeling process of skeletal muscle. While these parameters have been individually investigated before, no study has investigated all of these indices within the same cohort. Similarly, the literature is inconsistent. For example, overall, the research suggests a fiber type shift from oxidative to glycolytic; however, not all models or studies have agreed. Moreover, the investigation of fibrous infiltration into skeletal muscle in heart failure patients is limited and conflicting. Therefore, this dissertation expands the current literature's morphohistological characterization to include measures such as morphology, myonuclear counts, and fibrosis, all within the context of late-stage disease, providing a more complete examination of the skeletal muscle landscape.

The Approach

The primary objectives of this project were: 1) to characterize the intrinsic contractile properties of skeletal muscle in late-stage heart failure patients compared to controls, 2) to conduct a comprehensive morphohistological assessment of fiber size, type, morphology, and fibrous infiltration, and 3) to quantify skeletal muscle mitochondrial content and neutral lipid accumulation.

Ten patients with AHA/ACC Stage D heart failure undergoing VAD implantation or heart transplant at the University of Wisconsin Hospital were enrolled in the study. Eight non-HF organ donors were included as controls and collected at the University of Kentucky. Skeletal muscle biopsies of the sternal pectoralis major and proximal rectus abdominis were collected during their respective surgeries. Biopsy samples were subdivided for subsequent analysis for individual aims. Detailed methods for each aim are presented within their respective chapters (Chapters II-IV).

Conclusion

In summary, this is the first study to simultaneously investigate multiple domains of skeletal muscle dysfunction within a late-stage heart failure population. By studying the most critically ill and using a multi-biopsy approach this project aims to provide novel and clinically translatable insights into cardiac-induced skeletal myopathy.

Each chapter herein will contain a detailed introduction to the aim of the chapter, an in-depth methods section, a results section, and a detailed discussion section considering the significance of the findings and clinical impact. Chapter II addresses Aim 1 (SMF contractile properties), Chapter III addresses Aim 2 (Morphohistological assessment), and Chapter IV addresses Aim 3 (Mitochondrial content and lipid accumulation). Chapter V provides a brief

summary of the findings within each chapter, an integrated interpretation of the project, project-wide limitations, and future directions. The collective hope is that the findings of this dissertation will contribute to a better mechanistic understanding of skeletal myopathy in heart failure, provide a foundation for future research, improve risk stratification and post-operative care in patients undergoing advanced cardiac intervention, and ultimately aid in the development of novel interventions to reduce the burden imposed by peripheral maladaptations within this disease.

References

1. Heidenreich, P. A. *et al.* 2022 AHA/ACC/HFSA Guideline for the Management of Heart Failure: A Report of the American College of Cardiology/American Heart Association Joint Committee on Clinical Practice Guidelines. *Circulation* vol. 145 E895–E1032 Preprint at https://doi.org/10.1161/CIR.0000000000001063 (2022).

2. Heidenreich, P. A. *et al.* Forecasting the Impact of Heart Failure in the United States. *Circ. Heart Fail.* **6**, 606–619 (2013).

3. United Nations Department of Economic and Social Affairs. *World Social Report 2023*. (United Nations, 2023). doi:10.18356/9789210019682.

4. Martin, S. S. *et al.* 2025 Heart Disease and Stroke Statistics: A Report of US and Global Data from the American Heart Association. *Circulation* **151**, e41–e660 (2025).

5. Kilgore, M., Patel, H. K., Kielhorn, A., Maya, J. F. & Sharma, P. Economic burden of hospitalizations of Medicare beneficiaries with heart failure. *Risk Manag. Healthc. Policy* **10**, 63–70 (2017).

6. National data - OPTN. https://optn.transplant.hrsa.gov/data/view-data-reports/national-data/.

7. UNOS Data and Transplant Statistics | Organ Donation Data. https://unos.org/data/.

8. Bentley, T. S. & Ortner, N. J. *2020 U.S. Organ and Tissue Transplants: Cost Estimates, Discussion, and Emerging Issues*. (2020).

9. United Network for Organ Sharing. About UNOS. (2026).

10. Health Resources and Services Administration. About the OPTN. (2026).

11. Szentgróti, R. *et al.* The Impact of Frailty Components and Preoperative Mechanical Cardiac Support Changes with Time after Heart Transplantation. *Biomedicines* **12**, (2024).

12. Bottiger, B. A. *et al.* Frailty in the End-Stage Lung Disease or Heart Failure Patient: Implications for the Perioperative Transplant Clinician. *Journal of Cardiothoracic and Vascular Anesthesia* vol. 33 1382–1392 Preprint at https://doi.org/10.1053/j.jvca.2018.08.002 (2019).

13. Keller-Ross, M. L., Larson, M. & Johnson, B. D. Skeletal muscle fatigability in heart failure. *Frontiers in Physiology* vol. 10 Preprint at https://doi.org/10.3389/fphys.2019.00129 (2019).

14. Kinugawa, S., Takada, S., Matsushima, S., Okita, K. & Tsutsui, H. Skeletal Muscle Abnormalities in Heart Failure. *Int. Heart J.* (2015).

15. Lavine, K. J. & Sierra, O. L. Skeletal muscle inflammation and atrophy in heart failure. *Heart Fail. Rev.* **22**, (2017).

16. Adams, V., Linke, A. & Winzer, E. Skeletal muscle alterations in HFrEF vs. HFpEF. *Curr. Heart Fail. Rep.* **14**, 489–497 (2017).

17. Kennel, P. J., Mancini, D. M. & Schulze, P. C. Skeletal muscle changes in chronic cardiac disease and failure. *Compr. Physiol.* **5**, 1947–1969 (2015).

18. Paneroni, M. *et al.* Skeletal Muscle Myopathy in Heart Failure: the Role of Ejection Fraction. *Curr. Cardiol. Rep.* **20**, (2018).

19. Konishi, M. *et al.* Impact of sarcopenia on prognosis in patients with heart failure with reduced and preserved ejection fraction. *Eur. J. Prev. Cardiol.* **28**, 1022–1029 (2021).

20. Konishi, M. *et al.* Prognostic impact of upper and lower extremity muscle mass in heart failure. *ESC Heart Fail.* **10**, 732–737 (2023).

21. Myers, J. Exercise capacity and prognosis in chronic heart failure. *Circulation* vol. 119 3165–3167 Preprint at https://doi.org/10.1161/CIRCULATIONAHA.109.873430 (2009).

22. Agdamag, A. C., Van Iterson, E. H., Tang, W. H. W. & Finet, J. E. Prognostic Role of Metabolic Exercise Testing in Heart Failure. *J. Clin. Med.* **12**, 4438 (2023).

23. Newman, A. B. *et al.* Associations of subclinical cardiovascular disease with frailty. *J. Gerontol. A Biol. Sci. Med. Sci.* **56**, M158–M166 (2001).

24. Fried, L. P. *et al.* Frailty in Older Adults: Evidence for a Phenotype. *The Journals of Gerontology: Series A* **56**, M146–M157 (2001).

25. Cacciatore, F. *et al.* Frailty predicts long-term mortality in elderly subjects with chronic heart failure. *Eur. J. Clin. Invest.* **35**, 723–730 (2005).

26. Pandey, A. *et al.* Frailty Among Older Decompensated Heart Failure Patients: Prevalence, Association With Patient-Centered Outcomes, and Efficient Detection Methods. *JACC Heart Fail.* **7**, 1079–1088 (2019).

27. Flint, K. M., Matlock, D. D., Lindenfeld, J. A. & Allen, L. A. Frailty and the selection of patients for destination therapy left ventricular assist device. *Circ. Heart Fail.* **5**, 286–293 (2012).

28. Mancini, D. Heart transplantation in adults: Indications and contraindications. in *UpToDate* (ed. Connor, R. F.) (Wolters Kluwer, Waltham, MA, 2023).

Chapter 2. Contractile function of skeletal muscle in late-stage heart failure

Introduction

Heart failure is a chronic, progressive condition in which the heart cannot match cardiac output to sustain sufficient perfusion to peripheral tissues. This inability to appropriately supply adequate perfusion leads to symptoms of shortness of breath, lethargy, peripheral edema, pulmonary congestion, and reduced exercise capacity. However, these symptoms are not dependent on the function of the heart alone. In fact, common clinical markers of heart function (e.g. ejection fraction) often poorly correlate to patients' symptoms.[1–4] Moreover, using pharmacological interventions to normalize hemodynamics of individuals with heart failure often fails to improve exercise capacity.[5] Finally, patients that have undergone orthotopic heart transplantation (OHT) or a ventricular assist device (VAD) implantation still demonstrate an attenuated VO_2max.[6] These data demonstrate that the symptoms associated with heart failure are not a cause of poor hemodynamic function alone. Instead, it suggests that peripheral maladaptations are also contributing to patient symptomology. As such, skeletal muscle, the primary determinant of exercise capacity, is an organ system that needs to be investigated in the setting of heart failure. In fact, skeletal muscle impairment is now a recognized consequence of heart failure.[7–10]

Impairments in various levels of the neuromuscular chain can lead to significant reductions in function and lead to exacerbated patient symptoms. Notably, the intrinsic function of skeletal muscle, or the ability to generate cross-bridges and undergo cross-bridge cycling, is the most downstream mechanism on this multilevel chain. As such, it is vital to understand the effects of heart failure on the intrinsic contractile properties of skeletal muscle fibers. In order to understand the pathophysiological mechanisms of heart failure-induced myopathy, the intrinsic function of skeletal muscle can be determined via skinned muscle fiber (SMF) preparations; where individual muscle fibers are isolated from a biopsy, permeabilized (i.e. skinned), and subjected to: a) length

and force perturbations, and b) changes in substrate content and concentration. Currently, previous human research in heart failure-induced myopathy utilizing this approach is limited, and the existing studies have demonstrated equivocal results. For example, specific force (peak isometric force [P_0] normalized to cross-sectional area [CSA] of the fiber) has been shown to decrease in all fiber types,[11] only Type 1 fibers,[12] or not decreased at all compared to controls in locomotive skeletal muscles.[13] Furthermore, the effects of heart failure on unloaded shortening velocity (V_{max}) has not been investigated directly. Photometric analysis of NADH oxidation used to indirectly assess the myosin ATPase has shown that heart failure causes significant declines in maximal ATPase rate compared to controls.[11] Moreover, sinusoidal wave analysis of SMFs from heart failure patients demonstrates a decreased transition rate for myosin from the weakly to strongly bound state compared to controls. This results in a longer duty cycle and would suggest a slower shortening velocity.[13] However, measurements of shortening velocity in a purified actin-myosin model suggest that heart failure does not attenuate V_{max}.[14] Not only have these studies utilized either surrogate measurements or simplified models to investigate changes to V_{max}, the collective results are ambiguous. Finally, to our knowledge, there are no studies in the literature that measure effects of heart failure-induced myopathy on peak power output, which may be more physiologically relevant than both P_0 and V_{max} measures.

These inconsistencies make it difficult to draw a general conclusion about the effects of the intrinsic function of skeletal muscle fibers in the setting of heart failure. However, these disagreements may be a product of subject selection or use of single site biopsies and not experimental design or small effect sizes. Studies that utilize human subjects often recruit patients with stable heart failure, usually with a New York Heart Association (NYHA) classification of 2 or 3. However, the NYHA classification is based on reported patient symptoms and is therefore innately subjective. A more objective measure for patient selection is necessary in order to generate a more

homogenous sample population. Furthermore, often-cited issues with methodology that relies on a single biopsy site are that 1) conclusions drawn from the results are inferred to all skeletal muscle within the subject, or 2) differences between groups may not be captured as the changes do not occur in that biopsy location.[15] For this reason, multiple biopsy sites, from a variety of functionally distinct muscle groups is suggested.[15–17]

Therefore, the purpose of this study is to investigate the effects of heart failure on the intrinsic contractile properties of single muscle fibers in patients with advanced heart failure (ACC/AHA Stage D) who were actively undergoing a ventricular assist device (VAD) implantation or orthotopic heart transplant (OHT). Two functionally distinct skeletal muscle biopsy sites were used to assess the contractile properties of SMFs, such as specific force, V_{max}, and normalized power.

Methods

Muscle biopsy and tissue processing

All experiments were reviewed and approved by the University of Wisconsin-Madison Institutional Review Board. Subjects were recruited from clinical patients at the University of Wisconsin Hospital (HF; n = 10) or from organ donors at the University of Kentucky (non-HF controls; n = 8). Informed consent was obtained from all clinical subjects. Inclusion criteria included the following: patients with advanced heart failure (ACC/AHA Stage D) that required implantation of a VAD or OHT.

Following the opening incision of the respective surgery, roughly 200-300 mg of the sternal pectoralis major and proximal rectus abdominis was collected by the cardiothoracic surgeon. The sample was stored in relax solution[18] for ~1 hour until it could be divided manually, under guidance of a dissecting microscope, to generate bundles of roughly 20-30 muscle fibers. Each bundle was

tied to a capillary tube, placed in a skinning solution,[19] and stored in the fridge at 4°C for roughly 24 hours to allow for permeabilization of the membranes. Finally, the permeabilized fibers were stored in fresh skinning solution at -20°C until contractile analysis.

SMF contractile experiments

Contractile experiments of SMFs were conducted as described previously [20] with some modifications. Briefly, on the day of an experiment, a SMF at least 2 mm in length was manually dissected from a bundle and transferred to an experiment trough on the Permeabilized Fiber Apparatus (802D, Aurora Scientific) filled with relax solution. Each end of the SMF was securely fastened between a force transducer (403A, Aurora Scientific) and DC torque motor (6220H, Aurora Scientific), which was connected to a High-Speed length controller (322C, Aurora Scientific). The apparatus was then mounted on an Olympus IX50 Inverted Phase Contrast Microscope during the experiment. Under high-power (150x) magnification, the sarcomere lengths were set to roughly 2.6 µm by altering the length of the fiber until the desired sarcomere length was reached. The total length of the fiber was noted. Furthermore, the diameter of the fiber was measured at three points along the length of the fiber in two planes of view. The average diameter within each plane was used to determine CSA as determined by the equation for an ellipse. Finally, all the following SMF contractile experiments were carried out at 15°C by utilizing a thermometer/TEC controller (825A, Aurora Scientific) to maintain the temperature of the solutions in the troughs.

A slack test, as previously described [21], was conducted on the SMF mounted in the apparatus. Briefly, following setting the sarcomere length, the fiber was moved from relax solution into a trough with pCa 9.0 solution for priming. Afterwards, the fiber was transferred into another trough with maximally activating (pCa 4.5) solution (see 17 for solutions). The fiber was allowed to undergo an isometric contraction, and force was generated until saturation, at which point the fiber was then slacked to 80% of its original length. Once force began to regenerate following the slack,

the fiber was quickly transferred back into the pCa 9.0 solution prior to stretching back to the original length to avoid damaging the fiber. The length of time from fiber transfer into the maximally activating solution and the saturation point of the force curve (time to peak tension) was noted and constantly used throughout the subsequent contractile experiments. Peak isometric force was determined by subtracting the highest measured force value prior to the slack by the lowest measured force value immediately following the slack.

To determine the loaded shortening velocity of the fibers, a series of force steps was conducted (described previously at [22]). Each series contained three steps of descending force, to allow for three brief isotonic concentric contractions, followed by a slack to ~80% of the fibers' original length (Figure 1, top two inserts). Similarly to the slack test, the fiber was transferred into pCa 9.0 solution prior to stretching back to the original length. The individual forces used during the force steps were determined and selected by the researcher to allow for a broad range of values between the measured maximum and minimum force values (Figure 1, middle two inserts). At least 4 and up to 6 series of force steps were completed, resulting in 12-18 isotonic concentric contractions of varying intensities.

Determination of the shortening velocity of each force step was as follows: a linear regression was fit to the final half (100 msec) of each force step length curve, and the slope of that line was used as the shortening velocity (Figure 2). To establish the percentage of P_0 elicited by each force step, the maximum isometric force within each series was determined as described above. Following this, the mean force during the last 100 msec of the force step was divided by the maximum isometric force within each series and then multiplied by 100. This was completed for each force step, while adjusting the maximum isometric force within each series. Finally, in order to ensure preserved contractile function of the fiber, the maximum isometric force within each series was compared to the P_0 of the fiber. Each series of force steps was considered valid as long as the

maximum isometric force within the series was at least 90% or greater of the fibers' P_0. Following contractile experiments, SMFs were stored in microcentrifuge tubes at -80°C for later fiber typing.

To generate a force-velocity curve for a fiber, at least 12 valid force steps were present. For each force step, the absolute value and its respective loaded shortening velocity were exported to GraphPad Prism. An XY plot was created with force as the X-axis and shortening velocity as the Y-axis. The modified Hill equation (presented below) was fit to the data.

$$\text{Hill Equation: } \left(\frac{(X_{max}+a)*b}{X+a}\right) - b$$

Where X_{max} is peak isometric force, the variable "*a*" is a force constant, and variable "*b*" is a shortening velocity constant. Following the completion of the force-velocity curve, the velocity from the Hill's nonlinear line was transformed into power by multiplying velocity by force. This created a force-power curve where peak power output (PPO), percentage of P_0 at which PPO is attained, and normalized power (PPO normalized to CSA) were gathered (Figure 1, bottom two inserts).

Snap freezing tissue pilot study

Biopsies from HF patients were collected fresh and never frozen prior to contractile experiments, however, non-HF controls were collected during organ donation and subsequently snap frozen. In order to determine the effects of snap freezing skeletal muscle tissue on contractile function, a pilot study was conducted. A subset of samples from HF patients were divided, where half the sample was kept fresh and underwent typical contractile experiments. The other half of the sample was snap frozen in liquid nitrogen, stored at -80°C for a couple of months (to mimic the time from biopsy acquisition until experimentation), thawed at room temperature in relax solution, and then bundled as usual. All other procedural steps were carried out the same as the fresh section.

SMF myosin heavy chain determination

Myosin heavy chain (MHC) isoform expression of SMFs that completed contractile experiments was conducted utilizing sodium dodecyl sulfate-polyacrylamide gel electrophoresis (SDS-PAGE) as previously described.[23] Briefly, on the day of or day prior to gel electrophoresis, a separating gel was made utilizing Criterion MIDI 12+2 well cassettes (Bio-Rad). On the day of the experiment, a 4% stacking gel was made and added on top of the fully polymerized separating gel and a well comb inserted into the top to generate 12+2 wells. Upon polymerization, the cassette was placed into the Criterion Cell (Bio-Rad) and filled with the appropriate upper and lower running buffer. Then, fibers were removed from -80°C freezer and 10 µL of modified Laemmli buffer (2% SDS, 15% glycerol, 5% β-mercaptoethanol, 0.002% bromophenol blue dye, and 62.5 mM Tris [pH 6.7]) was added into the tube for each mm of fiber length (roughly 20-30 µL total). The fibers were then placed on a heat block at 95°C for 5 minutes, after which the tubes were quickly vortexed for ~30 seconds. Afterwards, 10 µL of the fiber-Laemmli solution were loaded into each well, except for two wells that contained controls. The controls were homogenized human skeletal muscle tissue which expressed all three skeletal muscle isoforms of MHC. The Criterion Cell was connected to a PowerPac Universal Power Supply (Bio-Rad) and ran at 250 V for ~15 hours at 4°C. After the run, the gels were stained using Silver Stain Plus (Bio-Rad) according to the manufacturer's instructions. Individual fiber MHC isoform expression was determined by the migration pattern of the myosin band as shown in Figure 3.

Physiological measurements correlated to clinical data

In order to determine if single muscle fiber contractile data in fibers from HF patients varied along with other aspects of heart failure symptoms, we correlated SMF contractile data with clinical data. Clinical data was acquired through a query of the HF patients' electronic medical records. The following is a non-inclusive list of relevant clinical information gathered: BNP, duration

of heart failure, frailty status/score (measured using the Fried Frailty Phenotype), and most recent chest CT prior to cardiac intervention. Duration of heart failure was determined as the difference (in months) from the first reported date of diagnosis to date of cardiac intervention. From the chest CT, the total area of pectoralis, minimum, maximum, and mean attenuation (HU), was extracted. Throughout the query process, patient confidentiality was maintained, and all data handling adhered to HIPAA guidelines.

Statistical analysis

Skinned muscle fiber contractile data were analyzed using GraphPad Prism (version 10.4 for Windows). A paired T-test was used to assess pilot data addressing the effects of freezing on contractile function of SMFs with a significance set at $p \leq 0.05$. A freezing correction factor was then derived from the difference of means between the fresh and frozen samples. A Shapiro-Wilk test of normality was used to assess normal distribution of data. Pooled analysis of fibers was conducted utilizing an independent T-test or Wilcoxon rank-sum test if normality was violated.

Due to unequal biopsy sites from subjects within each group, we used linear mixed-effects (LME) modeling to compare the effects of heart failure on contractile function. The initial modeling for each dependent variable considered biopsy site as a repeated measure, and therefore biopsy site and fiber type, and their interaction, were modeled as repeated within-subjects factors (compound symmetry for covariance structure). This approach allowed us to account for non-independence among repeated observations obtained within the same participant. Subjects were included as a random intercept to account for multiple observations obtained from the same individual. Fixed effects included heart failure status, biopsy site, and fiber type, along with all two and three-way interactions. Age and sex were examined as additional fixed effect covariates. Models were fit in SPSS (V31.0, IBM) using restricted maximum likelihood (REML) estimation and Satterthwaite approximation for denominator degrees of freedom. Statistical significance was

assessed using Type III tests of fixed effects and estimated marginal means were calculated to aid in interpretation of significant main effects and interactions. Because model stability differed across dependent variables, convergence and fit diagnostics were evaluated for each model. If nonconvergence occurred, a simplified model that removed the repeated covariance structure or age and sex covariates was used. Final reported models were the best-fitting converged models, as judged by model estimability and AIC criterion, while retaining biologically relevant fixed effects and interactions.

Correlation of physiological measurements to clinical data was conducted using a Pearson correlation if normally distributed, or a Spearman correlation if normality was violated or use of an ordinal variable. Data is presented as means ± SD.

Results

Effect of snap freezing on contractile function

Snap freezing of skeletal muscle tissue prior to permeabilization and SMF contractile analysis led to significantly reduced P_0 compared to fresh tissue (0.591 mN ± 0.344 vs 1.579 mN ± 0.782, $p < 0.0001$). Furthermore, PPO was significantly attenuated (38.01 μN FL sec^{-1} ± 22.00 vs 89.98 μN FL sec^{-1} ± 47.98, $p = 0.002$). However, freezing did not affect the measured CSA of the SMFs (16648 μm^2 ± 7032 vs 14990 μm^2 ± 6258, $p = 0.441$). After normalizing for CSA, as expected, this resulted in reduced specific force and normalized power. To amend for the effect of freezing on contractile function, a correction factor was derived as the percentage change from fresh to frozen for both P_0 and PPO. This correct factor was utilized moving forward on all non-HF control contractile data.

Contractile function across biopsy sites

Subject characteristics are presented in Table 1. Comparison of intrinsic properties of SMF contractile function across the two muscle biopsy sites was conducted by binning all fibers together by biopsy site. Pairwise comparisons demonstrated a significant difference in PPO (26.76 μN FL sec^{-1} ± 26.67 pec vs 11.55 μN FL sec^{-1} ± 8.641 ab, p = 0.039), while CSA trended toward larger fibers in the pec biopsy sites relative to ab (8545 μm^2 ± 3558 vs 6129 μm^2 ± 2362, p = 0.064). There were no differences in any other contractile characteristics between biopsy sites (Figure 4).

Pooled fiber analysis

Pooled fiber contractile data is presented in Table 3. Pooling of all fibers (global) based on the condition of heart failure showed that fibers in the HF group consistently demonstrated reduced CSA and contractile function, even when normalizing by fiber size. Namely, there was a ~16% reduction in fiber size (8270 vs 6967 μm^2), a ~63% decrease in P_0 (1.133 vs 0.414 mN), and a ~16% reduction in V_{max} (0.418 vs 0.338 Fl sec^{-1}). Accordingly, the decrease in both force and velocity led to a significantly diminished PPO (50.18 vs 19.68 μN Fl sec^{-1}). Moreover, contractile data normalized to fiber CSA were attenuated (specific force: 137.8 vs 50.97 kN m^{-2}; normalized power: 5.579 vs 2.081 W L^{-1}). In order to further validate our freeze correction method, SMF data from our lab of vastus lateralis biopsies taken from both young and old individuals (treated in the same manner as the HF samples) are presented concurrently with HF and non-HF control in Figure 5.

Effect of heart failure on SMF contractile properties

Descriptive statistics of contractile function separated by condition, biopsy site, and fiber type are presented in Table 2. We conducted linear mixed effects modeling to assess the impact of heart failure on contractile function of SMFs. The study design is depicted in Figure 6 demonstrating the need for repeated measures LME models with biopsy by fiber type as within-subjects factors. Table 4 summarizes the structure of the model used for each dependent variable. There was a

significant main effect of condition for CSA, P_0, and specific force ($p = 0.029$, 0.044, and 0.006, respectively) with trends in PPO and normalized power ($p = 0.071$ and 0.053). Biopsy site significantly affected CSA and P_0 ($p = 0.013$ and 0.028), but not specific force, V_{max}, PPO, or normalized power. Moreover, there were significant main effects of fiber type for CSA ($p < 0.001$), P_0 ($p = 0.01$), V_{max} ($p = 0.014$), PPO ($p < 0.001$), and normalized power ($p < 0.001$), but not for specific force. There were no significant two-way or three-way interaction effects detected for any dependent variable; however, there was a trend present in condition x fiber type for PPO ($p = 0.073$). Therefore, we conducted an exploratory simple effects analysis and found a significant mean difference in Type 2 fibers between condition (38.4 μN Fl sec^{-1}; $p = 0.008$), but not between Type 1 fibers. Finally, age and sex were not significant covariates in any model (all $p > .05$) (See Table 5 for complete main and interaction effects data). These findings demonstrate that heart failure causes a significant reduction in P_0 and specific force, with possible reductions in PPO and normalized power.

Contractile function and clinical correlations

Tables 6-8 detail correlations between clinically relevant data and global, Type 1 fibers, and Type 2 fibers SMF contractile function respectively. Correlational analysis of global contractile function and age of HF patients revealed no significant correlations. Similarly, frailty showed no significant correlations with fiber functional parameters. Moreover, there were no correlations for global function and the gold standard heart failure biomarker BNP, however, there was a trend seen in V_{max} ($r = 0.744$, $p = 0.090$). There was no correlation between duration of HF and global fiber contractile data. Moreover, we saw no correlation between pectoralis area acquired through chest CT and pec only contractile information, although CSA, P_0, and PPO approached significance ($r = 0.771$, $p = 0.103$; $r = 0.829$, $p = 0.058$; $r = 0.900$, $p = 0.083$; respectively). Nevertheless, contractile function normalized to fiber size (i.e. specific force and normalized power) showed no correlations.

In addition to global fiber contractile characteristics, correlational analysis was conducted on a fiber type basis. Type 2 fiber CSA and P_0 were significantly correlated to pec CT area ($r = 0.932$, $p = 0.021$ and $r = 0.943$, $p = 0.016$ respectively). No other fiber type correlations were significant with any clinical marker. Of note, however, there was a trend for duration of HF and Type 2 CSA ($r = 0.680$, $p = 0.093$) as well as BNP and Type 2 V_{max} ($r = 0.769$, $p = 0.074$).

Discussion

This study demonstrates that late-stage heart failure induces profound intrinsic contractile dysfunction in skeletal muscle fibers. Moreover, these differences in intrinsic function are independent of muscle fiber atrophy. Specifically, single muscle fibers from heart failure patients exhibited significantly reduced peak isometric force (~70%) and specific force (~61%), with trends suggested reduced peak power output (~68%), and normalized power (~55%) compared to non-HF controls. Additionally, these heart failure-induced contractile deficits (normalized to fiber size) were not dependent on biopsy sites. This novel finding of skeletal muscle contractile dysfunction in heart failure suggests a systemic skeletal myopathy rather than a localized, muscle-specific pathology. These findings have important implications for understanding the mechanisms of cardiac-induced skeletal myopathy and exercise intolerance in patients with heart failure. Moreover, these, and future findings, may help in identifying potential therapeutic targets to restore muscle function, ameliorate patient symptoms, and slow disease progression.

Analysis of pooled fibers (i.e. regardless of biopsy site) from HF and non-HF controls demonstrated significant reductions to intrinsic contractile properties of SMFs. While this statistical approach has been utilized in the past,[24,25] it fails to account for individual differences. Due to our research design, a more comprehensive analysis was warranted. As such, we employed

linear mixed-effects modeling to ascertain the effects of heart failure on intrinsic skeletal muscle function. The main advantage of using these types of models, rather than pooled analysis or classic nested ANOVAs which have been used in the past, is that they accommodate missing observations, unbalanced data, and do not assume independence of observations, all which were present in the current study. Moreover, they are more flexible and allow for correction of covariates, such as age and sex. Using biopsy site and fiber type as within-subjects factors and a random intercept (see Figure 6 for the nested design), we detected significant impairments in contractile function. This approach was generally in agreement with those observed using the pooled fiber analysis. Patients with heart failure had significantly reduced CSA, P_0, and specific force compared to non-HF controls. Moreover, PPO and normalized power showed trend-level effects, suggesting that heart failure may cause an attenuation in power production in SMFs. Our findings are in agreement with those of some prior studies. Decrements in specific force have previously been observed in both animal[24] and human models.[11,12] However, Miller et al. reports that SMF experiments conducted near physiological temperatures and inorganic phosphate levels attenuate these differences in specific force.[13] Moreover, in vitro studies using isolated myosin and thin filament have shown no differences in specific force in patients with heart failure compared to controls.[14] The current study utilized a temperature of 15°C and 0 mM inorganic phosphate during SMF contractile function testing. Furthermore, our approach utilized skinned single muscle fibers, where permeabilization maintains the entire sarcomeric functional unit. These differences in methodological design may explain the differences seen between our study and those aforementioned.

While it is difficult to resolve the conflicting results of the effects of heart failure on the intrinsic contractile function of skeletal muscle fibers, these differences may also be explained by patient selection. Studies involving patients with heart failure often select individuals with stable

heart failure and a NYHA functional class of 3 or less. Additionally, they often involve an inclusion criterion of no recent hospitalizations (previous 6 months). This patient selection may not be the best representation of heart failure. Roughly 50% of heart failure patients are readmitted within a 6-month period.[26] Furthermore, it is plausible that the effect sizes of intrinsic contractile function are too small to determine during the early or mild stages of heart failure. For this reason, we selected patients with late-stage heart failure, who required advanced cardiac interventions. By selecting the most critically ill, we aimed to capture the largest possible changes to skeletal muscle function.

A unique contribution of this work is the direct comparison of intrinsic contractile properties across two functionally distinct skeletal muscle groups. Typically, studies using single muscle fiber analysis have relied on a single muscle biopsy, often from the vastus lateralis, raising questions about whether findings can be extrapolated to the broader skeletal musculature. While previous studies have investigated the effects of multiple biopsies on the same muscle group[15], or the number of micro-biopsies to determine a representative sample of the whole muscle[27], to our knowledge, only one other study has directly compared SMFs across different skeletal muscles, but only within a single individual and in Type 1 fibers only.[28] Initially, our reasoning for multiple biopsy sites was to capture potential disparate effects in the setting of heart failure. We hypothesized that changes in local blood flow, innervation, metabolic factors, or disuse may disproportionally affect some muscle groups from others; a phenomenon often seen in other settings, such as aging, disuse, and weightlessness.[29–35] Moreover, there is an increased incidence of heart failure in older populations compared to young.[36–38] Older individuals tend to have multiple comorbidities, many of which negatively impact skeletal muscle function.[39] Utilization of numerous muscle groups with various physiological tasks may better capture the complete picture of skeletal musculature. Our LME models showed a significant main effect of biopsy for CSA and P_0, but no other contractile measure. The observed changes in P_0 appear to be driven by the differences in measured CSA as

we did not see any significant difference between biopsy sites when normalizing force to CSA (specific force). Furthermore, as expected, we saw significant main effects of fiber type for CSA, P_0 V_{max}, PPO, and normalized power, with exception only to specific force. In SMFs, the primary determinant of force is fiber volume. As Type 2 fibers tend to be larger than Type 1, they often generate greater force. This difference disappears when normalizing force to cross-sectional area. Importantly, we do not see this effect when comparing normalized power. Power is the product of force and velocity and as such is strongly influenced by the significantly different shortening velocities between fiber types.

Together, our data demonstrates that 1) there is no difference in normalized contractile function across functionally distinct skeletal muscles when accounting for MHC content, and 2) late-stage heart failure does not appear to have a disparate effect on muscle groups, and instead results in a systemic skeletal myopathy, leading to worsening patient symptoms and prognosis.[40–44] These findings substantially strengthen the validity of previous single-site biopsy studies and provide reassurance that conclusions drawn from vastus lateralis samples can be reasonably extended to other skeletal muscles in the setting of heart failure. Furthermore, the lack of site-specific differences suggests that therapeutic interventions targeting the molecular mechanisms of contractile dysfunction, may produce benefits across multiple muscle groups rather than being tissue specific.

While we have demonstrated that heart failure negatively impacts the contractile function of skeletal muscle, biopsies and subsequent single fiber analysis is not feasible in the clinical setting. For this reason, it is imperative that we make connections between SMF function and commonly utilized or readily accessible clinical measures. Accordingly, we investigated the correlations between SMF contractile characteristics and regularly acquired clinical data. Using Pearson and Spearman correlations, we found that global pec fiber CSA showed a positive trend

with pectoralis area assessed through CT imaging. This correlation appears to be driven by Type 2 fibers as there was a significant correlation between Type 2 fiber CSA and pectoralis area but not Type 1. Moreover, Type 2 fibers P_0 was significantly correlated with pectoralis area. However, normalized contractile characteristics were not correlated. These findings suggest that repurposing of the commonly acquired thoracic CT imaging prior to advanced cardiac intervention may be useful in indirectly assessing pectoralis fiber atrophy; however, it does not appear to describe intrinsic contractile properties. Brain natriuretic peptide (BNP) is the gold standard biomarker of heart failure and is also closely monitor in these patients.[45,46] We saw a positive trend for global fiber V_{max} and BNP levels. This increased V_{max} may be indirectly measuring fiber type, as all the fibers are pooled together within an individual for these global measures. As V_{max} increases, that may reflect an increase in the number of Type 2 fibers present. It has been shown that heart failure may result in a fiber type shift from oxidative to faster, glycolytic fibers.[47] This positive trend with BNP levels may reflect this shift in fiber type and should be investigated further as a possible clinical marker of skeletal muscle impairment.

Interestingly, frailty, as assessed by the Fried Frailty Phenotype (FFP), did not correlate with any single fiber characteristic measured. The purpose of this measurement tool is to quantify the degree of frailty within an individual and classify them as non-frail, prefrail, or frail. As frailty is primarily driven by skeletal muscle mass and function,[32,48] we believed that the FFP would strongly correlate with single fiber contractile properties, the primary drivers of whole muscle function. However, this does not appear to be the case. Moreover, the ability to appropriately capture frailty, especially in this patient population, is vital. A variety of factors need to be considered during assessment for heart transplantation or VAD placement, including frailty. In fact, frailty is considered a relative contraindication for OHT.[49] The lack of a correlation between frailty and the

driving components of whole muscle function suggests that we may not be adequately capturing the physiological underpinnings driving frailty in this patient population.

In conclusion, the aim of this study was to investigate the effects of late-stage HF on the contractile properties of skeletal muscle fibers. We have demonstrated that HF has a profound effect on the intrinsic contractile function of SMFs, with significant declines in the force generating capacity and shortening velocity in both Type 1 and Type 2 fibers from multiple biopsy sites. The systemic nature of the skeletal myopathy and its persistence when accounting for fiber atrophy indicates a pathophysiological mechanism beyond muscle wasting that is contributing to symptomology and disease progression in this patient population. These findings underscore the necessity of skeletal muscle targeted therapies and rehabilitation in heart failure management.

References

1. Agdamag, A. C., Van Iterson, E. H., Tang, W. H. W. & Finet, J. E. Prognostic Role of Metabolic Exercise Testing in Heart Failure. *J. Clin. Med.* **12**, 4438 (2023).

2. Azul Freitas, A. *et al.* Heart failure with reduced ejection fraction: predicting exercise intolerance with echocardiography. *Eur. Heart J.* **42**, (2021).

3. Franciosa, J. A., Park, M. & Levine, T. B. Lack of Correlation Between Exercise Capacity and Indexes of Resting Left Ventricular Performance in Heart Failure. *Am. J. Cardiol.* **47**, 33 (1981).

4. Myers, J. Exercise capacity and prognosis in chronic heart failure. *Circulation* vol. 119 3165–3167 Preprint at https://doi.org/10.1161/CIRCULATIONAHA.109.873430 (2009).

5. Maskin, C. S., Forman, R., Sonnenblick, E. H., Frishman, W. H. & LeJemtel, T. H. Failure of dobutamine to increase exercise capacity despite hemodynamic improvement in severe chronic heart failure. *Am. J. Cardiol.* **51**, (1983).

6. Wilson, R. F., Johnson, T. H., Haidet, G. C., Kubo, S. H. & Mianuelli, M. Sympathetic Reinnervation of the Sinus Node and Exercise Hemodynamics After Cardiac Transplantation. *Circulation* 2727–2733 (2000).

7. Kinugawa, S., Takada, S., Matsushima, S., Okita, K. & Tsutsui, H. Skeletal Muscle Abnormalities in Heart Failure. *Int. Heart J.* (2015).

8. Tucker, W. J., Haykowsky, M. J., Seo, Y., Stehling, E. & Forman, D. E. Impaired Exercise Tolerance in Heart Failure: Role of Skeletal Muscle Morphology and Function. *Current Heart Failure Reports* vol. 15 323–331 Preprint at https://doi.org/10.1007/s11897-018-0408-6 (2018).

9. Bekfani, T. *et al.* Skeletal Muscle Function, Structure, and Metabolism in Patients With Heart Failure With Reduced Ejection Fraction and Heart Failure With Preserved Ejection Fraction. *Circ. Heart Fail.* **13**, E007198 (2020).

10. Heidenreich, P. A. *et al.* 2022 AHA/ACC/HFSA Guideline for the Management of Heart Failure: A Report of the American College of Cardiology/American Heart Association Joint Committee on Clinical Practice Guidelines. *Circulation* vol. 145 E895–E1032 Preprint at https://doi.org/10.1161/CIR.0000000000001063 (2022).

11. Szentesi, P. *et al.* Depression of force production and ATPase activity in different types of human skeletal muscle fibers from patients with chronic heart failure. *J. Appl. Physiol.* **99**, (2005).

12. Miller, M. S. *et al.* Mechanisms underlying skeletal muscle weakness in human heart failure: Alterations in single fiber myosin protein content and function. *Circ. Heart Fail.* **2**, 700–706 (2009).

13. Miller, M. S. *et al*. Chronic heart failure decreases cross-bridge kinetics in single skeletal muscle fibres from humans. *Journal of Physiology* **588**, 4039–4053 (2010).

14. Okada, Y., Toth, M. J. & VanBuren, P. Skeletal muscle contractile protein function is preserved in human heart failure. *J. Appl. Physiol.* **104**, 952–957 (2008).

15. Van de Casteele, F. *et al*. Does one biopsy cut it? Revisiting human muscle fiber type composition variability using repeated biopsies in the vastus lateralis and gastrocnemius medialis. *J. Appl. Physiol.* **137**, 1341–1353 (2024).

16. Prayson, R. A. Diagnostic yield associated with multiple simultaneous skeletal muscle biopsies. *Am. J. Clin. Pathol.* **126**, 843–848 (2006).

17. Long, D. E. *et al*. Short-term repeated human biopsy sampling contributes to changes in muscle morphology and higher outcome variability. *J. Appl. Physiol.* **135**, 1403–1414 (2023).

18. Diffee, G. M. & Chung, E. Altered single cell force-velocity and power properties in exercise-trained rat myocardium. *J. Appl. Physiol.* **94**, 1941–1948 (2003).

19. Diffee, G. M., Greaser, M. L., Reinach, F. C. & Moss, R. L. *Effects of a Non-Divalent Cation Binding Mutant of Myosin Regulatory Light Chain on Tension Generation in Skinned Skeletal Muscle Fibers*. *Biophysical Journal* vol. 68 (1995).

20. Moss, R. L., Giulian, G. G. & Greaser, M. L. Effects of EDTA Treatment upon the Protein Subunit Composition and Mechanical Mammalian Single Skeletal Muscle Fibers Properties of. *J. Cell Biol.* **96**, 970 (1983).

21. Edman, K. A. The velocity of unloaded shortening and its relation to sarcomere length and isometric force in vertebrate muscle fibres. *J. Physiol.* **291**, 143–159 (1979).

22. Gries, K. J. *et al*. Single-muscle fiber contractile properties in lifelong aerobic exercising women. *J Appl Physiol* **127**, 1710–1719 (2019).

23. Roberts, M. D., Dalbo, V. J., Sunderland, K. L. & Kerksick, C. M. Electrophoretic separation of myosin heavy chain isoforms using a modified mini gel system. *J. Strength Cond. Res.* **26**, 3461–3468 (2012).

24. van Hees, H. W. H. *et al*. Diaphragm single-fiber weakness and loss of myosin in congestive heart failure rats. *Am J Physiol Heart Circ Physiol* **293**, 819–828 (2007).

25. van Hees, H. W. H., Ottenheijm, C. A. C., Granzier, H. L., Dekhuijzen, P. N. R. & Heunks, L. M. A. Heart failure decreases passive tension generation of rat diaphragm fibers. *Int. J. Cardiol.* **141**, 275–283 (2010).

26. Heidenreich, P. A. *et al*. Forecasting the Impact of Heart Failure in the United States. *Circ. Heart Fail.* **6**, 606–619 (2013).

27. Hester, G. M. *et al.* Microbiopsy Sampling for Examining Age-Related Differences in Skeletal Muscle Fiber Morphology and Composition. *Front. Physiol.* **12**, (2022).

28. Frontera, W. R. & Larsson, L. Contractile studies of single human skeletal muscle fibers: A comparison of different muscles, permeabilization procedures, and storage techniques. *Muscle Nerve* **20**, 948–952 (1997).

29. Miokovic, T., Armbrecht, G., Felsenberg, D. & Belavy, D. L. Heterogeneous atrophy occurs within individual lower limb muscles during 60 days of bed rest. *J. Appl. Physiol.* **113**, (2012).

30. Gallagher, P. *et al.* Effects of 84-days of bedrest and resistance training on single muscle fibre myosin heavy chain distribution in human vastus lateralis and soleus muscles. *Acta Physiol. Scand.* **185**, 61–69 (2005).

31. Fitts, R. H. *et al.* Prolonged space flight-induced alterations in the structure and function of human skeletal muscle fibres. *Journal of Physiology* **588**, 3567–3592 (2010).

32. Faulkner, J. A., Larkin, L. M., Claflin, D. R. & Brooks, S. V. Age-related changes in the structure and function of skeletal muscles. *Clin. Exp. Pharmacol. Physiol.* **34**, 1091–1096 (2007).

33. Janssen, I., Heymsfield, S. B., Wang, Z. M. & Ross, R. Skeletal muscle mass and distribution in 468 men and women aged 18-88 yr. *J. Appl. Physiol.* **89**, 81–88 (2000).

34. Kemmler, W., Von Stengel, S. & Schoene, D. Longitudinal Changes in Muscle Mass and Function in Older Men at Increased Risk for Sarcopenia — The FrOST-Study. *Journal of Frailty and Aging* **8**, 57–61 (2019).

35. Candow, D. G. & Chilibeck, P. D. *Differences in Size, Strength, and Power of Upper and Lower Body Muscle Groups in Young and Older Men*. https://academic.oup.com/biomedgerontology/article/60/2/148/563279 (2005).

36. Gielen, S. *et al.* Heart Failure Exercise Training Attenuates MuRF-1 Expression in the Skeletal Muscle of Patients With Chronic Heart Failure Independent of Age The Randomized Leipzig Exercise Intervention in Chronic Heart Failure and Aging Catabolism Study. https://doi.org/10.1161/CIRCULATIONAHA (2012) doi:10.1161/CIRCULATIONAHA.

37. Martin, S. S. *et al.* 2025 Heart Disease and Stroke Statistics: A Report of US and Global Data from the American Heart Association. *Circulation* **151**, e41–e660 (2025).

38. Tsao, C. W. *et al.* Heart Disease and Stroke Statistics-2022 Update: A Report from the American Heart Association. *Circulation* vol. 145 E153–E639 Preprint at https://doi.org/10.1161/CIR.0000000000001052 (2022).

39. Cruz-Jentoft, A. J. *et al*. Sarcopenia: Revised European consensus on definition and diagnosis. *Age and Ageing* vol. 48 16–31 Preprint at https://doi.org/10.1093/ageing/afy169 (2019).

40. Anker, S. D. *et al*. Wasting as independent risk factor for mortality in chronic heart failure. *The Lancet* **349**, 1050–1053 (1997).

41. Coats, A. J. S. The "Muscle Hypothesis" of Chronic Heart Failure. *J. Mol. Cell. Cardiol.* **28**, 2255–2262 (1996).

42. Coats, A. J. S., Clark, A. L., Piepoli, M., Volterrani, M. & Poole-Wilson, P. A. Symptoms and quality of life in heart failure: the muscle hypothesis. *Br. Heart J.* **72**, S36 (1994).

43. Harrington, D. *et al*. Skeletal muscle function and its relation to exercise tolerance in chronic heart failure. *J. Am. Coll. Cardiol.* **30**, 1758–1764 (1997).

44. Aimo, A. *et al*. The ergoreflex: how the skeletal muscle modulates ventilation and cardiovascular function in health and disease. *Eur. J. Heart Fail.* **23**, 1458–1467 (2021).

45. Shrivastava, A., Haase, T., Zeller, T. & Schulte, C. Biomarkers for Heart Failure Prognosis: Proteins, Genetic Scores and Non-coding RNAs. *Frontiers in Cardiovascular Medicine* vol. 7 Preprint at https://doi.org/10.3389/fcvm.2020.601364 (2020).

46. Nadar, S. K. & Shaikh, M. M. Biomarkers in Routine Heart Failure Clinical Care. *Card. Fail. Rev.* **5**, 50–56 (2019).

47. Kaneguchi, A., Sakitani, N. & Umehara, T. Histological changes in skeletal muscle induced by heart failure in human patients and animal models: A scoping review. *Acta Histochem.* **126**, 152210 (2024).

48. Bortz, W. M. *A Conceptual Framework of Frailty: A Review*. *Journal of Gerontology* vol. 57 https://academic.oup.com/biomedgerontology/article/57/5/M283/620581 (2002).

49. Mancini, D. Heart transplantation in adults: Indications and contraindications. in *UpToDate* (ed. Connor, R. F.) (Wolters Kluwer, Waltham, MA, 2023).

Tables and Figures

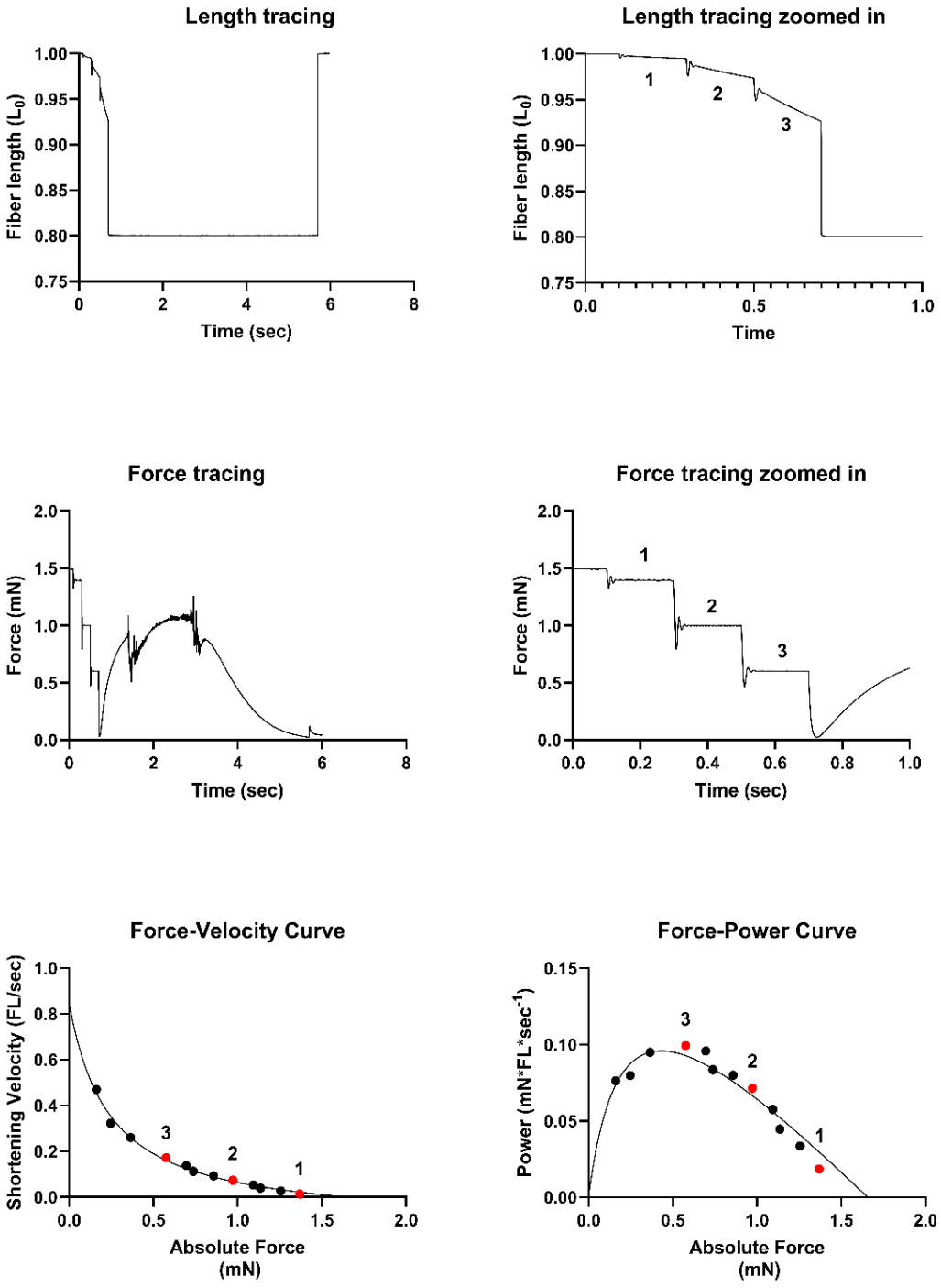

Figure 1. Force and length tracing during force step protocol and subsequent force-velocity and force-power curves.

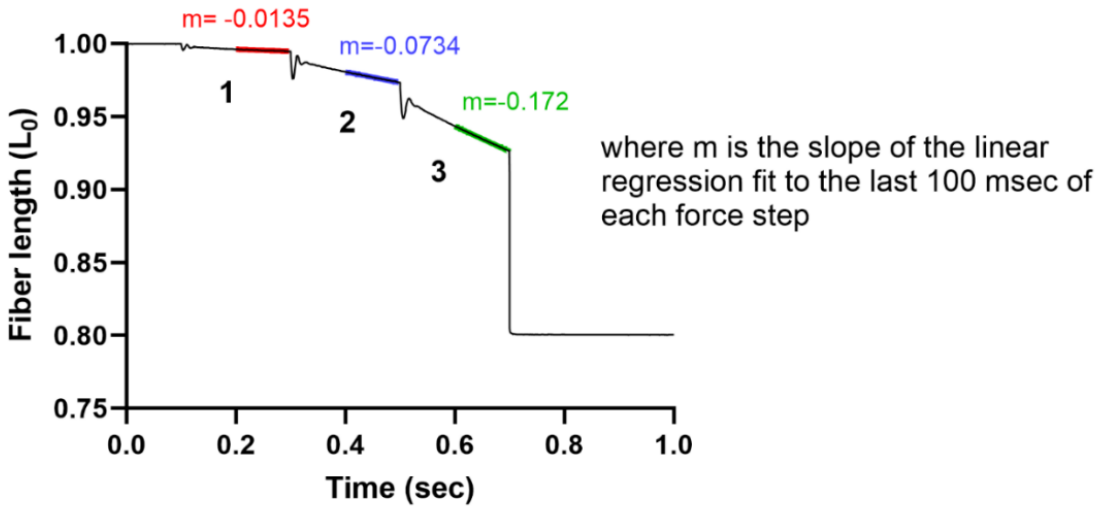

Figure 2. Demonstration of shortening velocity calculation within a series of force steps.

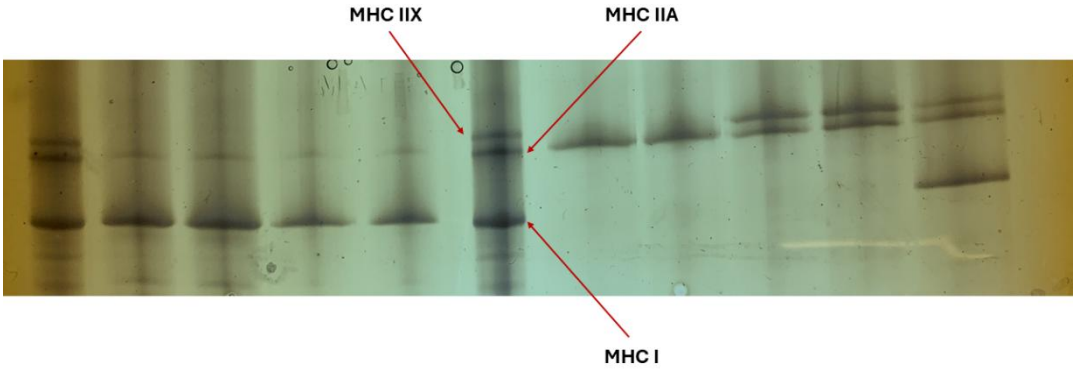

Figure 3. Representative image of SDS-PAGE gel for myosin heavy chain determination. Controls in far left, right, and middle (labeled) lanes.

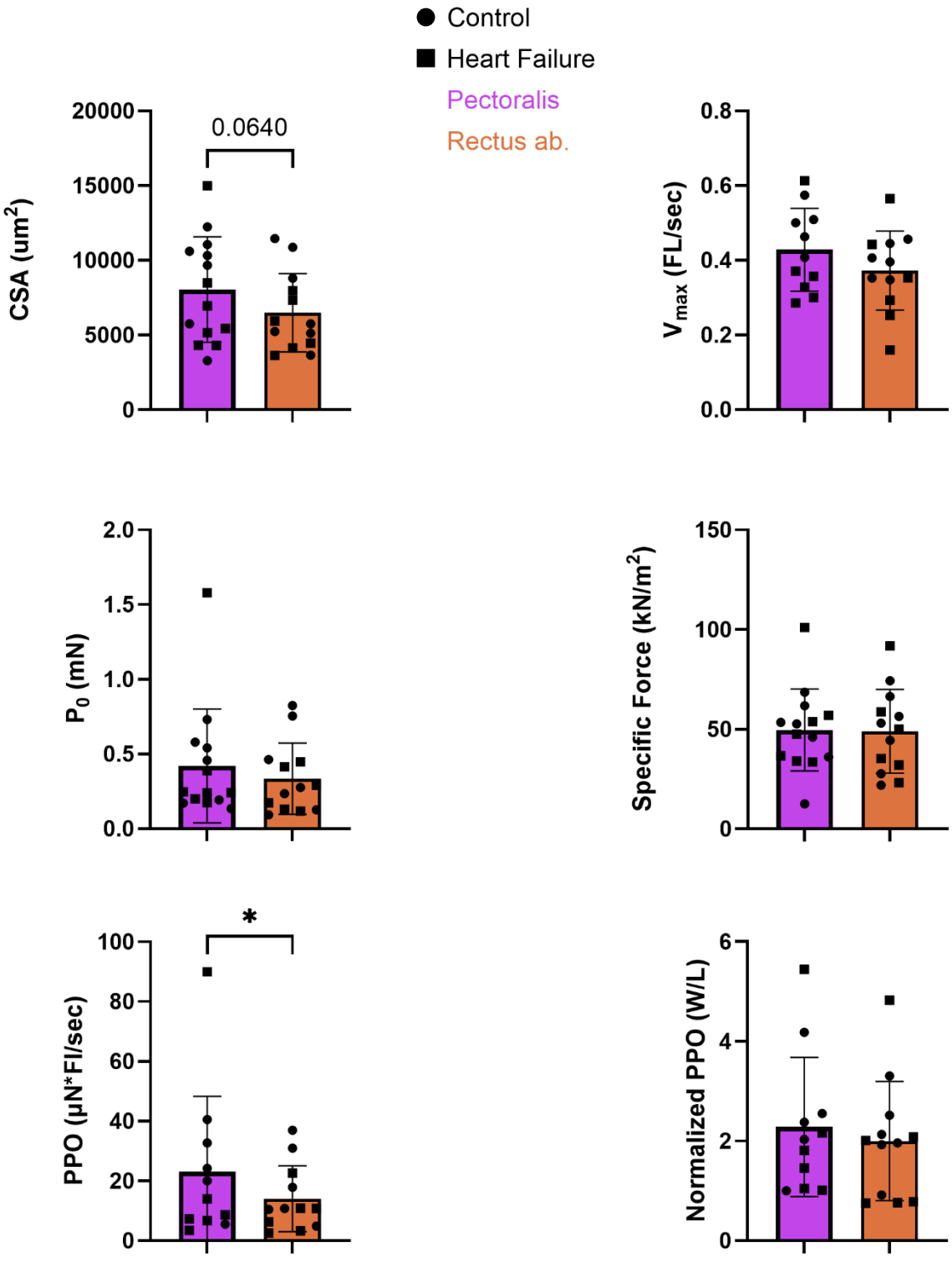

*Figure 4. Comparison of contractile characteristics between biopsy sites in both HF and control. Fibers from both groups are pooled together. Each symbol represents a biopsy site from a single individual. * signifies $p < 0.05$.*

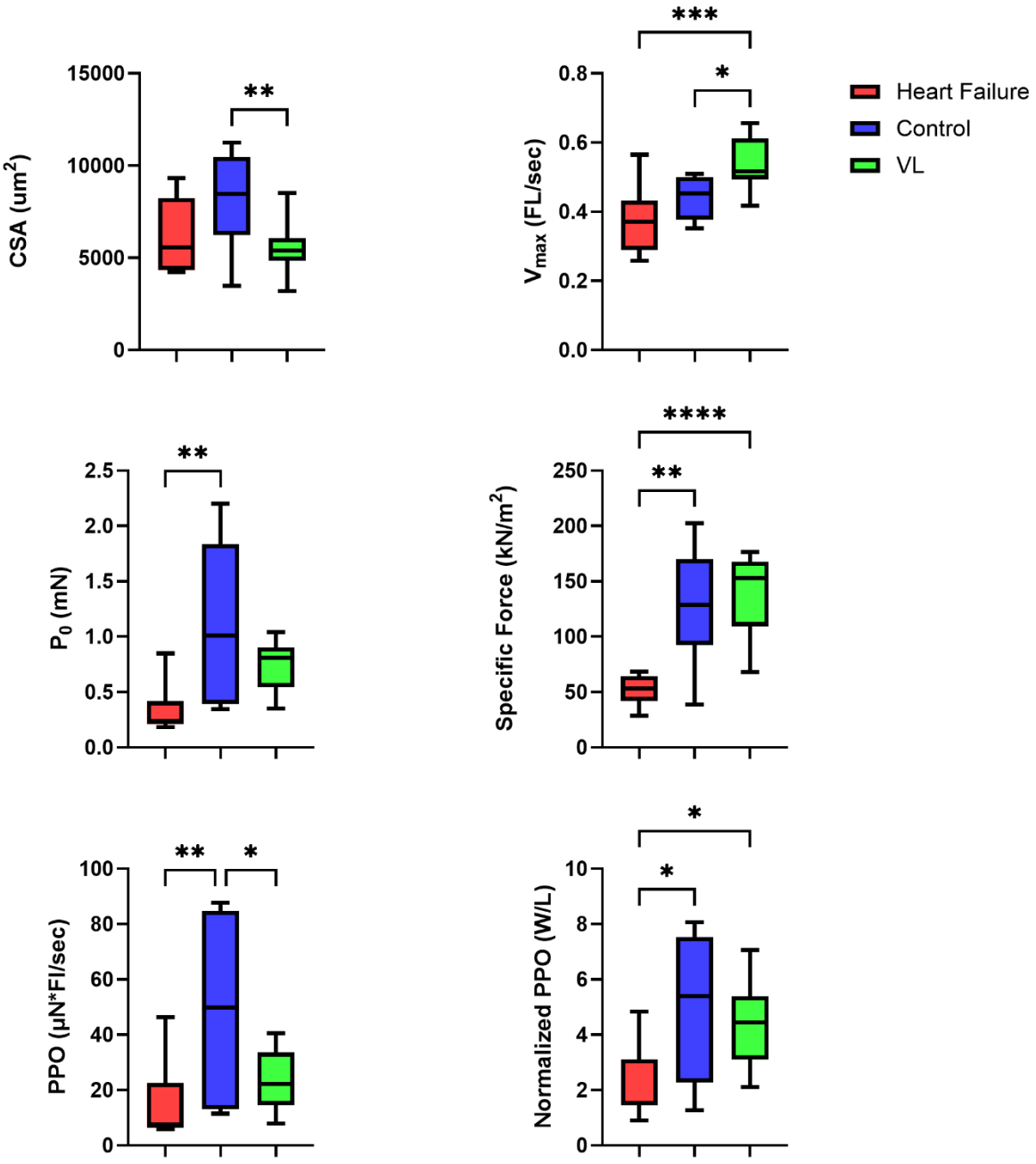

*Figure 5. Box and whiskers plots of contractile parameters. A one-way ANOVA was used for the comparison of contractile characteristics between groups. Vastus lateralis biopsies (VL) were from healthy young and old individuals. * signifies $p < 0.05$. ** signifies $p < 0.01$. *** signifies $p < 0.001$. **** signifies $p < 0.0001$.*

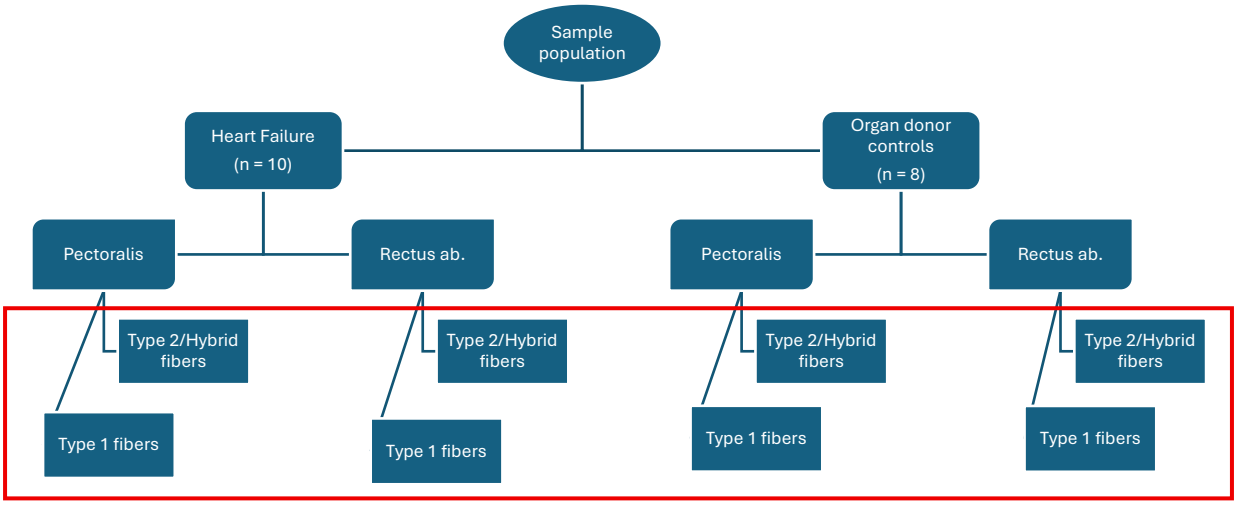

Figure 6. Graphical representation of study design and nesting features. Boxed section represents factors within the repeated measures (biopsy site).

Subject Characteristics		
Variable	**Heart Failure**	**Organ Donor Controls**
Number of subjects	7	8
Age (range)	47.0 (20-63)	55.5 (47-66)
Sex	5 Male/2 Female	5 Male/3 Female
BMI	25.54 ± 4.29	27.97 ± 9.38
Surgery type	4 OHT/3 VAD	-
Frailty	3.4 ± 1.3	-
MELD 3.0	18.83 ± 5.88	-

Table 1. Subject and advanced cardiac intervention specific characteristics. Data presented as mean ± SD unless otherwise specified.

Descriptive Statistics

Dependent variable	Control (n= 8)		Heart failure (n = 7)	
Biopsy site	Type 1 fibers	Type 2 fibers	Type 1 fibers	Type 2 fibers
CSA				
Pec	6396.6 ± 2489.9	11833.3 ± 706.2	5453.0 ± 976.6	7844.4 ± 3969.8
Ab	5174.7 ± 3683.1	7645.8 ± 3131.4	4500.6 ± 531.3	6349.6 ± 2572.9
P_0				
Pec	0.779 ± 0.307	1.332 ± 0.649	0.317 ± 0.129	0.497 ± 0.557
Ab	0.735 ± 0.550	1.150 ± 0.882	0.221 ± 0.144	0.294 ± 0.170
SF				
Pec	125.38 ± 26.33	119.35 ± 60.22	55.67 ± 14.17	54.24 ± 27.35
Ab	138.04 ± 37.74	134.90 ± 58.39	47.71 ± 27.03	48.24 ± 29.17
V_{max}				
Pec	0.385 ± 0.110	0.492 ± 0.108	0.318 ± 0.040	0.429 ± 0.118
Ab	0.363 ± 0.031	0.420 ± 0.065	0.298 ± 0.123	0.376 ± 0.180
PPO				
Pec	20.03 ± 5.16	73.23 ± 31.66	6.34 ± 2.60	30.04 ± 37.86
Ab	18.52 ± 8.80	56.23 ± 44.23	6.54 ± 4.66	11.77 ± 9.40
NP				
Pec	3.023 ± 0.609	6.302 ± 2.904	1.109 ± 0.335	2.962 ± 1.837
Ab	3.195 ± 0.444	5.993 ± 2.730	1.320 ± 0.893	2.288 ± 2.025

Table 2. Descriptive statistics of contractile parameters for SMFs. Data is presented as mean ± SD.

Pooled fiber data				
Variable		**Mean**	**Lower 95% CI**	**Upper 95% CI**
CSA	HF	6967	6298	7637
	Control	8270	7464	9077
P_0	HF	0.414	0.332	0.496
	Control	1.133	0.985	1.280
SF	HF	50.97	46.55	55.38
	Control	137.80	126.30	149.20
V_{max}	HF	0.372	0.338	0.406
	Control	0.442	0.418	0.467
PPO	HF	19.68	12.84	26.52
	Control	50.18	41.76	58.61
NP	HF	2.081	1.694	2.469
	Control	5.579	4.870	6.289

Table 3. Pooled fiber data.

LME Model Structure for Dependent Variables			
Dependent variable	**Repeated measures**	**Covariates**	**Random intercept**
CSA	-	-	+
P_0	-	+	+
SF	-	+	+
V_{max}	+	+	+
PPO	+	+	+
NP	-	+	+

Table 4. Linear mixed effects model structure for each dependent variable. + indicates present in the model structure. - indicates absence.

	Numerator df	Denominator df	F	Sig.
CSA				
Condition	1	38	5.184	0.029
Biopsy	1	38	6.716	0.013
FT	1	38	16.057	<.001
Condition x Biopsy	1	38	0.955	0.335
Condition x FT	1	38	1.463	0.234
Biopsy x FT	1	38	1.339	0.254
3-way interaction	1	38	0.639	0.429
P_0				
Condition	1	9.34	5.44	0.044
Biopsy	1	24.66	5.44	0.028
FT	1	23.82	7.92	0.010
Condition x Biopsy	1	24.37	0.39	0.541
Condition x FT	1	23.79	2.48	0.129
Biopsy x FT	1	23.67	0.03	0.869
3-way interaction	1	23.67	0.13	0.722
Age	1	8.76	0.01	0.932
Sex	1	10.20	0.07	0.804
SF				
Condition	1	9.23	12.43	0.006
Biopsy	1	24.95	0.17	0.683
FT	1	23.92	0.06	0.805
Condition x Biopsy	1	24.62	0.50	0.486
Condition x FT	1	23.89	0.00	0.958
Biopsy x FT	1	23.72	0.38	0.544
3-way interaction	1	23.72	0.06	0.812
Age	1	8.53	0.01	0.935
Sex	1	10.29	0.35	0.567
V_{max}				
Condition	1	8.36	0.92	0.365
Biopsy	1	27.13	1.82	0.189
FT	1	22.95	7.06	0.014
Condition x Biopsy	1	26.41	0.04	0.839
Condition x FT	1	23.27	0.10	0.753
Biopsy x FT	1	23.65	0.23	0.635
3-way interaction	1	24.31	0.00	0.947
Age	1	7.00	2.49	0.158
Sex	1	16.43	1.33	0.265
PPO				
Condition	1	4.66	5.46	0.071
Biopsy	1	21.78	2.59	0.122

FT	1	15.62	16.37	<.001
Condition x Biopsy	1	19.73	0.02	0.898
Condition x FT	1	16.18	3.68	0.073
Biopsy x FT	1	16.47	0.63	0.439
3-way interaction	1	17.07	0.11	0.750
Age	1	3.70	0.77	0.434
Sex	1	8.87	1.17	0.308
NP				
Condition	1	6.86	5.47	0.053
Biopsy	1	21.14	1.58	0.222
FT	1	17.31	22.06	<.001
Condition x Biopsy	1	19.35	0.03	0.858
Condition x FT	1	17.79	2.50	0.132
Biopsy x FT	1	17.78	0.01	0.938
3-way interaction	1	18.05	0.48	0.499
Age	1	5.81	0.32	0.591
Sex	1	9.82	1.03	0.335

Table 5. Main and interactions effects from LME models for each dependent variable. FT = fiber type, SF = specific force, NP = normalized power.

Correlation of clinical data with global fiber contractile data						
	Contractile variable					
Clinical variable	**CSA**	**P_0**	**SF**	**V_{max}**	**PPO**	**NP**
Age	-0.240	0.107	0.353	0.496	0.036	0.263
Frailty	0.655	0.225	-0.094	-0.019	0.505	0.112
Duration	0.462	0.234	-0.098	-0.059	0.414	-0.099
Pec area	0.771	0.829	0.140	-0.070	0.900	0.404
BNP	-0.467	0.086	0.409	0.744	0.200	0.596

Table 6. Clinical correlations and global SMF contractile function.

Correlation of clinical data with Type 1 fiber contractile data						
	Contractile variable					
Clinical variable	**CSA**	**P_0**	**SF**	**V_{max}**	**PPO**	**NP**
Age	-0.286	-0.185	0.034	0.548	-0.154	0.012
Frailty	0.430	0.543	0.225	-0.711	0.243	-0.187
Duration	0.559	0.436	0.181	0.218	0.369	0.200
Pec area	-0.046	0.037	0.022	-0.605	0.0812	0.038
BNP	-0.481	0.350	0.622	0.107	0.387	0.533

Table 7. Clinical correlations and Type 1 SMF contractile function.

Correlation of clinical data with Type 2 fiber contractile data						
	Contractile variable					
Clinical variable	**CSA**	**P_0**	**SF**	**V_{max}**	**PPO**	**NP**
Age	-0.332	0.071	0.402	0.364	0.372	0.334
Frailty	0.655	0.281	0.112	-0.075	0.281	0.056
Duration	0.680	0.396	-0.054	-0.090	-0.056	-0.077
Pec area	**0.932***	**0.943***	0.066	-0.298	0.8850	0.267
BNP	-0.521	-0.029	0.440	0.769	0.535	0.646

*Table 8. Clinical correlations and Type 2 SMF contractile function. Bold indicates statistically significant. * signifies ($p < 0.05$).*

Chapter 3. Morphohistological changes of skeletal muscle in late-stage heart failure

Introduction

Heart failure is a chronic condition often associated with skeletal muscle impairments. In fact, loss of muscle mass and function in heart failure is significantly correlated to patient symptoms and prognosis. [1–5] Yet, direct assessment of skeletal muscle mass and function is not common in the clinical setting. However, determining patient muscle mass is relatively available, with methods such as CT imaging- to obtain a skeletal muscle index- as well as dual-energy X-ray absorptiometry and bioelectrical impedance being possible.[6] In fact, patients undergoing assessment for advanced cardiac intervention (i.e. transplant or VAD placement) routinely receive thoracic CT imaging, a procedure that has already been repurposed and used to assess length of stay and survivability in transplant recipients.[7,8] Nevertheless, more research is necessary to connect these observed changes and the histological alterations occurring within the muscle itself.

Whole muscle mass and function are products of the individual fibers making them up, in addition to the composition of the muscle (i.e. contractile and extracellular tissues). Decrements in muscle mass and function can be the result of any impairment in these characteristics. For example, decreases in fiber CSA will decrease whole muscle size and have been previously demonstrated to occur in the heart failure population.[9] Moreover, changes to the fiber type makeup of the whole muscle can influence skeletal muscle function. Heart failure has been shown to cause a fiber type shift from oxidative to more glycolytic fiber types, and this fiber type shift can often be identified by the MHC content. This shift toward glycolytic fiber types would predict an increased fatiguability, which is often seen in the heart failure population. However, this finding is not ubiquitous, with a scoping review suggesting only ~60% of studies showing a slow to fast fiber transition.[10] Finally, changes to extracellular composition of whole muscle may directly influence function. Fibrosis of muscle, for example, can impair typical force transduction from sarcomere to tendon. In fact, fibrosis of skeletal muscle has been demonstrated in many conditions with

concomitant muscle dysfunction, such as injury,[11] genetic disorders,[12] chronic diseases,[13] and even in some models of heart failure.[14]

While histological changes to skeletal muscle are well known to affect muscle mass and function, few studies have investigated these changes in human models of heart failure. Furthermore, of the studies that involved human subjects, most histological assessments have been performed on the lower limb, with >90% of biopsies coming from the vastus lateralis.[10] While both histochemical and functional assessment of vastus lateralis biopsies have correlated with key clinical outcomes,[15–18] little work has been done in the upper body. Heart failure has been shown to cause a reduction in upper limb muscle mass and function and correlate with patient rehospitalization and mortality. [19–21] As such, it is imperative to also investigate histological changes to upper body musculature in the setting of heart failure.

In addition to changes of the histological composition of muscle, a newer type of analysis has begun to be utilized to aid in addressing changes in skeletal muscle quality- morphometric analysis. It has been proposed that in chronic diseases which induce skeletal muscle myopathy that small microanatomic changes to skeletal muscle may precede the more apparent changes, such as fiber atrophy or extracellular matrix changes.[22,23] Morphometric analysis has been used to appropriately classify muscle biopsies from control, moderate peripheral artery disease (PAD), and severe PAD subjects.[24] Furthermore, there is evidence that these minute morphological changes are fiber type specific,[25] similar to what is seen in heart failure fiber type shifts. As such, this tool needs to be investigated in the setting of heart failure-induced myopathy.

Therefore, in order to address the gaps in the literature, in this study we conducted a comprehensive morphohistological analysis of two functionally distinct skeletal muscles in late-stage heart failure patients. We assessed differences in CSA, morphology, and myonuclear counts

on the global and fiber type levels, as well as determined the extent of fibrosis compared to non-heart failure controls.

Methods

Muscle biopsy and tissue processing

All experiments were reviewed and approved by the University of Wisconsin-Madison Institutional Review Board. Subjects were recruited from clinical patients at the University of Wisconsin Hospital (HF; n = 10) or from organ donors at the University of Kentucky (non-HF controls [CON]; n = 8). Informed consent was obtained for all clinical subjects. Inclusion criteria included the following: patients with advanced heart failure (ACC/AHA Stage D) that required implantation of a VAD or OHT.

During the respective cardiothoracic surgery, roughly 200-300 mg of the sternal pectoralis major and proximal rectus abdominis were collected by the surgeon. The sample was briefly stored in chilled relax solution[26] until it could be returned to the lab and processed further. The biopsy was cleaned of any visible adipose and connective tissue as well as any damage secondary to acquisition (i.e. cautery burns). Sample was patted dry and oriented under guidance of a dissecting microscope. It was then covered in OCT, which was allowed to penetrate into the tissue for ~30 minutes.[27] Finally, the OCT covered biopsy was frozen utilizing the liquid nitrogen cooled isopentane method. The frozen samples were stored at -80°C until tissue slicing. On the day of the experiment, the frozen sample was allowed to acclimate to the cryostat (HM505E, Microm), which was maintained at -25°C. At least two serial sections were adhered to each microscope slide. Cross-sectional thicknesses of 6 and 10 µm were obtained for use in subsequent histological protocols. Slides were allowed to dry at room temperature for 1) 20 minutes and then stored in a slide box at -80°C for future staining, or 2) 60 minutes for immediate use. Non-heart failure control tissues were

obtained during organ donation and immediately flash frozen. Samples were then next-day transported from the University of Kentucky to the University of Wisconsin- Madison on dry ice. Upon arrival, samples were allowed to thaw in chilled relax buffer and thereafter treated the same as HF biopsies.

MHC isoform expression, morphology, and nuclei

For fiber type determination and CSA analysis, immunofluorescence was used as previously described by Murach et al.[28] Briefly, 6 µm cross-sections were removed from -80°C storage and allowed to equilibrate to room temperature. The slides were initially washed 2 x 5 minutes in PBS. Afterwards, the primary antibody cocktail (PBST-B: 0.1% Tween20, 2% BSA, 1x PBS, and antibodies) was applied and the slides were placed in a dark humidity box for 1 hour. The slides were rinsed 3 x 5 minutes in PBS, followed by the addition of a secondary antibody cocktail (same concentrations as primary cocktail) for 1 hour in a humidity box. Lastly, the slides were rinsed one last time 3x 5 minutes in PBS and the coverslip was mounted using Aqua-Mount (Epredia). The following antibodies were used in the primary antibody cocktail (see Table 1 for more details): anti-MHC1 [BA-D5], anti-MHC2a [SC-71], anti-MHC2x [6H-1], and anti-laminin gamma 1 [2E8] (DSHB). The following secondary antibodies conjugated to unique, non-overlapping fluorophores were used: Goat α-Mouse IgG2b [Fluor 647], Goat α-Mouse IgG1 [Fluor 488], Goat α-Mouse IgM [Fluor 555], Goat α-Mouse IgG2a [Fluor 350], respectively (Invitrogen). All primary antibodies were supernatants and diluted down to a final concentration of 1-4 µg/mL in the primary cocktail. The secondary antibodies were diluted down to concentrations as recommended by the manufacturer in the secondary antibody cocktail. The fluorescent nuclear stain DAPI (Tocris) was used for nuclear staining at a final concentration of 300 nM for ~2 minutes. However, due to potential spectral overlap of DAPI with Fluor 350, DAPI and MHC primary antibodies were applied to the serial section for nuclear localization. Images were taken utilizing a 10x objective on the SoRa/W1 Spinning Disk

Microscope. At least 3 images with a FOV clear of any apparent disturbances were acquired. Image preprocessing was completed using the freely available software Fiji [29] and final processing was completed with Myovision Basic (v 1.0, University of Kentucky).[28,30] Of note, a fiber was considered Type 2 if it stained positive for MHC 2A, 2X, or 2A/2X, as suggested by Murach and colleagues. Finally, nuclear counts, both peripheral and central, were determined by manually counting the number of nuclei directly surrounding the colocalized MHC primary antibody. Average nuclei was determined by dividing the sum of all nuclei in sample by the number of fibers. Average centronuclei was similarly determined by dividing the sum of all centronuclei by the total number of fibers. The percentage of centronucleated fibers was calculated as the number of fibers with at least one centronuclei divided by the total number of fibers. Finally, in order to account for CSA differences between fiber types, the normalized average nuclei was calculated by dividing the average nuclei by the mean CSA in mm^2 of the given fiber type.

In addition to fiber type determination, morphology of all the fibers (global) and individual fiber types was determined through three main parameters: 1) cross-sectional area (CSA), 2) roundness, and 3) convexity. To determine the roundness of the fibers, first the equivalent diameter was determined. The equivalent diameter is the diameter of a circle with the same area as the CSA of the fiber. Equation 1 demonstrates the calculation of the equivalent diameter.

$$\text{Equation 1}: \ \text{Equivalent diamter} = \sqrt{\frac{(4 \times \text{actual fiber area})}{\pi}}$$

Then, roundness was calculated utilizing the following equation:

$$\text{Equation 2}: \ \text{Roundness} = \frac{(\text{Equivalent diameter} \times \pi)}{\text{actual fiber perimeter}},$$

where the actual perimeter of the fiber is directly measured in the image processing software. Furthermore, the convexity measure is given by the Myovision software and defined by equation 3, listed below.

$$\text{Equation 3}: \ \text{Convexity} = \frac{\text{actual fiber area}}{\text{area of smallest surrounding convex hull}}$$

Fibrous infiltration

Fibrous content was assessed through collagen deposition (types I and III) staining with picrosirius red (PSR) as previously described by Hildyard et al.[31] First, previously cut 10 μm thick tissue cross-sections were removed from storage and allowed to equilibrate to room temperature. The samples were placed in xylene for 20 minutes, followed by rehydration through graded alcohol baths starting at 100% EtOH and subsequently moving down to 90%, 80%, 70%, and DH_2O each for 5 minutes. Next the slides were immersed in PSR stain for 45 minutes. Afterwards, the slides were washed briefly in DH_2O and differentiated in 0.5% acetic acid for 2 minutes. Finally, the samples were dehydrated in graded alcohol baths, cleared in xylene for 1 hour, and cover slipped with Permount (Fisher Scientific). Images were taken utilizing a 20x objective on the SoRa/W1 Spinning Disk Microscope using the red fluorescence channel. At least 3 images with a FOV clear of any apparent disturbances were acquired. Image analysis was conducted as previously described using the freely available image analysis software Fiji.[32] Total fibrous area was determined by thresholding the image (taking into account background fluorescence), binarizing the image, and then measuring total stained area. Percent fibrous area was determined by dividing the area stained by PSR by the total area.

Clinical correlations

In order to determine if changes in skeletal muscle quality from HF patients varied along with other aspects of heart failure symptoms, we correlated histological and morphological data with clinical data. Clinical data was acquired through a query of the HF patients' electronic medical records. The following is a non-inclusive list of relevant clinical information gathered: BNP, duration of heart failure, frailty status/score (measured using the Fried Frailty Phenotype), and most recent chest CT prior to cardiac intervention. Duration of heart failure was determined as the difference (in months) from the first reported date of diagnosis to date of cardiac intervention. From the chest CT, the total area of pectoralis and the minimum, maximum, and mean attenuation (HU) were extracted. Throughout the query process, patient confidentiality was maintained, and all data handling adhered to HIPAA guidelines.

Statistical analysis

Analysis of pooled fibers was performed using GraphPad Prism (version 11.0 for Windows). Normality of data was verified with a Shapiro-Wilk test. Differences between the two groups were tested using an unpaired T-tests of the mean of means. For a more robust analysis, linear mixed-effects (LME) modeling was used to compare the effects of heart failure on measures of skeletal muscle quality. We analyzed each outcome using a linear mixed model with condition (HF vs CON), biopsy site (pec vs ab), and fiber type (Type 1 vs Type 2) as fixed effects, including all interactions. Subject was included as a random intercept to account for within-subject dependence. Repeated observations across biopsy site and fiber type within subject were modeled using a compound symmetrical covariance matrix. Models were fit in SPSS (V31.0, IBM) using restricted maximum likelihood (REML) estimation and Satterthwaite approximation for denominator degrees of freedom. Statistical significance was assessed using Type III tests of fixed effects and estimated marginal means were calculated to aid in interpretation of significant main effects and interactions. Because

model stability differed across dependent variables, convergence and fit diagnostics were evaluated for each model. If nonconvergence occurred, a simplified model that removed the repeated covariance structure was used. Final reported models were the best-fitting converged models, as judged by model estimability and AIC criterion, while retaining biologically relevant fixed effects and interactions.

Fiber type prevalence was determined by dividing the number of fibers of a given fiber type with the total fiber count within a sample. In order to determine the total contribution of a given fiber type to the whole muscle, fiber type contribution was determined by multiplying the prevalence of a given fiber type with the average CSA of that same type within each sample. Comparison of prevalence and contribution between conditions was determined by Fishers Exact Test of the mean of means. Finally, correlations of morphohistological data to clinical data were performed using a Pearson or Spearman correlation, as dictated by the normality and type of data (e.g. ordinal vs continuous). Separate correlations were analyzed between morphohistological parameters for CT pec area and CT attenuation that included both biopsy sites and pec biopsy sites only (pec only). All correlational analyses were performed using GraphPad Prism A p-value <0.05 was considered statistically significant.

Results

Heart failure induced skeletal fiber atrophy and fiber type changes

Subject characteristics and baseline data are presented in Tables 2 and 3, respectively. Skeletal muscle fiber cross-sectional area was determined by immunofluorescence. A representative image of MHC immunostaining is presented in Figure 1. Pooling all fibers irrespective of biopsy site or fiber type showed a significantly reduced CSA in HF compared to control ($p <$

0.0001). However, while this statistical approach has been utilized historically, this analysis does not account for non-independence of measurements or individual differences. Therefore, in order to appropriately assess CSA, we performed linear mixed effects modeling (see Table 4 for model structure). There was a significant main effect for both condition and fiber type ($p = 0.015$ and <0.001, respectively). Pairwise comparisons demonstrated a significantly reduced CSA in the HF group compared to CON, and as expected, a significantly smaller CSA in Type 1 fibers compared to Type 2 fibers. No other main effect or interaction was significant. However, of note, there was a trend-level effect for the two-way interaction of condition by fiber type ($p = 0.051$) and therefore an exploratory simple effects comparison was conducted. Within Type 2 fibers, there was an estimated mean difference of 3321.14 μm^2 (CON-HF; $p = 0.005$) whereas within Type 1 fibers there was an estimated mean difference of 2072.64 μm^2 ($p = 0.06$). These results demonstrate that late-stage heart failure leads to significant skeletal muscle fiber atrophy and that there may be disparate effects of atrophy across skeletal muscle fiber types.

In addition to CSA, we assessed the prevalence of each fiber type utilizing a Fisher's Exact Test. There was a significantly different frequency of observed fiber types (HF) compared to expected (CON) ($p < 0.001$). Muscle biopsies from heart failure patients demonstrated a significantly reduced prevalence of Type 1 fibers (34.0% vs 54.8%) and a higher prevalence of Type 2 fibers (60.8% vs 41.6%) compared to control (Figure 2). Furthermore, in order to account for dissimilar CSA between fiber types, we also analyzed the total area contribution of each fiber type (Figure 3). A Fisher's Exact Test showed a significant difference in the observed proportions compared to expected (Type 1: HF- 34.2% CON- 49.1%; Type 2: HF- 60.8% CON- 48.6%). This data demonstrates that the area contribution from Type 1 fibers in heart failure is significantly diminished compared to control subjects. Moreover, this difference in relative proportion consists of an increased area contribution from Type 2 fibers.

Morphological fiber changes in heart failure

Besides fiber size, we assessed differences in skeletal muscle quality through morphometric analysis to quantify differences of fiber shape in heart failure subjects compared to control. Specifically, we used linear mixed effects modeling to investigate differences in roundness and convexity within biopsy site and fiber types (Table 4 for model structure). There was a significant main effect of condition for both morphological measures (roundness: $p = 0.028$, convexity: $p = 0.026$). Pairwise comparisons showed a reduced roundness but increased convexity of myofibers in heart failure subjects relative to control. No other main effect or interaction was significant; however, there was a trend-level effect of fiber type for roundness ($p = 0.074$), with pairwise comparisons suggesting rounder Type 1 fibers compared to Type 2 (estimated mean difference: 0.012 [Type 1- Type 2]). Overall, these results suggest that heart failure does indeed lead to changes in fiber shape, namely less circular, more convex fibers and that these changes may be fiber type specific.

Peripheral and centrally located nuclei

Figure 4 shows an example of nuclear staining with MyHC colocalization. Similarly to fiber CSA, we analyzed myonuclear counts with linear mixed effects modeling (Table 4 for model structure). There were no significant main effects or interactions for peripherally or centrally located nuclei parameters. However, there was a trend-level effect on the two-way interaction condition by biopsy for the normalized average myonuclei count. Therefore, we performed an exploratory simple effects comparison and saw the mean difference in the pec biopsies between the two groups was -593.51 (CON-HF; SE= 222.02, $p = 0.014$).

Fibrous content of skeletal muscle

Skeletal muscle fibrous content was approximated by PSR staining of collagen types I and III (Figure 5). There was no significance for main effects of condition or biopsy site, nor any significant interaction terms between the two groups.

Clinical correlations

Correlations between clinically relevant data and global, Type 1, and Type 2 morphohistological parameters are detailed in Table 5. Analysis of global parameters revealed significant positive relationships between CSA and duration, and CT pec area ($p = 0.028$ and <0.001, respectively). Moreover, there was a significant negative correlation between frailty and global roundness ($p = 0.036$). Furthermore, this relationship remained significant when separating by fiber type (Type 1: $p = 0.040$ and Type 2: $p = 0.026$).

Investigating correlations by fiber type demonstrated significant positive relationships for Type 1 CSA between duration of heart failure and CT pec area ($p = 0.020$ and 0.048). Similarly, Type 2 CSA was positively correlated with CT pec area ($p = 0.007$) as well as CT area of pec only ($p = 0.033$). Additionally, CT pec area was also positively correlated with Type 2 area contribution ($p = 0.012$). In addition to CT pec area, the average attenuation of the pec was positively correlated with Type 2 contribution ($p = 0.049$) with an inverse trend-level effect seen for Type 1 contribution ($p = 0.072$).

Finally, and as expected, the prevalence of Type 1 fibers positively correlated with age and was mirrored by a negative correlation with Type 2 prevalence ($p = 0.018$ and 0.019). Similarly, these relationships were reflected by fiber type area contribution (Type 1: $p = 0.007$ and Type 2: $p = 0.008$). There were no other significant correlations between clinical measures and morphohistological parameters.

In addition to morphohistological parameters, we utilized correlational analysis to assess the relationships between clinically relevant data and myonuclear and fibrous content parameters (Table 6). We found a significantly positive relationship between CT pec area and global average myonuclei and fibrous index ($p = 0.023$ and 0.048). Moreover, there were significant negative correlations for normalized average myonuclei between duration of heart failure and CT pec area ($p = 0.0013$ and 0.034). When separating myonuclear data by fiber type we found significant relationships for BNP and Type 1 average myonuclei and its cross-sectional area normalized counterpart ($p = 0.047$ and 0.016). Furthermore, Type 2 fiber average myonuclei positively correlated with both duration and CT attenuation ($p = 0.017$ and 0.018). Similarly, CT attenuation also was found to have a positive relationship with average centronuclei and percentage of fibers centronucleated ($p = 0.011$ and 0.028). Finally, there was a significant negative relationship between frailty and Type 2 fibers normalized average myonuclei ($p = 0.046$).

Discussion

The objective of this study was to conduct a comprehensive morphohistological assessment of skeletal muscle in the setting of late-stage heart failure. Herein we have demonstrated that heart failure causes significant atrophy of both Type 1 (~36%) and Type 2 (~41%) fibers. These decrements in CSA were coupled with a fiber type shift from oxidative Type 1 fibers to more glycolytic Type 2 fibers and this change is also reflected in the relative area contribution from each fiber type. Additionally, we have shown that in conjunction to fiber size, heart failure impacts the morphological features of myofibers. Specifically, we saw a reduction in fiber roundness and increase in the convexity of heart failure subjects compared to control. Finally, there were no significant differences seen between biopsy sites. These findings suggest that heart failure-induced

myopathy is driven not only by atrophogenic processes, but also extensive whole-muscle fiber type shifts and morphological changes.

We analyzed changes to fiber size both by the historically utilized pooled fiber analysis as well as the more robust LME modeling warranted by our repeated measures and within-subjects study design. Both analyses were in agreement, demonstrating that CSA was significantly attenuated in the HF group compared to CON. Additionally, as we expected to see, there was a main effect for fiber type on CSA, given that Type 2 fibers tend to be larger than Type 1 in humans. [33] Despite these absolute differences, we did observe a slightly larger relative decrease in the CSA of Type 2 fibers compared to Type 1 fibers, which may explain the noted trend-level effect for condition by fiber type. Despite that trend-level two-way interaction, the whole-muscle area contribution was dominated by Type 2 fibers in the heart failure subjects (60.8% vs Type 1: 34.3%) whereas the control subjects demonstrated a nearly 50-50 split. This significant difference in area contribution appears to be driven by the difference in prevalence of each fiber type between groups. Our data demonstrates a significant fiber type shift from oxidative Type 1 fibers (34.0%) to glycolytic Type 2 fibers (60.8%) in the setting of heart failure, consistent with that of previous studies.[9,10,14,34] Taken together, these findings suggest that heart failure induces a widespread atrophic response in skeletal muscle, albeit with a greater absolute loss of Type 2 size. Nonetheless, the fiber type shift from oxidative to glycolytic dominated fibers results in smaller, more fatigue prone whole muscle. These changes to fiber size and type may help to further explain the symptoms of heart failure, such as fatigue, shortness of breath, and exercise intolerance. However, while this study has demonstrated the alterations occurring in skeletal muscle, we have yet to elucidate the mechanisms driving these changes. Therefore, it is vital that future research continue to investigate this phenomenon by addressing systems upstream of the myofibers,

namely motor units and α-motor neurons, as these have been demonstrated affect MHC isoform expression.[33,35,36]

Fiber morphology, or the shape of myofibers, has been utilized to try and quantify qualitative changes to skeletal muscle fibers, irrespective of changes to size.[24,25,34] These changes to morphology may reflect early maladaptations to skeletal muscle prior to gross atrophy in myopathic conditions. In fact, morphometric analysis has been previously used to appropriately classify muscle biopsies from individuals with varying degrees of PAD and healthy controls.[24] In the current study, we assessed the morphological parameters roundness and solidity (also called convexity). Our data shows that heart failure results in a significant change to fiber morphology, specifically a reduction in roundness and increase in solidity leading to an overall less polygonal and more irregularly shaped convex fiber. Similarly to Larsen et al. in heart failure subjects and Koutakis and colleagues in PAD patients, we see that myopathy leads to less rounded fibers.[25,34] However, in contrast to PAD patients, we observed an increase in myofiber solidity. This difference in solidity may be a product of different measurement algorithms or clinical populations (heart failure vs PAD). Roundness and solidity measures are sensitive to partial pixel counting (i.e. subpixel measurement), and different image analysis programs may not have this feature on by default or measure subpixels differently (e.g. sub-pixel processing, weighted intensity, etc). As such, depending on the image processing software and algorithm being used, there can be summative divergent values that lead to discrepancies between studies. Moreover, regarding patient population, we initially hypothesized that fiber morphology would parallel that of the PAD patients as the pathophysiological hallmark of peripheral artery disease (reduced blood flow/ischemia) is similar to the clinical consequence of late-stage heart failure. However, heart failure is a systemic condition with a complex neurohormonal milieu that appears to differentially affect skeletal muscle compared to the more localized effects of PAD. Notwithstanding, this study

demonstrates that morphological changes do indeed occur in the setting of heart failure and helps to build a foundation for future research interested in utilizing morphometric analysis to aid heart failure prognostication.

In addition to fiber size and shape, we assessed peripheral and central nuclear counts in the muscle cross-sections. In contrast to our hypothesis, we found no significant differences in the average number of nuclei associated with a myofiber, the number of centronuclei, the percentage of fibers with centronuclei, or the cross-sectional area normalized average nuclei per myofiber (see Table 7 for F-statistics). It has been established that muscle fibers regenerating from damage demonstrate a centrally located nuclear chain that can persist for months following the initial insult.[37] Because heart failure produces such a robust atrophic response in skeletal muscle, we had hypothesized that there would be an increased number of centronuclei present in the skeletal muscle of heart failure patients. Moreover, we expected to see a larger proportion of fibers with the presence of centronuclei. However, our data does not suggest this to be the case. Nevertheless, the lack of a difference in normalized average nuclear count suggests that heart failure-induced skeletal muscle atrophy may coincide in parallel with myonuclear apoptosis. Indeed, this has been demonstrated previously in heart failure patients, especially those with significantly reduced exercise capacity.[38,39] However, this study did not directly measure markers of nuclear apoptosis and therefore should be interpreted cautiously. Finally, we visualized nuclei via the fluorescent dye DAPI, which binds to AT-rich regions of DNA, and as such is non-specific to myonuclei. While myonuclei specific antibodies do exist, we chose to use DAPI and therefore the possibility of nuclear staining from non-myofiber nuclei does exist.[40]

Fibrosis of skeletal muscle has been associated with damage, disease, and disuse.[11–13,41,42] Therefore, we aimed to compare the fibrous content of skeletal muscle in heart failure patients compared to control. We found no significant main effects or interactions utilizing linear mixed

effect modeling, suggesting there is no difference in the collagen content between heart failure and control subjects. Previous research in animal models shows equivocal results for heart failure-induced fibrosis of skeletal muscle.[14,43] Likewise, human studies have demonstrated various results.[14,44] However, these differences in fibrous content results may be a product of patient selection. Filippatos et al. demonstrated that individuals diagnosed with cardiac cachexia concurrent with heart failure had significantly more fibrosis of skeletal muscle compared to non-cachexic counterparts.[44] Overall, these findings suggest that heart failure itself may not lead to skeletal muscle fibrosis, however conditions associated with it may in fact be driving the collagen deposition and exacerbating impairments in skeletal muscle quality.

Currently, assessment of skeletal muscle quantity and quality is sparse in the clinical setting. However, the inclusion of muscle biopsies or additional imaging techniques (i.e. DEXA, MRI, or CT) is not always feasible. As such, it is vital that we uncover relationships between research-based metrics of skeletal muscle quality and those used in routine care of heart failure. Therefore, we conducted correlational analysis of morphohistological, myonuclear, and fibrotic parameters with common clinical heart failure variables. We found significant positive correlations between pec area calculated from thoracic CT and global, Type 1, and Type 2 fiber CSA (Figure 6 middle insert) and this relationship remained for Type 2 fibers when only assessing the pec biopsy site. Moreover, there was a positive relationship between Type 2 whole-muscle contribution and CT average attenuation, with an inverse trend-level effect seen in Type 1 contribution (Figure 6 bottom insert). These findings suggest that repurposing of the thoracic CT often used prior to advanced cardiac intervention may provide valuable insight into fiber type specific myofiber size and contribution to whole-muscle area and therefore help to optimize care and prognosticate recovery.[45,46] Additionally, we saw significant negative correlations between frailty and global, Type 1, and Type 2 fiber roundness, suggesting that morphological features of muscle fibers is able to

capture the complex clinical conditions such as frailty (Figure 6 top insert). Finally, we saw the expected inverse correlations with CT pec area between Type 1 fiber prevalence and contribution versus Type 2 fiber prevalence and contribution. Previous research has demonstrated that during aging there is a preferential atrophy and/or loss of Type 2 relative to Type 1 fibers. [47–49] We found positive correlations for age and Type 1 and an appropriate opposite correlation in Type 2 fibers with age. Therefore, despite the observed fiber type shift from Type 1 to Type 2 seen in heart failure, within our heart failure population, we can still observe the effects of aging. Because of these conflicting effects on fiber type distribution, it can be difficult to ascertain the effects of heart failure on an aged population; however, we have demonstrated that at least in the critically ill, skeletal muscle fiber type shifts follow that of a heart failure phenotype.

In conclusion, herein we have demonstrated that heart failure results in not only significant widespread atrophy but also morphological alterations to myofibers from two functionally diverse skeletal muscles. These maladaptations to skeletal muscle appear to be fiber type independent, yet we observed a significant fiber type shift from Type 1 to Type 2 fibers. Moreover, this muscle wasting and fiber type shift correlate with clinical parameters already acquired during routine care and therefore indicate the ability to indirectly assess skeletal muscle quantity and quality in this population aiding in improving personalized care plans and better prognostic ability.

References

1. Anker, S. D. *et al.* Wasting as independent risk factor for mortality in chronic heart failure. *The Lancet* **349**, 1050–1053 (1997).

2. Coats, A. J. S. The “Muscle Hypothesis” of Chronic Heart Failure. *J. Mol. Cell. Cardiol.* **28**, 2255–2262 (1996).

3. Coats, A. J. S., Clark, A. L., Piepoli, M., Volterrani, M. & Poole-Wilson, P. A. Symptoms and quality of life in heart failure: the muscle hypothesis. *Br. Heart J.* **72**, S36 (1994).

4. Aimo, A. *et al.* The ergoreflex: how the skeletal muscle modulates ventilation and cardiovascular function in health and disease. *Eur. J. Heart Fail.* **23**, 1458–1467 (2021).

5. Harrington, D. *et al.* Skeletal muscle function and its relation to exercise tolerance in chronic heart failure. *J. Am. Coll. Cardiol.* **30**, 1758–1764 (1997).

6. Cruz-Jentoft, A. J. *et al.* Sarcopenia: Revised European consensus on definition and diagnosis. *Age and Ageing* vol. 48 16–31 Preprint at https://doi.org/10.1093/ageing/afy169 (2019).

7. Kuchnia, A. J. *et al.* Computed tomography measured tissue density of pectoral muscle and liver predicts outcomes in heart transplant recipients. *JCSM Rapid Commun.* **5**, 171–181 (2022).

8. Khoshbin, E. & Schueler, S. Pre-transplant ventricular assist device explant. *Ann. Cardiothorac. Surg.* **7**, 160–168 (2018).

9. Mancini, D. *et al.* Contribution of Intrinsic Skeletal Muscle Changes to 31P NMR Skeletal Muscle Metabolic Abnormalities in Patients With Chronic Heart Failure. *Circulation* 1338–1346 (1989).

10. Kaneguchi, A., Sakitani, N. & Umehara, T. Histological changes in skeletal muscle induced by heart failure in human patients and animal models: A scoping review. *Acta Histochem.* **126**, 152210 (2024).

11. Davies, M. R. *et al.* Rat rotator cuff muscle responds differently from hindlimb muscle to a combined tendon-nerve injury. *Journal of Orthopaedic Research* **33**, 1046–1053 (2015).

12. Smith, L. R. & Barton, E. R. Regulation of fibrosis in muscular dystrophy. *Matrix Biology* vols 68–69 602–615 Preprint at https://doi.org/10.1016/j.matbio.2018.01.014 (2018).

13. Abramowitz, M. K. *et al.* Skeletal muscle fibrosis is associated with decreased muscle inflammation and weakness in patients with chronic kidney disease. *Am. J. Physiol. Renal Physiol.* **315**, F1658–F1669 (2018).

14. Saw, E. L. *et al.* Skeletal muscle phenotypic switching in heart failure with preserved ejection fraction. *Front. Cardiovasc. Med.* **9**, (2022).

15. Bassey, E. J. *et al*. *Leg Extensor Power and Functional Performance in Very Old Men and Women*. *Clinical Science* vol. 82 http://portlandpress.com/clinsci/article-pdf/82/3/321/463359/cs0820321.pdf (1992).

16. Jeon, Y., Lee, H., Kim, D.-Y., Lim, J.-Y. & Choi, S.-J. Hand Grip Strength and Its Relation to Thigh-derived Single Muscle Fiber Contractile Properties. *Exercise Science* **27**, 280–288 (2018).

17. Jeon, Y.-N. *et al*. Contractile Properties of Single Muscle Fiber and Their Relations to Whole Muscle Strength in Korean Young Male. *Exercise Science* **27**, 23–31 (2018).

18. Wang, Z. M. *et al*. Relationship of physical function to single muscle fiber contractility in older adults: Effects of resistance training with and without caloric restriction. *Journals of Gerontology - Series A Biological Sciences and Medical Sciences* **74**, 412–419 (2019).

19. Konishi, M. *et al*. Prognostic impact of upper and lower extremity muscle mass in heart failure. *ESC Heart Fail*. **10**, 732–737 (2023).

20. Wang, Y. *et al*. Handgrip strength and the prognosis of patients with heart failure: A meta-analysis. *Clin. Cardiol*. **46**, 1173–1184 (2023).

21. Umehara, T. *et al*. Reduced upper and lower limb muscle strengths without reduced skeletal muscle in elderly patients with heart failure. *Journal of Rural Medicine* **18**, 8–14 (2023).

22. Pipinos, I. I. *et al*. Chronically ischemic mouse skeletal muscle exhibits myopathy in association with mitochondrial dysfunction and oxidative damage. *Am J Physiol Regul Integr Comp Physiol* **295**, 290–296 (2008).

23. Pipinos, I. I. *et al*. The Myopathy of Peripheral Arterial Occlusive Disease: Part 1. Functional and Histomorphological Changes and Evidence for Mitochondrial Dysfunction. *Vasc. Endovascular Surg*. **41**, 481–489 (2008).

24. Cluff, K. *et al*. Morphometric analysis of gastrocnemius muscle biopsies from patients with peripheral arterial disease: objective grading of muscle degeneration. *Am J Physiol Regul Integr Comp Physiol* **305**, 291–299 (2013).

25. Koutakis, P. *et al*. Oxidative damage in the gastrocnemius of patients with peripheral artery disease is myofiber type selective. *Redox Biol*. **2**, 921–928 (2014).

26. Diffee, G. M. & Chung, E. Altered single cell force-velocity and power properties in exercise-trained rat myocardium. *J. Appl. Physiol*. **94**, 1941–1948 (2003).

27. Kumar, A., Accorsi, A., Rhee, Y. & Girgenrath, M. Do's and don'ts in the preparation of muscle cryosections for histological analysis. *Journal of Visualized Experiments* **2015**, (2015).

28. Murach, K. A. *et al*. Fiber typing human skeletal muscle with fluorescent immunohistochemistry. *REVIEW Cores of Reproducibility in Physiology J Appl Physiol* **127**, 1632–1639 (2019).

29. Schindelin, J. *et al.* Fiji: an open-source platform for biological-image analysis. *Nat. Methods* **9**, 676–682 (2012).

30. Yuan Wen, X. *et al.* MyoVision: software for automated high-content analysis of skeletal muscle immunohistochemistry. *J Appl Physiol* **124**, 40–51 (2018).

31. Hildyard, J. C. W., Foster, E. M. A., Wells, D. J. & Piercy, R. J. Rapid histological quantification of muscle fibrosis and lysosomal activity using the HSB colour space. *bioRxiv* 2022.08.02.502489 (2022) doi:10.1101/2022.08.02.502489.

32. Vogel, B., Siebert, H., Hofmann, U. & Frantz, S. Determination of collagen content within picrosirius red stained paraffin-embedded tissue sections using fluorescence microscopy. *MethodsX* **2**, 124–134 (2015).

33. Bottinelli, R. & Reggiani, C. Human skeletal muscle fibres: molecular and functional diversity. *Prog. Biophys. Mol. Biol.* **73**, 195–262 (2000).

34. Larsen, A. I. *et al.* Effect of exercise training on skeletal muscle fibre characteristics in men with chronic heart failure. Correlation between skeletal muscle alterations, cytokines and exercise capacity. *Int. J. Cardiol.* **83**, 25–32 (2002).

35. Schiaffino, S. & Reggiani, C. Fiber Types In Mammalian Skeletal Muscles. *Physiol Rev* **91**, 1447–1531 (2011).

36. Schiaffino, S., Chemello, F. & Reggiani, C. The Diversity of Skeletal Muscle Fiber Types. *Cold Spring Harb. Perspect. Biol.* a041477 (2024) doi:10.1101/cshperspect.a041477.

37. Collins, B. C. *et al.* Three-dimensional imaging studies in mice identify cellular dynamics of skeletal muscle regeneration. *Dev. Cell* **59**, 1457-1474.e5 (2024).

38. Vescovo, G. *et al.* Apoptosis in the skeletal muscle of patients with heart failure: investigation of clinical and biochemical changes. *Heart* **84**, 431–437 (2000).

39. Adams, V. *et al.* Apoptosis in skeletal myocytes of patients with chronic heart failure is associated with exercise intolerance. *J. Am. Coll. Cardiol.* **33**, 959–965 (1999).

40. Winje, I. M. *et al.* Specific labelling of myonuclei by an antibody against pericentriolar material 1 on skeletal muscle tissue sections. *Acta Physiologica* **223**, (2018).

41. Kok, H. J. *et al.* Transcriptomics reveals transient and dynamic muscle fibrosis and atrophy differences following spinal cord injury in rats. *J. Cachexia Sarcopenia Muscle* https://doi.org/10.1002/jcsm.13476 (2024) doi:10.1002/jcsm.13476.

42. Molina, T., Fabre, P. & Dumont, N. A. Fibro-adipogenic progenitors in skeletal muscle homeostasis, regeneration and diseases. *Open Biology* vol. 11 Preprint at https://doi.org/10.1098/rsob.210110 (2021).

43. Rehn, T. A. *et al*. Temporary fatigue and altered extracellular matrix in skeletal muscle during progression of heart failure in rats. *Am J Physiol Regul Integr Comp Physiol* **297**, 26–33 (2009).

44. Filippatos, G. S. *et al*. Studies on apoptosis and fibrosis in skeletal musculature: A comparison of heart failure patients with and without cardiac cachexia. *Int. J. Cardiol.* **90**, 107–113 (2003).

45. Rajabali, N., Rolfson, D. & Bagshaw, S. M. Assessment and Utility of Frailty Measures in Critical Illness, Cardiology, and Cardiac Surgery. *Canadian Journal of Cardiology* vol. 32 1157–1165 Preprint at https://doi.org/10.1016/j.cjca.2016.05.011 (2016).

46. Flint, K. M., Matlock, D. D., Lindenfeld, J. A. & Allen, L. A. Frailty and the selection of patients for destination therapy left ventricular assist device. *Circ. Heart Fail.* **5**, 286–293 (2012).

47. Grosicki, G. J., Zepeda, C. S. & Sundberg, C. W. Single muscle fibre contractile function with ageing. *J. Physiol.* **600**, 5005–5026 (2022).

48. Sundberg, C. W. *et al*. Cumulative effects of H + and P i on force and power of skeletal muscle fibres from young and older adults. *J. Physiol.* **603**, 187–209 (2025).

49. Trappe, S. *et al*. Single muscle fibre contractile properties in young and old men and women. *Journal of Physiology* **552**, 47–58 (2003).

Tables and Figures

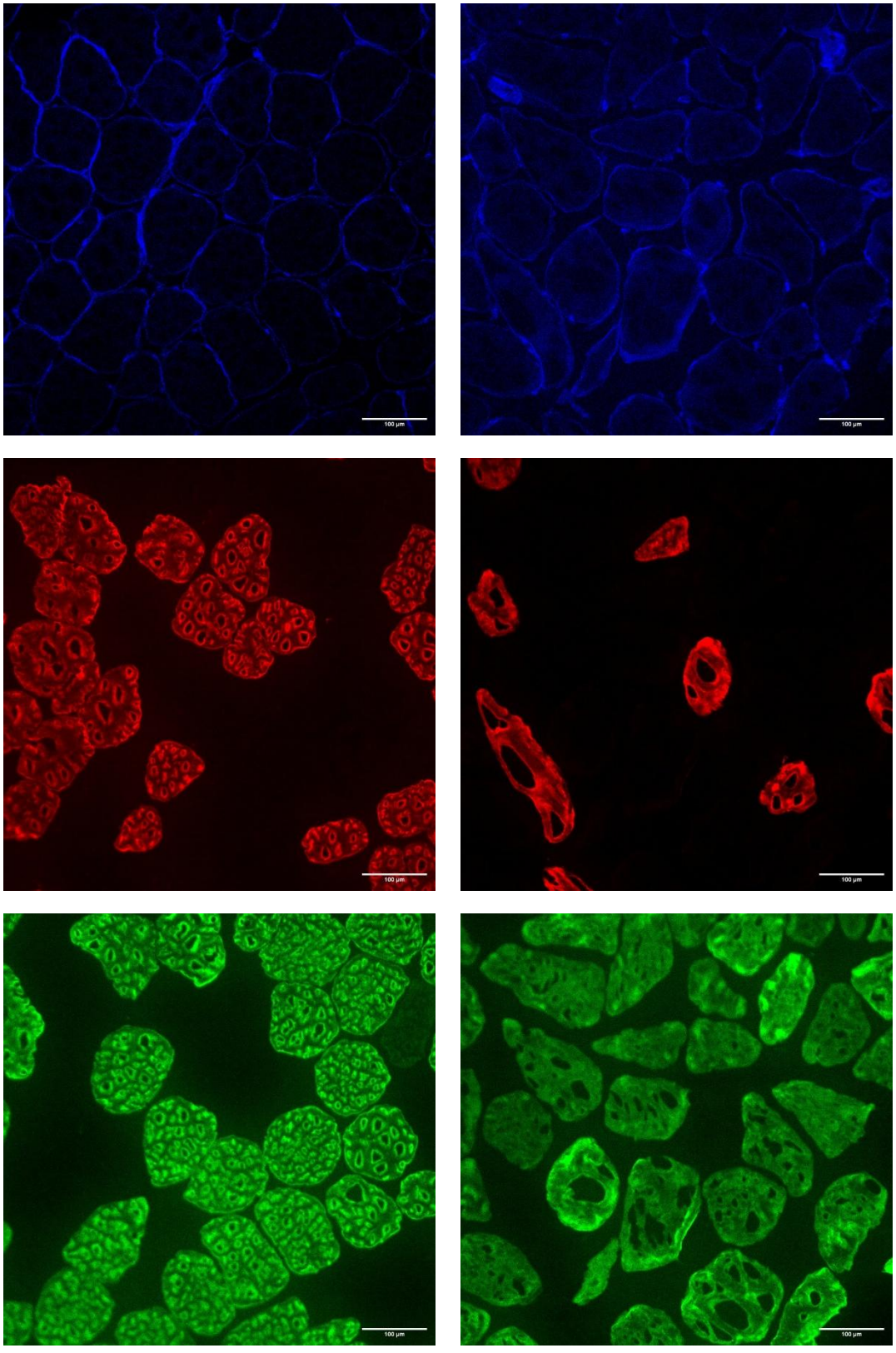

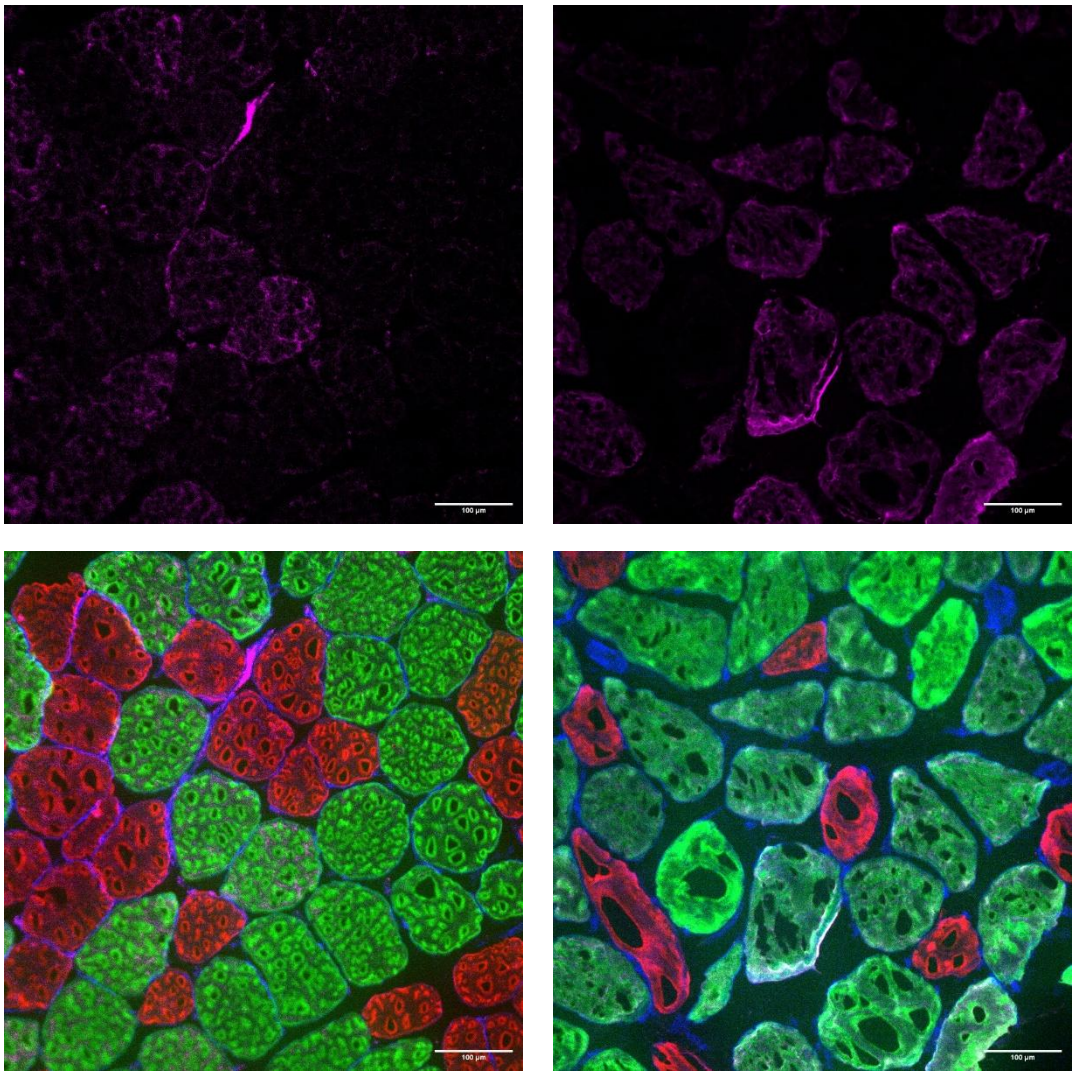

Figure 7. Example of fiber typing immunofluorescence. Left column is control. Right column is heart failure. From top to bottom: laminin, Type 1, Type 2A, Type 2X, and composite. In composite images, blue is laminin, red is Type 1, green is type 2A, and magenta is type 2X. Scale bars are 100 μm.

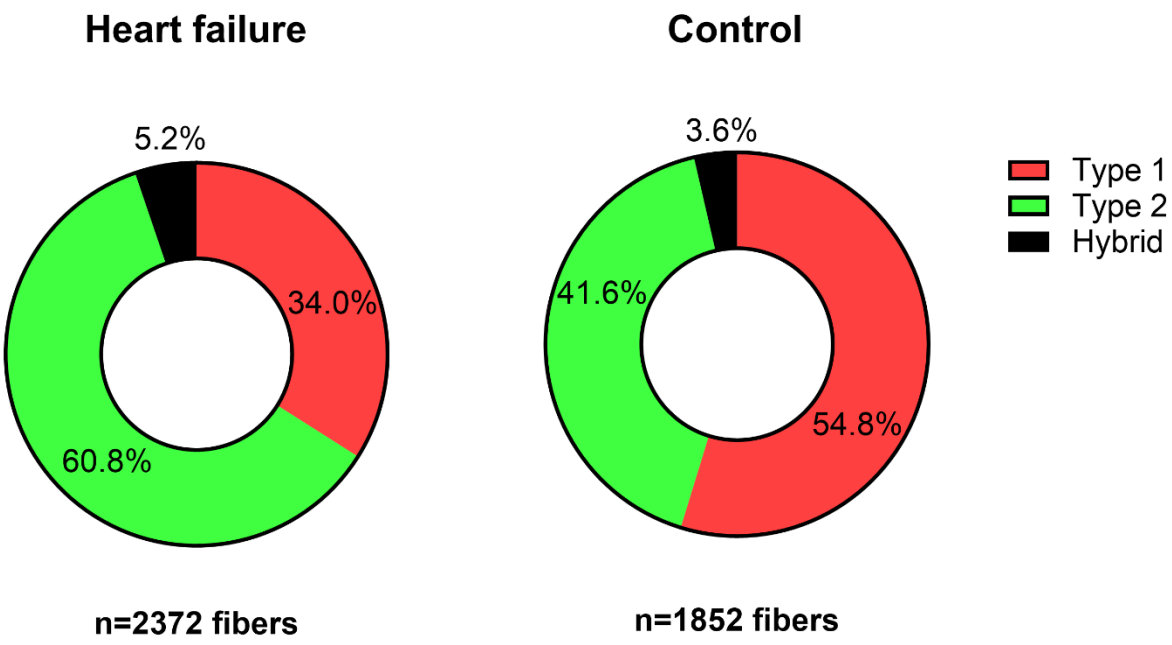

Figure 8. Prevalence of fiber type from skeletal muscle biopsies of heart failure and control subjects.

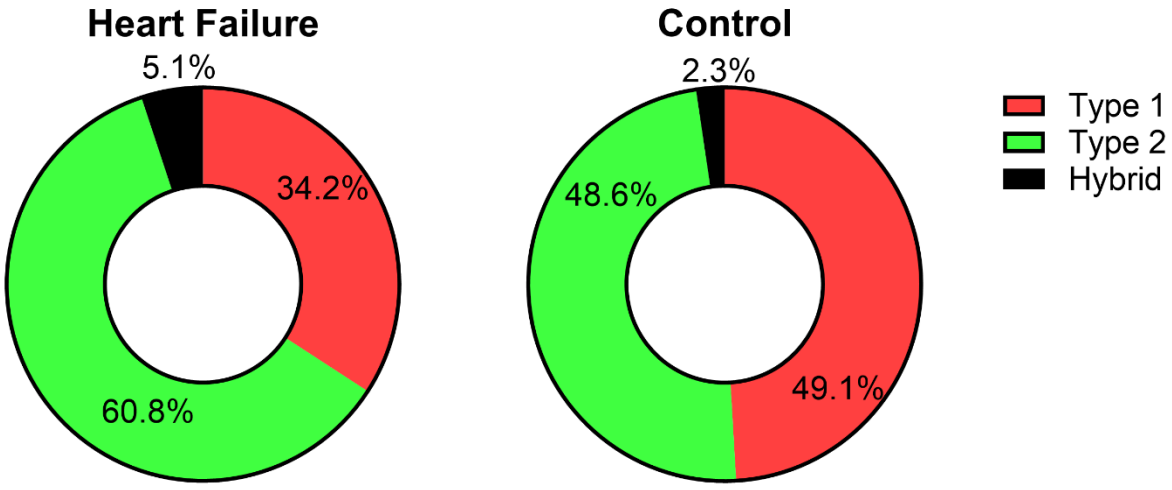

Figure 9. Area contribution (product of prevalence and average CSA) of fiber types from skeletal muscle biopsies of heart failure and control subjects.

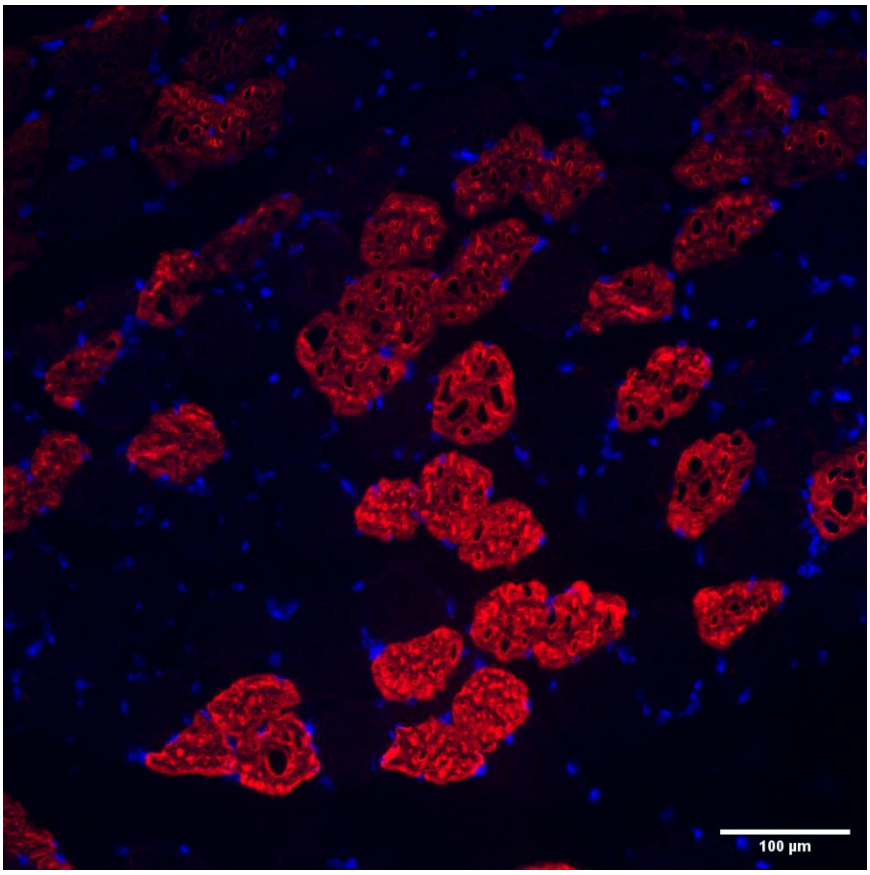

Figure 10. Example image of myonuclear staining with concurrent fiber type stain. Blue is DAPI stained nuclei. Red is MyHC Type 1. Scale bar is 100 µm.

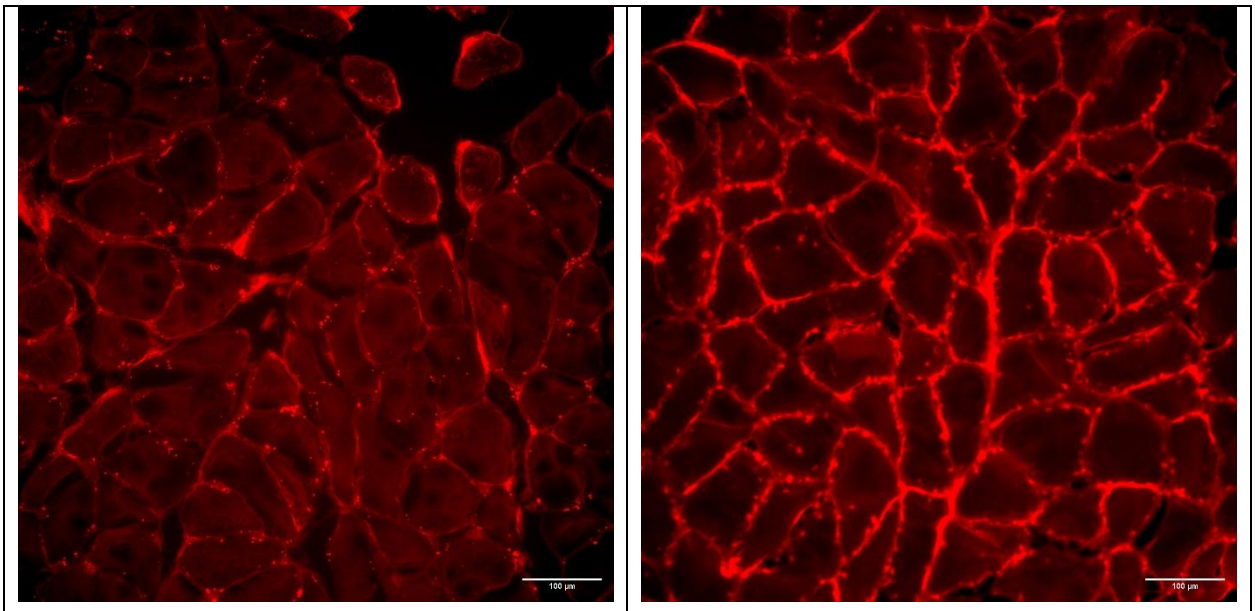

Figure 11. Example image of picrosirius red staining for collagen (Type I and III) in red fluorescence channel. Left image: Control. Right image: Heart failure. Scale bars are 100 µm.

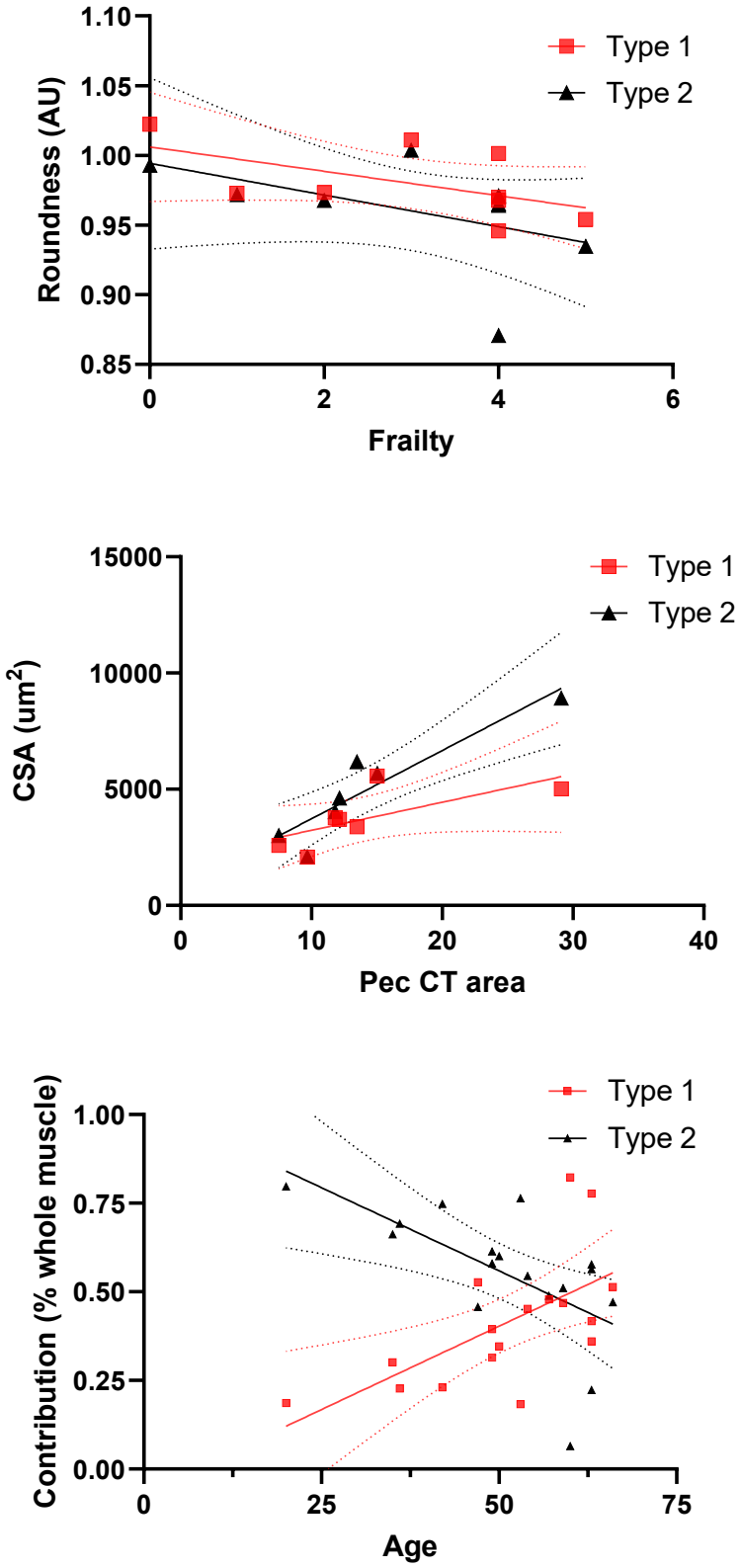

Figure 12. Linear regressions of physiologically and clinically relevant correlations.

Antibody	Isotype	Source
	Primary antibodies	
BA-D5 (MHC I)	αMsIgG2b	DSHB
SC-71 (MHC IIA)	αMsIgG1	DSHB
6H1 (MHC IIX)	αMsIgM	DSHB
2E8 (Laminin gamma 1)	αMsIgG2a	DSHB
	Secondary antibodies	
Fluor 647	GtαMsIgG2b	Invitrogen (A21242)
Fluor 488	GtαMsIgG1	Invitrogen (A21121)
Fluor 555	GtαMsIgM	Invitrogen (A21426)
Fluor 350	αMsIgG2a	Invitrogen (A21130)

Table 9. Fiber typing primary and secondary antibodies. MHC = myosin heavy chain. Ms = mouse. Gt = goat. α = "anti".

Subject Characteristics		
Variable	**Heart Failure**	**Organ Donor Controls**
Number of subjects	10	8
Age (range)	48.4 (20-63)	55.5 (47-66)
Sex	6 Male/4 Female	5 Male/3 Female
BMI	25.75 ± 4.72	27.97 ± 9.38
Surgery type	7 OHT/3 VAD	-
Frailty	3.0 ± 1.6	-
MELD 3.0	17.56 ± 5.34	-

Table 10. Subject and advanced cardiac intervention specific characteristics. MELD = model for end-stage liver disease. Data presented as mean ± SD unless otherwise specified.

Descriptive Statistics

Dependent variable	Control (n= 8)		Heart failure (n = 9)	
Biopsy site	Type 1 fibers	Type 2 fibers	Type 1 fibers	Type 2 fibers
CSA				
Pec	6271.5 ± 2586.2	8442.6 ± 3323.4	3749.5 ± 1220.1	4663.1 ± 2216.8
Ab	5204.5 ± 2063.8	7556.4 ± 3008.0	3612.2 ± 1255.7	4724.7 ± 2268.5
Roundness				
Pec	1.006 ± 0.021	1.001 ± 0.015	0.98632 ± 0.02859	0.97614 ± 0.03113
Ab	1.002 ± 0.022	0.993 ± 0.031	0.97984 ± 0.03373	0.95711 ± 0.04343
Convexity				
Pec	0.99 ± 0.01	0.99 ± 0.01	0.99208 ± 0.00254	0.98850 ± 0.00472
Ab	0.99 ± 0.00	0.98 ± 0.01	0.99138 ± 0.00265	0.98974 ± 0.00419
Prevalence				
Pec	55.7% ± 12.3%	42.3% ± 11.9%	30.8% ± 13.6%	65.9% ± 14.6%
Ab	51.2% ± 12.9%	43.3% ± 9.5%	39.5% ± 19.3%	53.6% ± 20.7%
Contribution				
Pec	49.2% ± 13.1%	49.4% ± 13.0%	28.6% ± 16.3%	68.5% ± 17.6%
Ab	43.5% ± 11.4%	52.3% ± 7.0%	34.4% ± 19.2%	59.2% ± 22.0%
Fibrosis Index				
Pec	4.36% ± 3.94%		6.20% ± 3.86%	
Ab	4.11% ± 3.80%		4.51% ± 2.60%	

Table 11. Descriptive statistics of morphological data. Please note fibrosis index is not separated by fiber type, only condition and biopsy site. Pec = pectoralis. Ab = rectus abdominis. Data is presented as means ± SD.

LME Model Structure for Dependent Variables

Dependent variable	Repeated measures	Random intercept
CSA	-	+
Roundness	+	+
Convexity	-	+
Fibrous Index	-	+
Avg Nuclei	-	+
Avg Centronuclei	-	+
% Centronucleated Fibers	-	+
CSA-normalized Avg Nuclei	-	+

Table 12. Linear mixed effects model structure for each dependent variable.

Correlation of clinical data with skeletal muscle data					
	Morphohistological parameters				
Clinical variable	**CSA**	**Roundness**	**Convexity**	**Prevalence**	**Area contribution**
Global					
Age	-0.311	0.139	-0.211	-	-
Frailty	0.514	**-0.714***	-0.531	-	-
Duration	**0.722***	0.184	0.153	-	-
BNP	-0.093	-0.451	-0.329	-	-
CT Pec area	**0.964*****	-0.571	-0.143	-	-
Pec only	0.771	-0.200	0.371	-	-
Avg Attenuation (HU)	0.646	0.297	0.308	-	-
Pec only	0.456	-0.029	0.147	-	-
Type 1					
Age	-0.134	0.149	-0.327	**0.567***	**0.630*****
Frailty	0.200	**-0.705***	-0.514	-0.409	-0.540
Duration	**0.751***	0.153	0.060	-0.258	-0.275
BNP	-0.188	-0.367	-0.278	-0.186	-0.275
CT Pec area	**0.786***	-0.571	-0.286	-0.679	-0.750
Pec only	0.771	-0.200	-0.029	-0.886	-0.886
Avg Attenuation (HU)	0.542	0.034	0.536	-0.608	-0.665
Pec only	0.392	-0.143	0.506	-0.091	-0.138
Type 2					
Age	-0.277	0.100	-0.053	**-0.560***	**-0.620*****
Frailty	0.574	**-0.749***	0.000	0.165	0.496
Duration	0.655	-0.167	0.012	0.268	0.285
BNP	-0.051	-0.143	-0.311	0.188	0.290
CT Pec area	**0.929****	-0.714	0.071	0.643	**0.893***
Pec only	**0.886***	-0.200	0.314	0.943	0.943
Avg Attenuation (HU)	0.693	0.214	-0.242	0.647	**0.708***
Pec only	0.453	-0.029	0.042	0.172	0.203

*Table 13. Pearson and Spearman r values for correlations between morphohistological variables and clinically relevant parameters. BNP = brain natriuretic peptide. Bolded values imply significance. * signifies p < 0.05. ** signifies p < 0.01. *** signifies p < 0.001.*

Correlation of clinical data with skeletal muscle data					
	Myonuclear and fibrous content parameters				
Clinical variable	**Avg Myonuclei**	**Avg Centronuclei**	**Centronucleated Fibers**	**Normalized Avg Myonuclei**	**Fibrous Index**
Global					
Age	-0.461	-0.384	-0.289	0.166	-0.329
Frailty	0.523	0.069	-0.061	0.079	0.395
Duration	0.365	0.397	0.197	**-0.891****	0.509
BNP	0.261	0.133	0.327	0.459	-0.200
CT Pec area	**0.857***	0.393	0.179	**-0.821***	**0.786***
Pec only	-	-	-	-	0.429
Avg Attenuation	0.647	0.685	0.647	-0.534	0.177
Pec only	-	-	-	-	0.281
Type 1					
Age	-0.050	-0.112	-0.086	-0.303	-
Frailty	0.702	0.176	0.295	0.944	-
Duration	-0.563	-0.309	-0.383	-0.827	-
BNP	**0.953***	0.632	0.723	**0.984***	-
CT Pec area	0.500	-0.500	-0.500	0.500	-
Avg Attenuation	-0.995	-0.751	-0.805	-0.963	-
Type 2					
Age	-0.563	-0.545	-0.338	0.438	-
Frailty	0.228	-0.017	-0.289	**-0.819***	-
Duration	**0.893***	0.681	0.457	-0.757	-
BNP	-0.489	-0.405	-0.305	-0.226	-
CT Pec area	0.600	0.500	0.100	-0.800	-
Avg Attenuation	**0.887***	**0.913***	**0.860***	-0.445	-

*Table 14. Pearson and Spearman r values for correlations between myonuclear and fibrous variables and clinically relevant parameters. Bolded values imply significance. * signifies $p < 0.05$. ** signifies $p < 0.01$.*

	Numerator df	Denominator df	F	Sig.
CSA				
Condition	1	15.53	7.49	0.015
Biopsy	1	38.84	2.27	0.140
FT	1	37.51	27.97	<.001
Condition x Biopsy	1	38.84	1.61	0.212
Condition x FT	1	37.51	4.07	0.051
Biopsy x FT	1	37.51	0.09	0.761
3-way interaction	1	37.51	0.00	0.988
Roundness				
Condition	1	13.53	6.02	0.028
Biopsy	1	39.75	1.75	0.194
FT	1	35.84	3.38	0.074
Condition x Biopsy	1	39.75	0.01	0.938
Condition x FT	1	35.84	0.53	0.472
Biopsy x FT	1	35.84	0.45	0.508
3-way interaction	1	35.84	0.10	0.758
Convexity				
Condition	1	13.99	6.23	0.026
Biopsy	1	41.37	0.68	0.416
FT	1	36.75	1.95	0.171
Condition x Biopsy	1	41.37	1.59	0.214
Condition x FT	1	36.75	0.58	0.450
Biopsy x FT	1	36.75	0.44	0.511
3-way interaction	1	36.75	0.02	0.892
Fibrous Index				
Condition	1	12.75	0.74	0.404
Biopsy	1	12.48	0.71	0.415
Condition x Biopsy	1	12.48	0.36	0.561
Avg Nuclei				
Condition	1	24.90	1.75	0.198
Biopsy	1	13.47	0.02	0.888
FT	1	22.45	1.06	0.313
Condition x Biopsy	1	12.18	2.18	0.165
Condition x FT	1	21.86	0.95	0.340
Biopsy x FT	1	13.47	0.65	0.433
Avg Centronuclei				
Condition	1	25.39	0.00	0.975

Biopsy	1	13.04	0.29	0.600
FT	1	22.53	0.43	0.521
Condition x Biopsy	1	11.46	0.16	0.695
Condition x FT	1	22.19	0.09	0.766
Biopsy x FT	1	13.24	0.04	0.841
% Centronucleated fibers				
Condition	1	25.53	0.84	0.367
Biopsy	1	11.70	2.78	0.122
FT	1	22.51	0.60	0.446
Condition x Biopsy	1	9.93	0.64	0.441
Condition x FT	1	22.52	0.01	0.935
Biopsy x FT	1	12.31	0.91	0.360
Normalized avg nuclei				
Condition	1	23.92	1.85	0.186
Biopsy	1	12.43	1.04	0.326
FT	1	20.93	0.00	0.975
Condition x Biopsy	1	11.37	4.25	0.063
Condition x FT	1	20.24	0.11	0.742
Biopsy x FT	1	12.23	0.30	0.592

Table 15. F-statistics and p values for main effects and interactions of linear mixed effects models. FT = fiber type.

Chapter 4. Skeletal muscle mitochondrial content and function in heart failure

Introduction

Heart failure is associated with a marked decrease in physical capacity and increased fatigability that are not fully explained by impaired cardiac function alone. While hemodynamic limitations can contribute to the observed exercise intolerance, a substantial portion of functional impairment in heart failure is attributed to peripheral maladaptations, namely of skeletal muscle.[1–4]

When thinking about the components of VO_2max (Q x ΔA-V O_2), the reduction in peripheral function would be seen as a decrease in the A-V O_2 difference.[5] Consistent with this theoretical framework, studies have both indirectly[6] and directly[7] demonstrated this attenuation in the heart failure population. Furthermore, these deficits in oxygen utilization are not simply due to reduced blood flow to working skeletal muscle.[8,9] Together with work showing a reduced diffusive component of VO_2[10] and observed fiber type shifts from oxidative to glycolytic fibers,[11] indicate the presence of intrinsic deficits in skeletal muscle oxidative metabolism. As such, mitochondria are central to this phenotype: reduced mitochondrial content and/or impaired function would be predicted to limit oxygen extraction and blunt ATP production, thereby contributing to early fatigue and reduced physical capacity. However, while there is broad agreement that heart failure induces mitochondrial maladaptations,[12–14] the underlying cellular features that accompany the reduced oxidative capacity are not fully characterized across subpopulations of patients, sampling sites, and method of measurement. Furthermore, the extent to which mitochondrial content tracks with other metabolic features of tissue remains an important area of investigation.

Concurrently, there is a growing body of evidence to suggest that lipid accumulation in skeletal muscle negatively impacts both contractile and metabolic function.[15–17] Intramyocellular lipids are an important cellular energy source; however, excess storage or altered distribution may negatively affect the skeletal muscle contractile function. In conditions of impaired oxidative capacity, such as heart failure, lipids may accumulate due to reduced oxidative flux, altered

mitochondrial density, or shifts in substrate preference, potentially linking mitochondrial abnormalities with changes in intramuscular lipid content. In respect to heart failure, lipid accumulation in skeletal muscle has shown equivocal results.[10,18] However, evidence from the Health ABC study demonstrates a significantly elevated incidence of heart failure in individuals with high intramuscular fat levels.[19] Together these data make it difficult to determine the cause and effect relationship between intramuscular lipid content and the established mitochondrial maladaptations that occur with heart failure.

Therefore, in this study, we quantified skeletal muscle neutral lipid accumulation and mitochondrial content in individuals with late-stage (ACC/AHA Stage D) heart failure and non-heart failure organ donor controls. In addition, we assessed these measures across two functionally distinct skeletal muscle groups in order to better understand the effects of heart failure on the musculature as a whole.

Methods

Muscle biopsy and tissue processing

All experiments were reviewed and approved by the University of Wisconsin-Madison Institutional Review Board. Heart failure subjects were recruited from clinical patients at the University of Wisconsin Hospital (HF) or from organ donors at the University of Kentucky (non-HF controls [CON]). Informed consent was obtained for all clinical subjects. Inclusion criteria was as follows: patients with advanced heart failure (ACC/AHA Stage D) that required implantation of a ventricular assist device (VAD) or orthotopic heart transplant (OHT).

During the respective cardiothoracic surgery, roughly 200-300 mg of the sternal pectoralis major and proximal rectus abdominis were collected by the surgeon. The sample was briefly stored

in chilled relax solution[20] until it could be returned to the lab and processed further. The biopsy was cleaned of any visible adipose and connective tissue as well as any damage secondary to acquisition (i.e. cautery burns). Sample was patted dry and oriented under guidance of a dissecting microscope. It was then covered in OCT, which was allowed to penetrate into the tissue for ~30 minutes.[21] Finally, the OCT covered biopsy was frozen utilizing the liquid nitrogen cooled isopentane method. The frozen samples were stored at -80 °C until tissue slicing. On the day of the experiment, the frozen sample was allowed to acclimate to the cryostat (HM505E, Microm), which was maintained at -25 °C. At least two 10 µm thick serial sections were adhered to each microscope slide for use in subsequent histological protocols. Slides were allowed to dry at room temperature for 1) 20 minutes and then stored in a slide box at -80 °C for future staining, or 2) 60 minutes for immediate use.

Skeletal muscle lipid content

Lipid content was assessed by Oil Red O staining as previously described by Goodpaster et al. with some modification.[22,23] Briefly, a stock solution of Oil Red O stain was made by dissolving 300 mg of Oil Red O powder into 100 mL of 99% isopropanol and stored at room temperature. On the day of staining, a working solution was made by adding three parts stock solution to two parts nanopure H_2O. The working solution was filtered through a Whatman #1 filter to remove crystallized stain. Previously cut and air-dried 10-µm cross sections were removed from -80 °C storage and allowed to equilibrate to room temperature. Slides were then placed in PBS for 10 minutes, removed, and allowed to dry for 10 minutes. Tissue was then fixed with 3.7% formaldehyde for 1 hour, followed by 2 x 20 seconds rinse in DH_2O. Slides were then placed into Oil Red O stain for 10 minutes and again rinsed 2 x 20 seconds in DH_2O immediately afterwards. Finally, staining was completed with a 10-minute tap water wash, and a coverslip was mounted using Aqua-Mount (Epredia). Images were taken utilizing a 10x objective on a SoRa/W1 Spinning Disk Confocal

Microscope. At least three images with a clear FOV, free of any artefacts due to tissue cutting or improper attachment were acquired. Image processing was completed using the freely available software Fiji.[24] Image analysis was performed as previously described by Bhullar and colleagues without Z-stacking and single plane merging.[25] Briefly, quantification of lipids was conducted by establishing thresholds for Oil Red O stain (red channel) and image binarization. Determination of area was handled using Fiji's "analyze" tool to determine measured lipid area in μm^2 and measured percent lipid area to tissue area (lipid area index [LAI]). Lipid droplet count and mean size (droplet size) was assessed through the "analyze particles" tool, with a limit of 0.5-50 μm^2 for each particle in order to limit single pixel counts and potential remaining stain crystals from being included in the analysis. Droplet density was determined by dividing droplet by the area of analyzed tissue. Following analysis of particles, the calculated lipid area and calculated LAI were determined by multiplying droplet count by mean droplet size.

Mitochondrial content

Mitochondrial content was assessed through citrate synthase (CS) activity. Briefly, roughly 20 mg of previously frozen tissue free of connective and adipose was collected. CelLytic MT cell lysis reagent (#C3238, Sigma-Aldrich) was added to the tissue as recommended by the manufacturer and was manually homogenized with microscissors and a tissue grinder. To determine protein concentration, we conducted a Bradford assay (Pierce Bradford Protein Assay Kit, #23200, Thermo Fisher Scientific Inc.) by following manufacturer instructions. Finally, to determine activity, the Citrate Synthase Assay Kit (#CS0720, Sigma-Aldrich) was used following directions from manufacturer. Colorimetric absorbance of light at 412 nm was detected using a multi-mode reader (Synergy LX, BioTek). Citrate synthase activity was calculated using the provided equation from the manufacturer and normalized for protein content.

Clinical correlations

In order to determine if changes in skeletal muscle mitochondrial or lipid content from HF patients varied along with other aspects of heart failure symptoms, we correlated citrate synthase and lipid droplet data with clinical data. Clinical data was acquired through a query of the HF patients' electronic medical records. The following is a non-inclusive list of relevant clinical information gathered: BNP, duration of heart failure, frailty status/score (measured using the Fried Frailty Phenotype), and most recent chest CT prior to cardiac intervention. Duration of heart failure was determined as the difference (in months) from the first reported date of diagnosis to date of cardiac intervention. From the chest CT, the total area of pectoralis and the minimum, maximum, and mean attenuation (HU) were extracted. Throughout the query process, patient confidentiality was maintained, and all data handling adhered to HIPAA guidelines.

Statistical analysis

All statistical analyses were conducted in SPSS (V31.0, IBM) and all figures made in GraphPad Prism (V11.0 for Windows). A Bland-Altman analysis was used to determine if measured values for lipid area and LAI were different than calculated values. Furthermore, we employed linear mixed effects (LME) modeling for the comparisons of mitochondrial and lipid content between groups and biopsy sites. We analyzed each dependent variable using a LME model with condition (HF vs CON), biopsy site (pec vs ab), and the two-way interaction as fixed effects. Subject was included as a random intercept to account for within-subject dependence. Repeated observations across biopsy sites within subjects were modeled using a compound symmetrical covariance matrix. Models were fit using restricted maximum likelihood (REML) estimation and Satterthwaite approximation for denominator degrees of freedom. Statistical significance was assessed using Type III tests of fixed effects and estimated marginal means were calculated to aid in interpretation of significant main effects and interactions. Because model stability differed

across dependent variables, convergence and fit diagnostics were evaluated for each model. If nonconvergence occurred, a simplified model that removed the repeated covariance structure was used. Final reported models were the best-fitting converged models, as judged by model estimability and AIC criterion, while retaining biologically relevant fixed effects and interactions.

Results

Agreement of measured and calculated lipid parameters

The Bland-Altman analysis demonstrated that the measured and calculated lipid area and LAI were not different (95% agreement limits overlapped with 0). Therefore, herein we used calculated lipid area and LAI as it eliminated single pixel counts and controlled for potential ORO crystals.

Lipid content of skeletal muscle

Subject characteristics are presented in Table 1. Lipid content was assessed by ORO stain (Figure 1) using multiple indices, including lipid droplet count, droplet size, droplet density, and lipid area index (Table 2). These variables were analyzed using LME models with condition, biopsy site, and the two-way interaction as fixed effects (see Table 3 for model structures). Across all lipid measures, there were no significant main effects of condition or biopsy site. Moreover, there were not significant two-way interactions. Collectively, these findings indicate that lipid content does not detectably differ between heart failure and control subjects, nor does it vary by muscle group within the present sample population.

Skeletal muscle mitochondrial content

Mitochondrial content as assessed by citrate synthase activity and analyzed using a LME model with repeated measures for biopsy site and condition, biopsy site, and the two-way

interaction as fixed effects. There was a significant main effect for condition ($p = 0.012$) demonstrating a 35.2% decrease in citrate synthase activity in HF compared to control when using the estimated marginal means (HF: 0.184 U/mg vs CON: 0.284 U/mg). There were no other significant main effects or interaction.

Correlations to clinical parameters

Correlations between lipid parameters and mitochondrial content with clinical data are detailed in Table 4. Correlational analysis revealed a significant negative relationship between CT pec average attenuation and lipid droplet size ($p = 0.017$). Furthermore, there was a positive correlation between average attenuation and droplet density of all muscles and pec biopsies only ($p = 0.035$ and 0.002, respectively). Finally, we found a negative correlation between lipid area index and levels of BNP (Figure 2). There were no other statistically significant correlations, however, we did see a trend for CT pec average attenuation and all biopsies LAI ($p = 0.071$) and pec only LAI (0.0501).

Discussion

In this study, we sought to investigate skeletal muscle neutral lipid accumulation and mitochondrial content across two functionally distinct muscle groups- the pectoralis major and rectus abdominis- in patients with late-stage heart failure compared to organ donor controls. Our findings demonstrate that advanced heart failure causes a significant, approximately 35% reduction in skeletal muscle mitochondrial content, as assessed by citrate synthase activity, while neutral lipid accumulation did not detectably differ between groups or biopsy sites. Notably, lipid parameters correlated significantly with clinically available markers, including relationships between CT derived pec attenuation and lipid droplet morphology. These findings advance our

understanding of the peripheral maladaptations that accompany late-stage heart failure and suggest that routinely acquired clinical data may offer valuable insight into skeletal muscle lipid biology without the need for invasive biopsies.

The principal finding of this study was the ~35% reduction in citrate synthase activity, a well-established marker of mitochondrial content, in the skeletal muscle of heart failure patients relative to controls. This finding is consistent with the broader literature characterizing heart failure as a systemic disease that profoundly disrupts skeletal muscle energetics.[10,12,14,26–28] In fact, mitochondrial dysfunction has been described as one of the earliest signs of skeletal muscle injury in heart failure,[29] and progressive mitochondrial dysfunction is associated with impairments in contractile coupling, muscle wasting, and exercise intolerance.[30–32] Importantly, reduced mitochondrial volume and oxidative capacity in skeletal muscle has been shown to strongly correlate with key functional measures, including VO_2max and the 6-minute walk test, further underscoring the clinical relevance of this peripheral maladaptation.[13] While the mechanisms driving the maladaptive mitochondrial response are not entirely understood, they are likely multifactorial and include oxidative stress, systemic inflammation, increased metabolic burden, and deconditioning.[33–35] It is crucial to note that in the current study we only utilized a measure of mitochondrial content, not function. While methods such as high-resolution mitochondrial respirometry allow for high sensitivity measurements during various respiratory states and in the presence of a variety of substrates, our control tissue was frozen and therefore prevented the use of high-resolution respirometry.[36,37] Although new protocols are being developed to allow for the use of previously frozen tissue,[38,39] they currently are limited to measuring maximal respiratory state capacities and cannot accommodate more complex substrate-uncoupler-inhibitor-titration (SUIT) protocols that lend more physiological relevance.[40] Moreover, there is limited data on the differences in mitochondrial intrinsic function between fiber types. Previous studies have

investigated markers of mitochondrial content and function in animal models, where muscles are more homogenous and have demonstrated disparate effects in the setting of heart failure.[41,42] More recently, Edman and colleagues developed a pipeline and quantified intrinsic mitochondrial function differences between skeletal muscle fiber types.[43] As expected, they observed an elevated Type 1 mitochondrial volume (~3x) compared to Type 2 fibers; however, Type 2 fibers have a greater maximal respiratory rate compared to Type 1 when normalizing for mitochondrial volume, suggesting that Type 2 fibers compensate for a reduced mitochondrial volume by increasing intrinsic capacity. This is a critical consideration when applying high-resolution respirometry to permeabilized muscle bundles from patients with heart failure, given that heart failure is associated with a fiber type shift from oxidative to glycolytic phenotypes. Taken together, these observations highlight the need for future investigations that incorporate fresh tissue preparations, fiber type specific analyses, and direct measures of intrinsic mitochondrial function in skeletal muscle from patients with heart failure. Such studies are crucial to disentangle the relative contributions of reduced mitochondrial volume, altered respiratory capacity, and disease-associated fiber type remodeling to the skeletal muscle phenotype. Ultimately, these studies will help to provide a more comprehensive understanding of peripheral energetic dysfunction in heart failure and aid in prognostication and the development of better therapies and interventions.

In contrast to the mitochondrial findings, neutral lipid content measured by Oil Red O staining and assessed across multiple indices, did not differ significantly between heart failure and controls, nor was there a biopsy site difference (Table 5). These findings warrant careful consideration, as previous studies have found evidence supporting and contesting skeletal muscle lipid accumulation in heart failure.[10,18] Prior work in patients with chronic heart failure have reported impaired lipid metabolism compared to healthy controls, partly attributable to reduced tricarboxylic acid cycle activity and subsequently causing ectopic lipid accumulation.[34,44] At the

same time, studies investigating skeletal muscle sublocation of lipid storage in healthy animals have demonstrated that increased intramuscular lipid content is driven primarily by accumulation of extramyocellular lipids- that is the growth and accumulation of intramuscular adipocytes.[45] Our study analyzed lipid content through ORO staining, which stains all neutral lipids- both intramyocellular and extramyocellular. As such, our null result for differences in lipid parameters may be a product of our visualization methodology. Prior work has successfully utilized immunofluorescence techniques that target perilipin isoforms specific to adipocytes and intramyocellular lipids independently, allowing for separate quantification.[45] In addition, heart failure is known to cause a fiber type shift in skeletal muscle from slow oxidative to fast glycolytic fibers. Fast glycolytic fibers tend to have a reduced content of intramyocellular lipids, resultant from a reduced mitochondrial volume.[43,46] Therefore, it is possible that our methodology failed to capture an elevated extramyocellular lipid content due to a reduced amount of intramyocellular lipids. Furthermore, our LME models did not control for comorbidities such as diabetes mellitus, which is known to cause increases in the amount of intramyocellular lipids, and is common in the heart failure population.[47–50] Finally, while our study aimed to investigate late-stage heart failure patients, we failed to account for the etiology of the condition (i.e. systolic vs diastolic dysfunction), which previous work has shown to have disparate peripheral metabolic effects.[51]

Despite the absence of condition-level difference in lipid content, we identified significant correlations between lipid parameters and two clinically relevant metrics: BNP and CT pec average attenuation. These findings suggest that, within the heart failure population, variation in skeletal muscle lipid biology does track with markers routinely acquired during clinical care. The strong negative correlation between lipid area index and BNP ($r = -0.786$, $p < 0.05$) is a notable finding with several potential interpretations. Brain natriuretic peptide is the gold standard marker for hemodynamic burden in heart failure, with higher levels indicating a greater cardiovascular strain.[52]

However, paradoxically, patients with the most elevated BNP may demonstrate lower skeletal muscle lipid accumulation, reflecting a catabolic state characterized by substrate mobilization rather than deposition. This interpretation aligns with observations of advanced heart failure concurrent with cardiac cachexia, where there is significant wasting and mobilization of peripheral energy stores.[53–55] Moreover, recent work has further demonstrated that NT-proBNP negatively correlates with skeletal muscle cellular features including cross-sectional area, capillarization, and muscle stem cell count, reinforcing the concept that natriuretic peptide levels infer information beyond their established cardiac utility.[56] In the current study, we did not account for a concurrent diagnosis of muscle wasting (i.e. cachexia) and therefore these correlations should be interpreted cautiously. Nonetheless, taken together, these data suggest that BNP may serve not only as a cardiac biomarker, but also an indicator of skeletal muscle lipid biology in patients with late-stage heart failure.

The CT attenuation findings further solidify the utility of clinically available imaging as a non-invasive tool into skeletal muscle lipid status. Average pec attenuation was negatively correlated with lipid droplet size ($p = 0.017$) and positively correlated with droplet density (all biopsies: $p = 0.035$; pec only: $p = 0.002$). CT muscle attenuation is well recognized as an inverse surrogate of intramuscular fat, where lower Hounsfield units (HU) reflect a greater lipid content within the muscle.[57] Our biopsy-level findings (pec only correlation) are in agreement with these prior observations. However, our observations that lower attenuation is associated with larger lipid droplets yet lower droplet density suggests that lipids detected by CT corresponds to large lipid droplets (extramyocellular), rather than numerous small, discrete lipids (intramyocellular). Interestingly, prior work has demonstrated an association between attenuation and muscle fiber composition, suggesting that lower attenuation is a surrogate measure for higher prevalence of oxidative fibers.[58] This does not seem to be the case in our study; however, caution should be taken

when interpreting these findings, as we did not compare intramyocellular and extramyocellular lipid content. Moreover, the glycolytic shift phenomenon often observed in heart failure may occur concurrently with extramyocellular lipid deposition, obscuring these results. Notwithstanding, increased pectoral muscle radiodensity has been shown to be independently associated with a one-year greater post-transplant survival in a cohort of heart failure patients undergoing orthotopic heart transplant.[59] The same anatomical site has shown both prognostic relevance as well as meaningful correlations with lipid droplet morphology in the present study, suggesting that CT-derived pectoral attenuation may serve as a clinically accessible indicator of the underlying skeletal muscle lipid environment in patients with heart failure. Together, these data support the concept that clinical indices collected during routine care of heart failure patients allow for insight into the skeletal muscle metabolic status and can be utilized to help guide improved patient care and clinical outcomes.

In conclusion, this study has demonstrated that late-stage heart failure causes significant reductions in mitochondrial content without any detectable changes to lipid biology compared to controls. Additionally, we have shown that commonly acquired clinical indices in the heart failure population significantly correlate to the lipid phenotype in skeletal muscle, providing a non-invasive approach to information regarding peripheral maladaptations. Future studies should focus on investigating fiber type specific differences and quantifying location of lipid deposition in this population in order to guide improved and novel treatment plans.

References

1. Maskin, C. S., Forman, R., Sonnenblick, E. H., Frishman, W. H. & LeJemtel, T. H. Failure of dobutamine to increase exercise capacity despite hemodynamic improvement in severe chronic heart failure. *Am. J. Cardiol.* **51**, (1983).

2. Coats, A. J. S. The "Muscle Hypothesis" of Chronic Heart Failure. *J. Mol. Cell. Cardiol.* **28**, 2255–2262 (1996).

3. Coats, A. J. S., Clark, A. L., Piepoli, M., Volterrani, M. & Poole-Wilson, P. A. Symptoms and quality of life in heart failure: the muscle hypothesis. *Br. Heart J.* **72**, S36 (1994).

4. Harrington, D. *et al.* Skeletal muscle function and its relation to exercise tolerance in chronic heart failure. *J. Am. Coll. Cardiol.* **30**, 1758–1764 (1997).

5. Wagner, P. D. A theoretical analysis of factors determining Vo2MAX at sea level and altitude. *Respir. Physiol.* **106**, 329–343 (1996).

6. Tucker, W. J. *et al.* Performance Limitations in Heart Transplant Recipients. *Exercise and Sport Sciences Reviews* vol. 46 144–151 Preprint at https://doi.org/10.1249/JES.0000000000000149 (2018).

7. Haykowsky, M. J. *et al.* Determinants of Exercise Intolerance in Elderly Heart Failure Patients With Preserved Ejection Fraction. *J. Am. Coll. Cardiol.* **58**, 265–274 (2011).

8. Massie, B. *et al.* Skeletal muscle metabolism in patients with congestive heart failure: relation to clinical severity and blood flow. *Circulation* **76**, 1009–1019 (1987).

9. Massie, B. M. *et al.* Skeletal Muscle Metabolism During Exercise Under Ischemic Conditions in Congestive Heart Failure Evidence for Abnormalities Unrelated to Blood Flow. *Circulation* **78**, 320–326 (1988).

10. Esposito, F., Mathieu-Costello, O., Shabetai, R., Wagner, P. D. & Richardson, R. S. Limited maximal exercise capacity in patients with chronic heart failure: Partitioning the contributors. *J. Am. Coll. Cardiol.* **55**, 1945–1954 (2010).

11. Kaneguchi, A., Sakitani, N. & Umehara, T. Histological changes in skeletal muscle induced by heart failure in human patients and animal models: A scoping review. *Acta Histochem.* **126**, 152210 (2024).

12. Guzmán Mentesana, G. *et al.* Functional and Structural Alterations of Cardiac and Skeletal Muscle Mitochondria in Heart Failure Patients. *Arch. Med. Res.* **45**, 237–246 (2014).

13. Scandalis, L. *et al.* Skeletal Muscle Mitochondrial Respiration and Exercise Intolerance in Patients With Heart Failure With Preserved Ejection Fraction. *JAMA Cardiol.* https://doi.org/10.1001/jamacardio.2023.0957 (2023) doi:10.1001/jamacardio.2023.0957.

14. Kumar, A. A., Kelly, D. P. & Chirinos, J. A. Mitochondrial Dysfunction in Heart Failure With Preserved Ejection Fraction. *Circulation* **139**, 1435–1450 (2019).

15. Bekfani, T. *et al.* Skeletal Muscle Function, Structure, and Metabolism in Patients With Heart Failure With Reduced Ejection Fraction and Heart Failure With Preserved Ejection Fraction. *Circ. Heart Fail.* **13**, E007198 (2020).

16. Biltz, N. K. *et al.* Infiltration of intramuscular adipose tissue impairs skeletal muscle contraction. *Journal of Physiology* **598**, 2669–2683 (2020).

17. Park, S. S. & Seo, Y. K. Excess accumulation of lipid impairs insulin sensitivity in skeletal muscle. *International Journal of Molecular Sciences* vol. 21 Preprint at https://doi.org/10.3390/ijms21061949 (2020).

18. Matsumoto, J. *et al.* Brain-Derived Neurotrophic Factor Improves Impaired Fatty Acid Oxidation Via the Activation of Adenosine Monophosphate-Activated Protein Kinase-α-Proliferator-Activated Receptor-r Coactivator-1α Signaling in Skeletal Muscle of Mice With Heart Failure. *Circ. Heart Fail.* **14**, E005890 (2021).

19. Huynh, K. *et al.* Association Between Thigh Muscle Fat Infiltration and Incident Heart Failure: The Health ABC Study. *JACC Heart Fail.* **10**, 485–493 (2022).

20. Diffee, G. M. & Chung, E. Altered single cell force-velocity and power properties in exercise-trained rat myocardium. *J. Appl. Physiol.* **94**, 1941–1948 (2003).

21. Kumar, A., Accorsi, A., Rhee, Y. & Girgenrath, M. Do's and don'ts in the preparation of muscle cryosections for histological analysis. *Journal of Visualized Experiments* **2015**, (2015).

22. Goodpaster, B. H., Theriault, R., Watkins, S. C. & Kelley, D. E. *Intramuscular Lipid Content Is Increased in Obesity and Decreased by Weight Loss*. (2000).

23. Koopman, R., Schaart, G. & Hesselink, M. K. Optimisation of oil red O staining permits combination with immunofluorescence and automated quantification of lipids. *Histochem. Cell Biol.* **116**, 63–68 (2001).

24. Schindelin, J. *et al.* Fiji: an open-source platform for biological-image analysis. *Nat. Methods* **9**, 676–682 (2012).

25. Bhullar, A. S. *et al.* Lipid is heterogeneously distributed in muscle and associates with low radiodensity in cancer patients. *J. Cachexia Sarcopenia Muscle* **11**, 735–747 (2020).

26. Minotti, J. R., Pillay, P., Chang, L., Wells, L. & Massie, B. M. Neurophysiological assessment of skeletal muscle fatigue in patients with congestive heart failure. *Circulation* **86**, 903–908 (1992).

27. De Sousa, E., Veksler, V., Bigard, X., Bing, P. M. & Ventura-Clapier, R. Heart failure affects mitochondrial but not myofibrillar intrinsic properties of skeletal muscle. *Circulation* **102**, (2000).

28. Drexler, H. *et al.* Alterations of skeletal muscle in chronic heart failure. *Circulation* **85**, 1751–1759 (1992).

29. Lv, J. *et al.* Skeletal muscle mitochondrial remodeling in heart failure: An update on mechanisms and therapeutic opportunities. *Biomedicine and Pharmacotherapy* vol. 155 Preprint at https://doi.org/10.1016/j.biopha.2022.113833 (2022).

30. Aimo, A. *et al.* The ergoreflex: how the skeletal muscle modulates ventilation and cardiovascular function in health and disease. *Eur. J. Heart Fail.* **23**, 1458–1467 (2021).

31. Weiss, K. *et al.* Fatigability, Exercise Intolerance, and Abnormal Skeletal Muscle Energetics in Heart Failure. *Circ. Heart Fail.* **10**, (2017).

32. Pipinos, I. I. *et al.* Chronically ischemic mouse skeletal muscle exhibits myopathy in association with mitochondrial dysfunction and oxidative damage. *Am J Physiol Regul Integr Comp Physiol* **295**, 290–296 (2008).

33. Mann, D. L. & Bristow, M. R. Mechanisms and Models in Heart Failure. *Circulation* **111**, 2837–2849 (2005).

34. Yokota, T. *et al.* Systemic oxidative stress is associated with lower aerobic capacity and impaired skeletal muscle energy metabolism in heart failure patients. *Sci. Rep.* **11**, (2021).

35. Gallagher, H., Hendrickse, P. W., Pereira, M. G. & Bowen, T. S. Skeletal muscle atrophy, regeneration, and dysfunction in heart failure: Impact of exercise training. *Journal of Sport and Health Science* vol. 12 Preprint at https://doi.org/10.1016/j.jshs.2023.04.001 (2023).

36. Doerrier, C. *et al.* High-resolution fluorespirometry and oxphos protocols for human cells, permeabilized fibers from small biopsies of muscle, and isolated mitochondria. in *Methods in Molecular Biology* vol. 1782 31–70 (Humana Press Inc., 2018).

37. Divakaruni, A. S. & Jastroch, M. A practical guide for the analysis, standardization and interpretation of oxygen consumption measurements. *Nature Metabolism* vol. 4 978–994 Preprint at https://doi.org/10.1038/s42255-022-00619-4 (2022).

38. Ebanks, B., Kwiecinska, P., Moisoi, N. & Chakrabarti, L. A method to assess the mitochondrial respiratory capacity of complexes I and II from frozen tissue using the Oroboros O2kFluoRespirometer. *PLoS One* **18**, (2023).

39. Acin-Perez, R. *et al.* A novel approach to measure mitochondrial respiration in frozen biological samples. *EMBO J.* **39**, (2020).

40. Elliehausen, C. J., Minton, D. M., Nichol, A. D. & Konopka, A. R. Skeletal muscle mitochondrial respiration in a model of age-related osteoarthritis is impaired after dietary rapamycin. *Exp. Gerontol.* **155**, (2021).

41. Delp, M. D., Duan, C., Mattson, J. P. & Musch, T. I. *Changes in Skeletal Muscle Biochemistry and Histology Relative to Fiber Type in Rats with Heart Failure*. *J. Appl. Physiol* vol. 83 http://www.jap.org (1997).

42. Larsen, S. *et al.* Biomarkers of mitochondrial content in skeletal muscle of healthy young human subjects. *J. Physiol.* **590**, 3349–3360 (2012).

43. Edman, S., Flockhart, M., Larsen, F. J. & Apró, W. Need for speed: Human fast-twitch mitochondria favor power over efficiency. *Mol. Metab.* **79**, 101854 (2024).

44. Takada, S., Sabe, H. & Kinugawa, S. Abnormalities of Skeletal Muscle, Adipocyte Tissue, and Lipid Metabolism in Heart Failure: Practical Therapeutic Targets. *Frontiers in Cardiovascular Medicine* vol. 7 Preprint at https://doi.org/10.3389/fcvm.2020.00079 (2020).

45. Gandolfi, G. *et al.* Perilipin 1 and perilipin 2 protein localization and gene expression study in skeletal muscles of European cross-breed pigs with different intramuscular fat contents. *Meat Sci.* **88**, 631–637 (2011).

46. Gueugneau, M. *et al.* Skeletal Muscle Lipid Content and Oxidative Activity in Relation to Muscle Fiber Type in Aging and Metabolic Syndrome. *J. Gerontol. A Biol. Sci. Med. Sci.* **70**, 566–576 (2015).

47. Li, Y., Xu, S., Zhang, X., Yi, Z. & Cichello, S. Skeletal intramyocellular lipid metabolism and insulin resistance. *Biophys. Rep.* **1**, 90–98 (2015).

48. Mezincescu, A. M. *et al.* Comparison of intramyocellular lipid metabolism in patients with diabetes and male athletes. *Nat. Commun.* **15**, 3690 (2024).

49. Martin, S. S. *et al.* 2025 Heart Disease and Stroke Statistics: A Report of US and Global Data from the American Heart Association. *Circulation* **151**, e41–e660 (2025).

50. Garnham, J. O. *et al.* Chronic heart failure with diabetes mellitus is characterized by a severe skeletal muscle pathology. *J. Cachexia Sarcopenia Muscle* **11**, 394–404 (2020).

51. Hunter, W. G. *et al.* Metabolomic Profiling Identifies Novel Circulating Biomarkers of Mitochondrial Dysfunction Differentially Elevated in Heart Failure With Preserved Versus Reduced Ejection Fraction: Evidence for Shared Metabolic Impairments in Clinical Heart Failure. *J. Am. Heart Assoc.* **5**, (2016).

52. Nadar, S. K. & Shaikh, M. M. Biomarkers in Routine Heart Failure Clinical Care. *Card. Fail. Rev.* **5**, 50–56 (2019).

53. Von Haehling, S. The wasting continuum in heart failure: from sarcopenia to cachexia. *Proc. Nutr. Soc.* **74**, 367–377 (2015).

54. von Haehling, S., Lainscak, M., Springer, J. & Anker, S. D. Cardiac cachexia: A systematic overview. *Pharmacology and Therapeutics* vol. 121 227–252 Preprint at https://doi.org/10.1016/j.pharmthera.2008.09.009 (2009).

55. Fülster, S. *et al.* Muscle wasting in patients with chronic heart failure: results from the studies investigating co-morbidities aggravating heart failure (SICA-HF). *Eur. Heart J.* **34**, 512–519 (2013).

56. Wang, J. *et al.* Functional capacity and skeletal muscle morphology are linked to N-terminal proBNP but not left ventricular ejection fraction in patients with heart failure. *Am. J. Physiol. Heart Circ. Physiol.* **328**, H1344–H1350 (2025).

57. Goodpaster, B. H., Kelley, D. E., Thaete, F. L., He, J. & Ross, R. Skeletal muscle attenuation determined by computed tomography is associated with skeletal muscle lipid content. *J. Appl. Physiol.* **89**, 104–110 (2000).

58. Simoneau, J., Colberg, S. R., Thaete, F. L. & Kelley, D. E. Skeletal muscle glycolytic and oxidative enzyme capacities are determinants of insulin sensitivity and muscle composition in obese women. *The FASEB Journal* **9**, 273–278 (1995).

59. Kuchnia, A. J. *et al.* Computed tomography measured tissue density of pectoral muscle and liver predicts outcomes in heart transplant recipients. *JCSM Rapid Commun.* **5**, 171–181 (2022).

Tables and Figures

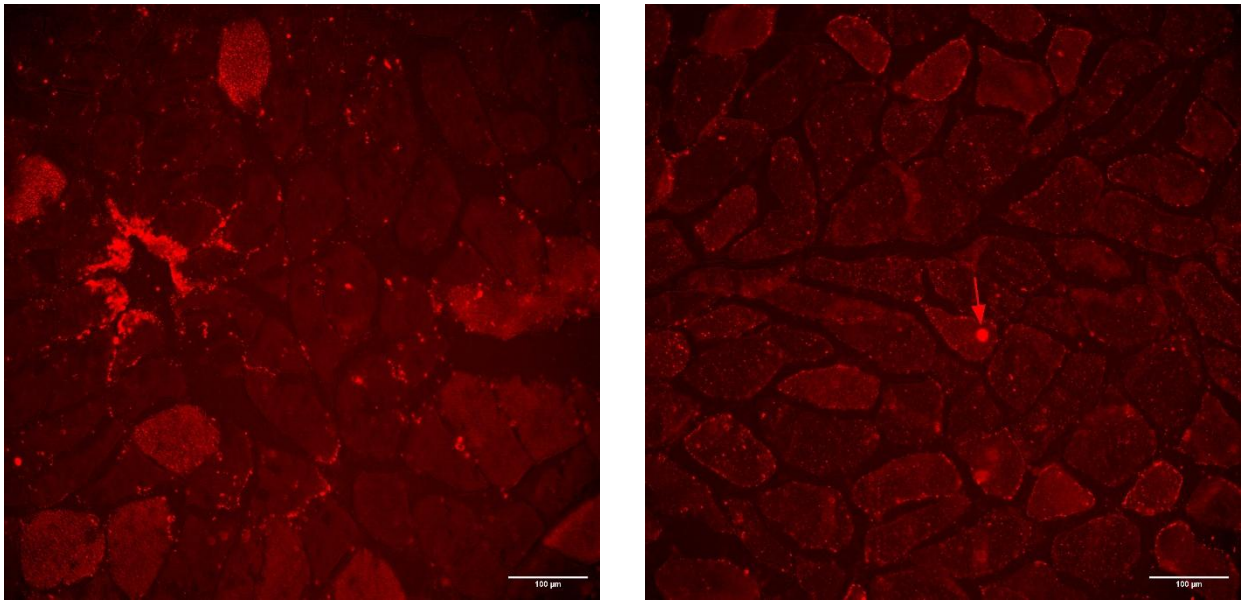

Figure 13. Representative images of Oil Red O staining. Left image: Control. Right image: Heart failure. Arrowhead indicates likely ORO crystal. Scale bars are 100 µm.

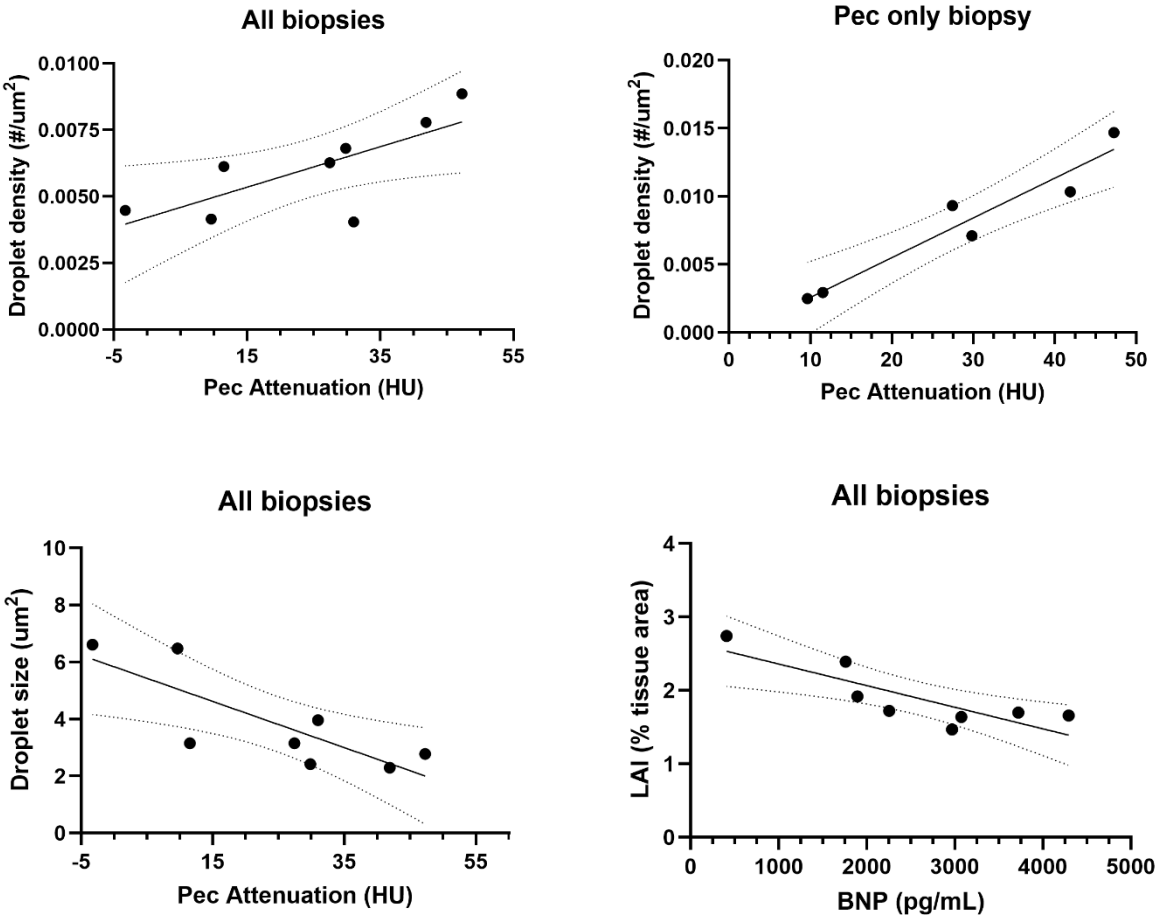

Figure 14. Linear regression of statistically significant correlations with 95% confidence intervals. Top left: Correlation between CT pec attenuation and droplet density from all biopsies. Top right: Correlation between CT pec attenuation and droplet density of pectoral biopsies only. Bottom left: Correlation between CT pec attenuation and mean droplet size from all biopsies. Bottom right: Correlation between BNP and lipid area index (LAI) of all biopsies. Symbols in all biopsy panels represent the mean value within a subject.

Subject Characteristics		
Variable	**Heart Failure**	**Organ Donor Controls**
Number of subjects	10	8
Age (range)	48.4 (20-63)	55.5 (47-66)
Sex	6 Male/4 Female	5 Male/3 Female
BMI	25.75 ± 4.72	27.97 ± 9.38
Surgery type	7 OHT/3 VAD	-
Frailty	3.0 ± 1.6	-
MELD 3.0	17.56 ± 5.34	-

Table 16. Subject and advanced cardiac intervention specific characteristics. MELD = model for end-stage liver disease. Data presented as mean ± SD unless otherwise specified.

Descriptive statistics		
Dependent variable		
Biopsy Site	**Control (n = 8)**	**Heart failure (n = 10)**
Citrate Synthase Activity		
Pec	0.189 ± 0.125	0.074 ± 0.045
Ab	0.200 ± 0.053	0.088 ± 0.044
Droplet count		
Pec	1778.0 ± 914.1	2310.6 ± 1137.4
Ab	1686.4 ± 864.0	1732.1 ± 533.1
Droplet size		
Pec	4.43 ± 1.62	3.41 ± 2.16
Ab	4.63 ± 1.32	3.67 ± 1.45
Droplet density		
Pec	0.0060 ± 0.0034	0.0086 ± 0.0047
Ab	0.0049 ± 0.0026	0.0055 ± 0.0021
Lipid Area Index		
Pec	2.31% ± 1.26%	2.23% ± 0.73%
Ab	1.96% ± 0.70%	1.79% ± 0.65%

Table 17. Baseline statistics of mitochondrial content and lipid parameters. Values are presented as mean ± SD.

LME Model Structure for Dependent Variables		
Dependent variable	**Repeated measures**	**Random intercept**
Droplet count	+	-
Droplet size	+	-
Droplet density	+	+
LAI	+	-
CS activity	+	-

Table 18. LME model structure for each dependent variable. – indicates absence.

Correlation of clinical data					
	Lipid and mitochondrial parameters				
Clinical variable	**Droplet count**	**Droplet size**	**Droplet density**	**LAI**	**CS activity**
Age	-0.141	0.333	-0.150	0.352	0.232
Frailty	0.017	0.003	-0.385	-0.557	-0.278
Duration	0.653	-0.318	0.645	-0.008	0.097
BNP	-0.440	-0.127	-0.553	**-0.786***	-0.278
CT Pec area	0.286	-0.250	0.214	-0.321	-0.524
Pec only	0.600	-0.371	0.371	0.257	-0.262
Avg Attenuation (HU)	0.595	**-0.801***	**0.742***	-0.381	-0.397
Pec only	0.810	-0.792	**0.961****	0.886	0.444

*Table 19. Correlational r values for clinical data with lipid and mitochondrial parameters. BNP = brain natriuretic peptide. Bold signifies a significant correlation. * signifies $p < 0.05$. ** signifies $p < 0.01$.*

	Numerator df	Denominator df	F	Sig.
Droplet count				
Condition	1	13.62	1.057	0.322
Biopsy	1	14.462	1.047	0.323
Condition x Biopsy	1	14.462	0.492	0.494
Droplet size				
Condition	1	13.315	1.421	0.254
Biopsy	1	10.584	0.105	0.752
Condition x Biopsy	1	10.584	0.118	0.738
Droplet density				
Condition	1	14.528	2.06	0.172
Biopsy	1	15.168	2.722	0.12
Condition x Biopsy	1	15.168	0.629	0.44
Lipid Area Index				
Condition	1	15.152	0.135	0.718
Biopsy	1	14.082	1.825	0.198
Condition x Biopsy	1	14.082	0.053	0.821
CS Activity				
Condition	1	13.454	8.545	0.012
Biopsy	1	14.618	1.385	0.258
Condition x Biopsy	1	14.618	0.393	0.541

Table 20. F-statistics and p values for main effects and interactions of linear mixed effects models.

Chapter 5. Project Summary, Limitations, and Future Directions

Project Summary

General Summary

Heart failure is a complex, progressive clinical syndrome defined not only by impaired cardiac function, but it is increasingly being recognized to cause significant peripheral maladaptations. Among these maladaptations, skeletal muscle dysfunction has emerged as a central contributor to the hallmark symptoms of exercise intolerance, fatigue, and dyspnea which profoundly diminish patient's quality of life and increase risk for morbidity and mortality.[1–3] While considerable attention has been directed toward understanding skeletal myopathy in stable, moderate-stage heart failure patients, peripheral phenotypes of patients with late-stage disease- those required advanced cardiac intervention- are poorly characterized. Therefore, the underlying aim of this project was to provide a thorough investigation into the intrinsic function and morphohistological indices of skeletal muscle in patients with ACC/AHA Stage D heart failure. Moreover, we aimed for a comprehensive assessment of the musculature by analyzing these parameters in two functionally distinct muscles groups. We developed and conducted the experiments described in Chapters II-IV in order to address these aims. The significant conclusions outlined in this dissertation are as follows:

1) In Chapter II, we described the effects of late-stage heart failure, biopsy site, and fiber type on the intrinsic contractile properties of SMFs, including peak isometric force, shortening velocity, and power output. We found SMFs from heart failure patients were significantly smaller and had reduced peak isometric force and specific force compared to controls. Additionally, while not significant, we saw trend-level interactions for a reduced power output and normalized power output in the heart failure group. We also saw that the intrinsic contractile properties did not differ between biopsy site when controlling for cross-sectional area of analyzed fibers. These findings suggest that heart failure has a profound negative impact on both the force generating capacity and

shortening velocity of both Type 1 and Type 2 fibers across multiply biopsy sites. The systemic nature of the myopathy and its persistence when account for fiber atrophy indicates a pathophysiological mechanism beyond muscle wasting that contributes to patient symptoms and disease progression.

We also investigated correlations between clinically acquired metrics used in routine care of heart failure patients and the contractile parameters obtained from skeletal muscle biopsies. There were significant positive relationships between global and Type 2 cross-sectional area with pec area assessed from thoracic CT. Moreover, peak isometric force of Type 2 fibers positively correlated with CT pec area. Collectively, these findings suggest that repurposing of the routinely acquired thoracic CT during pre-assessment for advanced cardiac intervention may provide useful information about fiber atrophy and force generating capacity.

2) In Chapter III, we provide a comprehensive and fiber type specific morphohistological assessment of skeletal muscle in the setting of heart failure. We analyzed the differences in cross-sectional area, fibrosis, and two morphological measures- roundness and convexity- both globally and within fiber types and between heart failure and control subjects. Our data showed that heart failure induces a significant atrophogenic effect in skeletal muscle that is not fiber type specific (Type 1: ~36%; Type 2: ~41%). Additionally, we found a marked shift in fiber type composition from Type 1 oxidative fibers (HF: 34%; CON 54.8%) toward Type 2 glycolytic fibers (HF: 68%; CON: 41.6%), similarly to the broader literature.[4] Beyond these changes to fiber size and prevalence, we noted significant alterations in fiber morphology, namely a reduced roundness and increased solidity, a pattern that is consistent with previous work.[5] Similarly to Chapter II, correlational analysis revealed significant positive relationships between global, Type 1, and Type 2 cross-sectional area with CT pec area. Furthermore, Type 2 whole-muscle area contribution was positively correlated with CT pec average attenuation, a finding seen in prior investigations.[6] There

was no significant differences in fibrous collagen content or myonuclear parameters between conditions, biopsy sites or fiber types. Overall, these findings demonstrate that heart failure incites a profound and widespread skeletal muscle atrophy that does not appear to have disparate effects on the musculature.

3) In Chapter IV, we investigated peripheral metabolic remodeling through mitochondrial content and lipid deposition in skeletal muscle. Our data revealed that late-stage heart failure is associated with a significant reduction (~35%) in mitochondrial content as measured by citrate synthase activity. Interestingly, we did not detect any differences in neutral lipid accumulation when assessed through multiple indices of Oil Red O staining. However, despite the absence of significant condition level effects, we discovered significant correlations between lipid parameters and clinical markers. This includes a significant negative relationship between lipid area index and BNP, the gold standard biomarker of heart failure.[7] Moreover, lipid morphology showed key significant relationships with radiodensity measures from thoracic CT. Collectively, these findings suggest that commonly acquired clinical indices in the heart failure population provide a non-invasive approach to analyze skeletal muscle energetics and substrate deposition.

Integrated interpretation

While the findings for each aim are impactful, jointly this dissertation's findings provides a compelling picture of the extensive, multi-domain skeletal myopathy present in patients with late-stage heart failure. It is well established that skeletal abnormalities are important determinants of exercise intolerance, patient symptoms, and prognosis in heart failure.[8–10] Broadly, these abnormalities include mitochondrial dysfunction, fiber type transitions, atrophy, and impaired contractile characteristics. However, few human studies have simultaneously characterized all of these dimensions within the same late-stage population, and fewer still with multiple biopsy sites of functionally distinct skeletal muscles. The current dissertation addresses these gaps by

demonstrating that the heart failure-induced skeletal myopathy is not dysfunction within a single domain, but rather encompasses concurrent functional, structural, and metabolic impairments that are systemic in nature.

The first integrative observation emerging from the three aims is the converging evidence that the pathophysiological mechanisms resulting in peripheral maladaptations are systemic rather than muscle specific. In Chapter II, we discovered that intrinsic contractile dysfunction occurred between conditions, but did not differ by biopsy site, indicating that functional impairments are not disparate between muscle groups. Similarly, in Chapter III, morphohistological parameters did not differ significantly between pec and ab. Finally, in Chapter IV, we did not observe any difference in mitochondrial content between sites but instead showed that the mitochondrial volume was equivalently reduced in the heart failure group. Altogether, these consistent findings across all three aims supports the concept that heart failure-induced myopathy is a systemic response rather that site-specific.

The second integrative theme is the relationship between the structural and metabolic findings. We demonstrated that there was a profound fiber type shift from oxidative Type 1 to glycolytic Type 2 fibers, which provides appropriate biological rationale for the reduced mitochondrial content observed in Chapter IV as Type 1 fibers inherently contain more mitochondrial volume than Type 2 fibers. [11] Reduced mitochondrial content and impaired oxidative capacity lead to accelerated fatigue due to impaired aerobic metabolism.[12,13] Within of heart failure subjects, the combination of a significant fiber type shift, impaired force generating capacity, and reduced mitochondrial content cumulatively impair the muscle's oxidative capacity at a given workload and offer an explanation for exercise intolerance in this population.

Finally, the morphological changes observed in Chapter III, namely the reduced roundness, provide yet another dimension to heart failure-induced myopathy. Alterations in fiber morphology may reflect several remodeling processes, including denervation, injury, and cytoskeletal alterations. While this dissertation did not utilize these measures for prognostication, the significant negative correlation between fiber roundness and frailty is intriguing and suggests that these minute morphological changes may hold clinical meaningful significance about the patient's functional status. This finding underscores the value of in-depth histological phenotyping in order to understand the functional capacity and increased risks of critically ill heart failure patients.

Limitations

While aim specific limitations were discussed in their respective chapters, there are several project-wide limitations that must be acknowledged in order to contextualize findings. First and foremost, our project had a relatively small sample size (10 heart failure and 8 controls). This limited sample size reduces our statistical power and ability to detect smaller effect sizes, especially in our repeated measures mixed design. While the use of linear mixed effects models mitigates some of these power limitations, we still remain underpowered for widespread, definitive conclusions. This is especially true regarding the two-way and three-way interaction terms within the models. Despite our small sample size, our the age of heart failure patients was quite heterogeneous (range: 20-63 years old). This sample may not appropriately represent the heart failure population, which is biased towards individuals in their sixth and seventh decades of life.[2]

A second limitation is that of our controls. Because we wanted to maintain consistency in biopsy sites between control and heart failure groups, we required a creative means to obtain pectoralis major and rectus abdominis tissue since these muscle sites are seldomly utilized for

biopsies. Therefore, control tissue was obtained from organ donors. As such, age and sex matching, as well as a comprehensive past medical history, was not possible. Although the contractile function LME models utilized age and sex as covariates, we could not feasibly match demographics between the two groups. Moreover, organ donors, though absent from heart failure, may not be the best representation of a healthy control population. Finally, because the organ donor skeletal muscle was collected at the University of Kentucky, it was necessary to snap freeze the tissue for transport to the University of Wisconsin- Madison. This snap freezing process required us to utilize a correction factor in Chapter II regarding contractile function. While correction factors for freezing have been utilized in the past, [14] it is not a true representation of the values measured during the control SMF contractile experiments and therefore should be interpreted cautiously. Finally, because the control tissue was snap frozen, there was observed freeze artifacts contained within the histological cross-sections. As such, morphometric parameters of control tissue may have been altered by the incorporation of ice crystals into the tissue and suggest that these results should be interpreted with caution.

The third limitation is our choice of muscle groups- pectoralis major and rectus abdominis. These skeletal muscles were easily accessible during the patients' respective cardiothoracic surgeries. While our integrated interpretation (above) of this project discussed how the consistent findings between aims suggest a systemic myopathic effect from heart failure, these are not the most commonly utilized sites for skeletal muscle biopsies, nor are they majorly involved in clinical measures of function and exercise capacity.[4] While most literature focuses on the limb musculature, especially the vastus lateralis, we assessed more central muscles. For this reason, this data should be treated cautiously and should not be used to extrapolate to skeletal muscle as a whole.

Fourth, this study did not account for the etiology of heart failure (i.e., systolic vs. diastolic dysfunction, ischemic vs. non-ischemic cardiomyopathy), which has been shown to produce disparate peripheral metabolic effects in the skeletal muscle. Similarly, important comorbidities known to independently impact skeletal muscle including diabetes mellitus, which elevates intramyocellular lipid content; cardiac cachexia, which drives catabolic substrate mobilization; and chronic kidney disease were not systematically controlled for in the analyses. The prevalence of comorbidities in this population is high, especially those that are known to impact parameters of skeletal muscle, and their confounding influence may have contributed to the variability observed across outcomes.

Finally, the fifth limitation is the cross-sectional design of the study, which prevents any causal inference, temporal sequence of myopathic changes, and prognostic abilities. Heart failure is a difficult condition to assess longitudinally as progressive of the disease has a significantly high variability. As such it is not feasible to acquire skeletal muscle biopsies prior to heart failure diagnosis or in the early stages, during the intermediate stages, and late stages. However, a longitudinal study employing patients undergoing advanced cardiac intervention allows for greater insight into the mechanisms driving heart failure-induced myopathy.

Future Directions

The findings from this dissertation generate several key questions that should be answered by future work. First, the most immediate need is replication and extension of the current findings to larger, more well-powered studies with prospectively matched controls and documentation of comorbidities, etiology of heart failure, and pharmacological treatment. Given the current design and logistical challenges for biopsy acquisition during surgery, a multi-center approach may be

warranted. Moreover, the studies should include measures of functional capacity, such as dynamometry, handgrip strength, and 6-minute walk test, as well as measures of whole muscle mass, such as DEXA.

Secondly, the current study design was cross-sectional in nature, observing skeletal muscle functional from a single time point. A natural extension to this project would be a longitudinal study design examining how functional, structural, and metabolic features of skeletal muscle change prior to and following OHT or VAD implantation. Prior work has demonstrated that despite the improved hemodynamics following transplantation, individuals still demonstrate a ~20% reduction in predicted VO_2max, suggesting persistent skeletal myopathy.[15] A longitudinal design would allow for us to investigate the changes to the skeletal muscle landscape following hemodynamic restoration. Understanding the temporal component of peripheral tissue recovery would inform us of the post-operative recovery process and identify potential key therapeutic windows.

Third, future studies should investigate skeletal muscle lipid compartmentalization, likely through immunofluorescence techniques, targeting intramyocellular and extramyocellular lipids independently. Furthermore, due to the documented fiber type shift, characterization of fiber type specific intramyocellular lipids is a compelling research aim. This topic would be complemented by high-resolution mitochondrial respirometry utilizing a SUIT protocol for physiologically relevant oxidative capacities for a variety of substrates.[16] Furthermore, assessment of fiber type specific mitochondrial respiration utilizing the pipeline developed by Edman and colleagues would significantly strengthen the literature on skeletal muscle mitochondrial function in the setting of heart failure.[11]

The fourth and final key question to address is the mechanisms underlying the observed intrinsic contractile dysfunction. Reductions is cross-sectional area, peak isometric force, and

specific force suggest an intrinsic dysfunction in crossbridge cycling of myofibers from heart failure patients. This intrinsic dysfunction could be driven by a variety of factors including sarcomeric isoform shifts, post-translation modifications, lattice disruption, and sarcomeric protein loss. Future studies could employ single fiber proteomics,[17] x-ray diffraction, sinusoidal wave analysis, or in vitro motility assays to ascertain the molecular basis for the reduced intrinsic function and aid in targeted therapy development.

Conclusion

In summary, this dissertation demonstrates that late-stage heart failure imposes a profound, systemic skeletal myopathy spanning functional, structural, and metabolic domains, encompassing intrinsic contractile dysfunction, widespread atrophy and fiber type remodeling, and significant mitochondrial depletion that together provide a mechanistic basis for the exercise intolerance and functional decline characteristic of this population. The consistency of these impairments across two functionally distinct muscle groups reinforces that the peripheral consequences of heart failure are systemic rather than site-specific, while convergent correlations between biopsy-derived parameters and routinely acquired clinical indices underscore a translational opportunity for non-invasive skeletal muscle phenotyping in this population. Collectively, these findings establish a mechanistic foundation for future therapeutic efforts that target the peripheral musculature as an integral component of advanced heart failure management.

References

1. Anker, S. D. *et al.* Wasting as independent risk factor for mortality in chronic heart failure. *The Lancet* **349**, 1050–1053 (1997).

2. Martin, S. S. *et al.* 2025 Heart Disease and Stroke Statistics: A Report of US and Global Data from the American Heart Association. *Circulation* **151**, e41–e660 (2025).

3. Heidenreich, P. A. *et al.* 2022 AHA/ACC/HFSA Guideline for the Management of Heart Failure: A Report of the American College of Cardiology/American Heart Association Joint Committee on Clinical Practice Guidelines. *Circulation* vol. 145 E895–E1032 Preprint at https://doi.org/10.1161/CIR.0000000000001063 (2022).

4. Kaneguchi, A., Sakitani, N. & Umehara, T. Histological changes in skeletal muscle induced by heart failure in human patients and animal models: A scoping review. *Acta Histochem.* **126**, 152210 (2024).

5. Larsen, A. I. *et al.* Effect of exercise training on skeletal muscle fibre characteristics in men with chronic heart failure. Correlation between skeletal muscle alterations, cytokines and exercise capacity. *Int. J. Cardiol.* **83**, 25–32 (2002).

6. Simoneau, J., Colberg, S. R., Thaete, F. L. & Kelley, D. E. Skeletal muscle glycolytic and oxidative enzyme capacities are determinants of insulin sensitivity and muscle composition in obese women. *The FASEB Journal* **9**, 273–278 (1995).

7. Shrivastava, A., Haase, T., Zeller, T. & Schulte, C. Biomarkers for Heart Failure Prognosis: Proteins, Genetic Scores and Non-coding RNAs. *Frontiers in Cardiovascular Medicine* vol. 7 Preprint at https://doi.org/10.3389/fcvm.2020.601364 (2020).

8. Keller-Ross, M. L., Larson, M. & Johnson, B. D. Skeletal muscle fatigability in heart failure. *Frontiers in Physiology* vol. 10 Preprint at https://doi.org/10.3389/fphys.2019.00129 (2019).

9. Kinugawa, S., Takada, S., Matsushima, S., Okita, K. & Tsutsui, H. Skeletal Muscle Abnormalities in Heart Failure. *Int. Heart J.* (2015).

10. Lavine, K. J. & Sierra, O. L. Skeletal muscle inflammation and atrophy in heart failure. *Heart Fail. Rev.* **22**, (2017).

11. Edman, S., Flockhart, M., Larsen, F. J. & Apró, W. Need for speed: Human fast-twitch mitochondria favor power over efficiency. *Mol. Metab.* **79**, 101854 (2024).

12. Weiss, K. *et al.* Fatigability, Exercise Intolerance, and Abnormal Skeletal Muscle Energetics in Heart Failure. *Circ. Heart Fail.* **10**, (2017).

13. De Sousa, E., Veksler, V., Bigard, X., Bing, P. M. & Ventura-Clapier, R. Heart failure affects mitochondrial but not myofibrillar intrinsic properties of skeletal muscle. *Circulation* **102**, (2000).

14. Claflin, D. R. *et al.* Effects of high-and low-velocity resistance training on the contractile properties of skeletal muscle fibers from young and older humans. *J Appl Physiol* **111**, 1021–1030 (2011).

15. Wilson, R. F., Johnson, T. H., Haidet, G. C., Kubo, S. H. & Mianuelli, M. Sympathetic Reinnervation of the Sinus Node and Exercise Hemodynamics After Cardiac Transplantation. *Circulation* 2727–2733 (2000).

16. Elliehausen, C. J., Minton, D. M., Nichol, A. D. & Konopka, A. R. Skeletal muscle mitochondrial respiration in a model of age-related osteoarthritis is impaired after dietary rapamycin. *Exp. Gerontol.* **155**, (2021).

17. Wilson, M. C. *et al.* Top–Down Proteomics of Skinned Human Muscle Fibers Reveals Proteoform-Resolved Fiber-to-Fiber Variability. *Journal of Mass Spectrometry* **61**, (2026).